Characteristics of Atmospheric Aerosols in Kitakyushu, Japan: Sources, Secondary Formation, Reduction Mechanism, and Risk Assessment

By

Xi ZHANG

Thesis submitted to the Graduate School of Environmental Engineering, The University of Kitakyushu in fulfillment of the requirement for the degree of Doctor of Engineering

September, 2021

Declaration

I hereby declare that this thesis has not been previously submitted to any other university or institution for obtaining any academic degree. Accept quotation and data which are properly cited, this thesis contains my original works. The thesis is only submitted to The University of Kitakyushu in fulfillment of the requirement for a Degree of Doctor of Engineering.

<div align="right">

Kitakyushu, Japan

September, 2021

Xi ZHANG

</div>

CONTENTS

Abstract. The sampling campaign of atmospheric aerosols (total particulate matter (TPM) and $PM_{2.5}$) was carried out in Kitakyushu, Japan. For TPM, five main sources (industrial combustion plus ship emissions, secondary sulfates, secondary nitrates plus biomass burning, marine aerosols, and dust) were identified in this study, accounting for 26%, 23%, 22%, 19%, and 10%, respectively. Secondary inorganic aerosols (SIA) had the largest contribution for total particle mass concentration, and its formation process is significantly influenced by Ox, NO_2, NH_3, HNO_3, HCl, T, and RH. Based on the sensitive tests of ISORROPIA II model, it can be known that controlling SIA concentrations was an effective and realistic method to mitigate particle pollution in Kitakyushu, Japan. The inorganic aerosol mass concentration (IAM) changed nonlinearly when we reduced TNH_4^+ and TSO_4^{2-} concentrations, while IAM decreased linearly when we control TNO_3^- concentration (the fitting curves: $y = -5.11x - 13.82x^2 + 9.21x^3$, $y = -12.89x + 10.47x^2$, and $y = -6.74x$, respectively (y and x presents IAM variation [$\mu g \cdot m^{-3}$] and concentration reduction ratio (CRR)/100 [dimensionless]). As the most sensitive aerosol component, aerosol liquid water content (ALWC) was statistically and strongly related to the variations of NO_3^-, Cl^-, SO_4^{2-}, HSO_4^-, HNO_3, and NH_3 ($P < 0.05$), with coefficients of 1.68, 5.23, 1.83, 2.81, 0.34, and 0.57, respectively. In addition, the concentration level of ALWC could affect aerosol pH; the reductions of TSO_4^{2-} and TNO_3^- concentrations caused the obvious increase of aerosol pH, with the fitting equations of $y = 0.97x + 0.54x^2$ and $y = 0.49x$, respectively (y and x presents the inorganic aerosol pH variation [dimensionless] and CRR/100 [dimensionless]). Only the inorganic aerosol pH after controlling TNH_4^+ was lower than that in base case, and the variations of aerosol pH followed the fitting equation of $y = -0.35x - 1.50x^2$.

Except for particle mass concentration and aerosol pH, the risk level of toxic components for the ecological system was also one of the parameters for atmospheric particle pollution. As compared with coarse-mode particles, fine-mode particles are easier to adsorb harmful substances due to the higher

surface/mass ratio; thus, the risk assessment of $PM_{2.5}$-bound heavy metals were further investigated in this study. Among 29 heavy metals, Se, Mo, Pb, As, Zn, W, Sb, Cu, V, Cr, Ni, and Cs were mainly from anthropogenic sources, which had the EF values larger than 10, and Igeo values larger than 0. The comprehensive ecological risk index for these 12 anthropogenic metals was far greater than 600. This large index showed the severe metal pollution and very high ecological risk in Kitakyushu, Japan, which should be paid great attention. The human health assessment result further revealed that children living here faced severe non-carcinogenic risk (HI=7.8) and moderate carcinogenic risk (CR=1.2×10^{-4}), and oral ingestion was basically the most important exposure pathway, followed by dermal contact and inhalation. The priority control metals included Mo, Se, As, Pb, Sb, and Cr, moreover, the concentration-weighted trajectory analysis (CWT) indicated that Mo, Sb, and Cr were from ship emissions because some shipping routes around Kyushu area were identified as their potential pollution source regions, while Se, As, and Pb were carried by the air masses from Asian landmass. Overall, our results clearly demonstrate the characteristics of atmospheric particles, providing policy makers with basic and effective ideas for mitigating particle pollution.

Keywords: filter-pack method; pollution source; sensitive tests; anthropogenic metals; human health risk; ship emissions.

Chapter 1: Introduction

1.1 Overview of aerosol types, sources, and atmospheric processing

Atmospheric aerosols, also known as particulate matters, are minute particles suspended in the ambient atmosphere, with the size range from a few nanometers to tens of micrometers in diameters (McNeill, 2017). The whole life cycle of aerosols is shown in Fig. 1-1. First, primary particles and some gaseous pollutants could be directly emitted from a wide variety of natural and anthropogenic sources, such as forest fire, volcanic eruption, sea salts, biomass burning, desert dust, construction activity, traffic emission, industrial emission, incomplete combustion of fossil fuels, and biological materials (plant fragments, pollen, micro-organisms, etc.) (Wen et al., 2018; Li et al., 2019; Duan et al., 2020; Hao et al., 2020; Tsai et al., 2020; Behrooz et al., 2021). Then, secondary particles could be formed by the gas-to-particle conversion in the ambient atmosphere and/or the condensation of gaseous compounds on pre-existing particles (Hama et al., 2017; Wang et al., 2017; Kim and Zhang, 2019; Svedova et al., 2019). Once airborne, these particles can change their size, structure, and composition by coagulating with other particles, by chemical reactions, by condensation or evaporation of vapor species, or by activation in the presence of water supersaturation (Seinfeld et al., 2006; Monks et al., 2009). In general, the total particle number and mass concentrations in the lower atmosphere (troposphere) typically vary in the range of about 10^2–10^5 cm^3 and 1–100 $\mu g \cdot m^{-3}$, respectively (Monks et al., 2009). The predominant chemical components of atmospheric aerosols are nitrate, sulfate, ammonium, organic carbon, and black or elemental carbon, each of which typically contribute about 10–30% to the overall mass load (Morakinyo et al., 2016; Liu et al., 2020; Ren et al., 2021; Shao et al., 2021; Zhang et al., 2021).

Atmospheric particles are eventually removed from ambient air by two deposition mechanisms (dry deposition and wet deposition) (Li et al., 2018). Dry deposition refers to the deposition of particles or

gases from the atmosphere through the direct delivery of mass to the surface (i.e. via non-precipitation) (Dolske and Gatzet, 1985). On the other hand, wet processes are often referred to as rain or snow scavenging (Tai et al., 2017), with rain-scavenged particles being generally classified as 'rainout particles' (serving as cloud-condensation nuclei or undergoing capture by cloud water) and as 'washout' (i.e. removal of below-cloud particles by raindrops as they fall) (Chate et al., 2003). Depending on aerosol properties and meteorological conditions, the characteristic residence times (lifetimes) of particles in the atmosphere range from hours to weeks (Pöschl, 2005; Monks et al., 2009).

Today there is a growing interest and concern in improving air quality by both the general public and governments. These interests and concerns have prompted an important increase in atmospheric particle pollution research, which is a complex task requiring knowledge of all the factors and processes involved: the emission sources, the transport process, the chemical and physical transformations, deposition mechanisms, and, finally, their effects on the environment and living beings. All these processes must be considered from different perspectives and at several scales, both spatial and temporal.
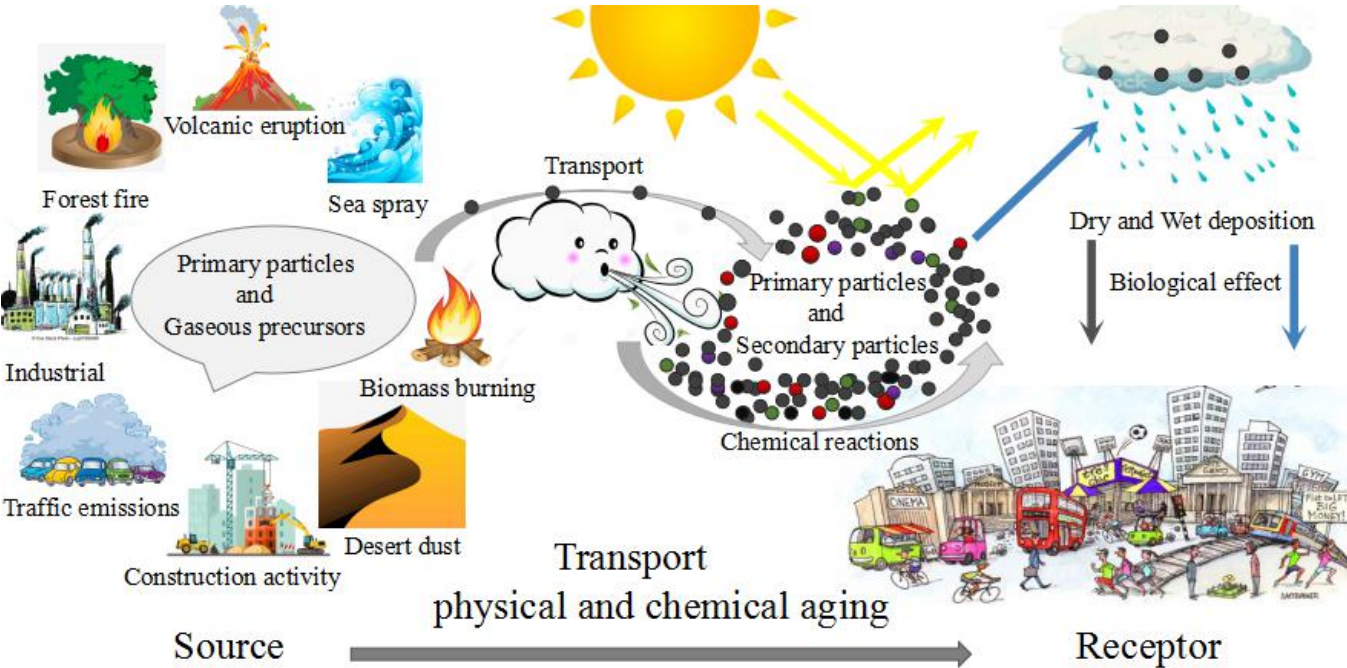
Fig. 1-1 Primary emissions, secondary formations, and atmospheric processing of natural and anthropogenic aerosols.

1.2 Global particle pollution

Over the past few decades, atmospheric particle pollution has aroused great attention on a global scale. Fig. 1-2 shows the spatial distributions of PM_{10} and $PM_{2.5}$. As we can see that particle pollution was most pronounced in China, India, Saudi Arabia, and some countries in northern Africa. Previous researches have confirmed that the formation process, component distribution, and risk level of atmospheric particles among regions vary greatly due to the difference of meteorological conditions, precursor concentrations, atmospheric oxidation level, etc (Monks et al., 2009; Fuzzi et al., 2015; Mukherjee et al., 2017; Hopke et al., 2020; Lim et al., 2020).
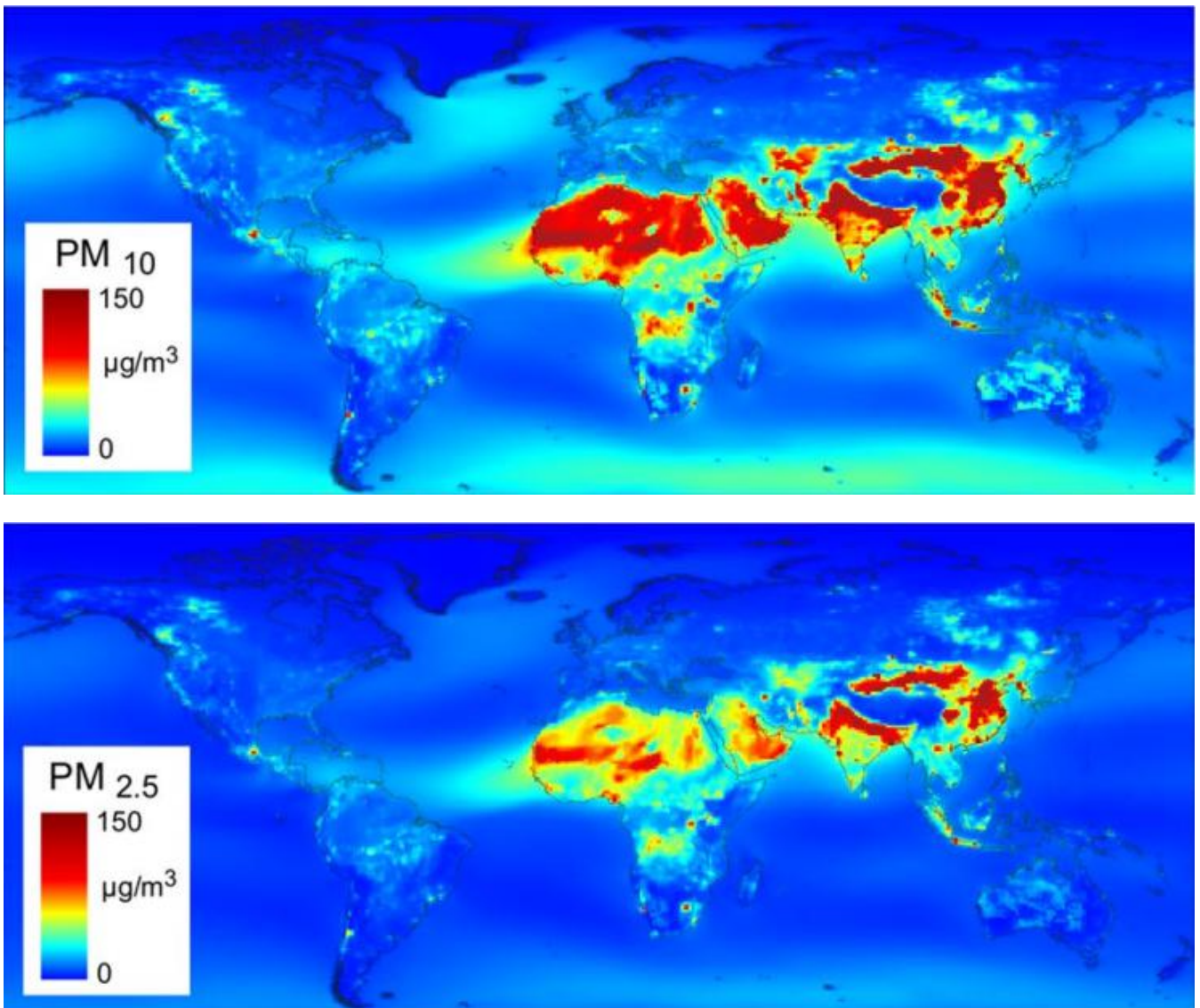
Fig. 1-2 PM_{10} and $PM_{2.5}$ concentration levels on the global scale over 2015-2018 (Solimini et al., 2021).

1.3 Particle monitoring in Japan

Compared with other countries, the concentration level of PM$_{2.5}$ in Japan was relatively low (Khan et al., 2010; Inomata et al., 2016; Phung et al., 2020; Ikemori et al., 2021). The Ministry of the Environment of Japan have conducted particle monitoring for a long time. The average PM$_{2.5}$ mass concentration in Japan was about 12.5 µg·m^{-3} from 2015 to 2018. Among 179 monitoring sites, there were 25 sites with the PM$_{2.5}$ concentration level larger than the annual National Ambient Air Quality Standards of the United States Environmental Protection Agency (15 µg·m^{-3}), and the highest PM$_{2.5}$ mass concentration (20.5 µg·m^{-3}) was observed at Kitakyushu monitoring site (Fig. 1-3). Hence, the particle pollution in Japan still needs attention, especially in Kitakyushu City.
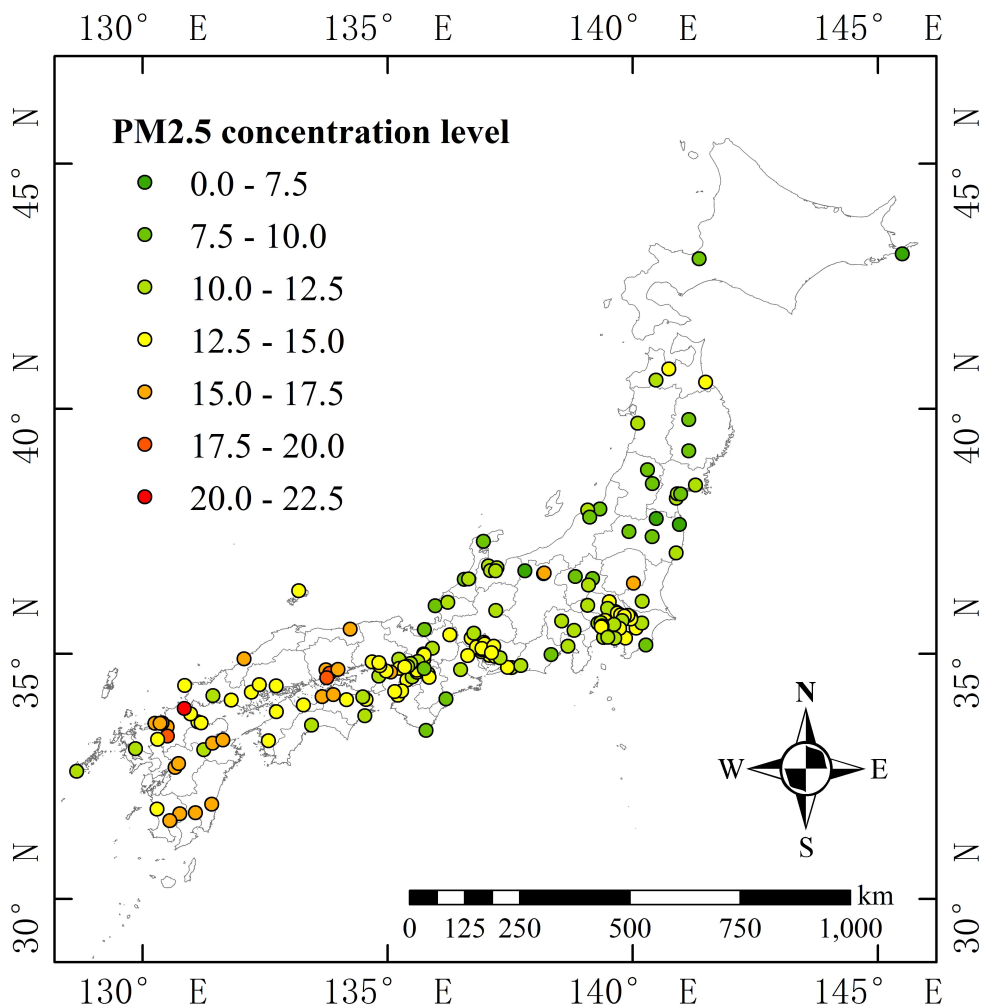
Fig. 1-3 PM$_{2.5}$ concentration levels (µg·m^{-3}) at 179 monitoring sites in Japan over 2015-2018 (Data source: http://www.env.go.jp/air/osen/pm/monitoring.html).

1.4 Research objectives of the present study

Kitakyushu City is a well-known urbanized and industrial area in Japan, with about one million inhabitants. The atmospheric particles in Kitakyushu City are double-influenced not only by in-country transport but also by trans-boundary transport. The main objectives of this study are as follows: (1) to quantify the contribution of each pollution source and distinguish the potential pollution source regions, especially for secondary aerosol; (2) to analyze the factors driving secondary formation; (3) to assess the calculation bias of the nitrogen oxidation rate when the presence of atmospheric HNO_3 is ignored; (4) to comprehensively assess the responses of inorganic aerosols to the reductions in precursor concentrations; (5) to evaluate the integrated environmental risk due to the exposure of particle-bound heavy metals, and the human health risk via oral ingestion, inhalation, and dermal contact, and (6) to identify the high-risk metal sources and their potential pollution source regions. Our comprehensive study about atmospheric aerosols could provide scientific reference to formulate countermeasures for air pollution issue on aerosol.

References

Behrooz, R.D., Kaskaoutis, D.G., Grivas, G., Mihalopoulos, N., 2021. Human health risk assessment for toxic elements in the extreme ambient dust conditions observed in Sistan, Iran. Chemosphere 262, 127835.

Chate, D.M., Rao, P.S.P., Naik, M.S., Momin, G.A., Safai, P.D., Ali, K., 2003. Scavenging of aerosols and their chemical species by rain. Atmospheric Environment 37, 2477-2484.

Dolske, D.A., Gatz, D.F., 1985. A field intercomparison of methods for the measurement of particle and gas dry deposition. Journal of Geophysical Research: Atmospheres 90, 2076-2084.

Duan, X., Yan, Y., Li, R., Deng, M., Hu, D., Peng, L., 2020. Seasonal variations, source apportionment, and health risk assessment of trace metals in $PM_{2.5}$ in the typical industrial city of changzhi, China.

Atmospheric Pollution Research.

Fuzzi, S., Baltensperger, U., Carslaw, K., Decesari, S., Denier van der Gon, H., Facchini, M.C., Fowler, D., Koren, I., Langford, B., Lohmann, U., Nemitz, E., Pandis, S., Riipinen, I., Rudich, Y., Schaap, M., Slowik, J.G., Spracklen, D.V., Vignati, E., Wild, M., Williams, M., Gilardoni, S., 2015. Particulate matter, air quality and climate: lessons learned and future needs. Atmospheric Chemistry and Physics 15, 8217-8299.

Hama, S.M.L., Cordell, R.L., Monks, P.S., 2017. Quantifying primary and secondary source contributions to ultrafine particles in the UK urban background. Atmospheric Environment 166, 62-78.

Hao, Y., Luo, B., Simayi, M., Zhang, W., Jiang, Y., He, J., Xie, S., 2020. Spatiotemporal patterns of $PM_{2.5}$ elemental composition over China and associated health risks. Environmental Pollution 265, 114910.

Hopke, P.K., Dai, Q., Li, L., Feng, Y., 2020. Global review of recent source apportionments for airborne particulate matter. Science of The Total Environment 740, 140091.

Ikemori, F., Uranishi, K., Sato, T., Fujihara, M., Hasegawa, H., Sugata, S., 2021. Time-resolved characterization of organic compounds in $PM_{2.5}$ collected at Oki Island, Japan, affected by transboundary pollution of biomass and non-biomass burning from Northeast China. Science of The Total Environment 750, 142183.

Inomata, Y., Ohizumi, T., Take, N., Sato, K., Nishikawa, M., 2016. Transboundary transport of anthropogenic sulfur in $PM_{2.5}$ at a coastal site in the Sea of Japan as studied by sulfur isotopic ratio measurement. Science of The Total Environment 553, 617-625.

Khan, M.F., Shirasuna, Y., Hirano, K., Masunaga, S., 2010. Characterization of $PM_{2.5}$, $PM_{2.5-10}$ and $PM_{>10}$ in ambient air, Yokohama, Japan. Atmospheric Research 96, 159-172.

Kim, H., Zhang, Q., 2019. Chemistry of new particle growth during springtime in the Seoul metropolitan area, Korea. Chemosphere 225, 713-722.

Li, F., Wu, Y., Liu, J., Zhai, J., Cong, L., Wang, Y., Ma, W., Zhang, Z., Li, C., 2018. Comparison of dry and wet deposition of particulate matter in near-surface waters during summer. Plos One 13, e0199241.

Li, P.h., Yu, J., Bi, C.l., Yue, J.j., Li, Q.q., Wang, L., Liu, J., Xiao, Z., Guo, L., Huang, B.j., 2019. Health risk assessment for highway toll station workers exposed to $PM_{2.5}$-bound heavy metals. Atmospheric Pollution Research 10, 1024-1030.

Lim, C.H., Ryu, J., Choi, Y., Jeon, S.W., Lee, W.K., 2020. Understanding global $PM_{2.5}$ concentrations and their drivers in recent decades (1998–2016). Environment International 144, 106011.

Liu, T., Hu, B., Xu, X., Hong, Y., Zhang, Y., Wu, X., Xu, L., Li, M., Chen, Y., Chen, X., Chen, J., 2020. Characteristics of $PM_{2.5}$-bound secondary organic aerosol tracers in a coastal city in Southeastern China: Seasonal patterns and pollution identification. Atmospheric Environment 237, 117710.

McNeill, V.F., 2017. Atmospheric Aerosols: Clouds, Chemistry, and Climate. Annual Review of Chemical and Biomolecular Engineering 8, 427-444.

Monks, P.S., Granier, C., Fuzzi, S., Stohl, A., Williams, M.L., Akimoto, H., Amann, M., Baklanov, A., Baltensperger, U., Bey, I., Blake, N., Blake, R.S., Carslaw, K., Cooper, O.R., Dentener, F., Fowler, D., Fragkou, E., Frost, G.J., Generoso, S., Ginoux, P., Grewe, V., Guenther, A., Hansson, H.C., Henne, S., Hjorth, J., Hofzumahaus, A., Huntrieser, H., Isaksen, I.S.A., Jenkin, M.E., Kaiser, J., Kanakidou, M., Klimont, Z., Kulmala, M., Laj, P., Lawrence, M.G., Lee, J.D., Liousse, C., Maione, M., McFiggans, G., Metzger, A., Mieville, A., Moussiopoulos, N., Orlando, J.J., O'Dowd, C.D., Palmer, P.I., Parrish, D.D., Petzold, A., Platt, U., Pöschl, U., Prévôt, A.S.H., Reeves, C.E., Reimann, S., Rudich, Y., Sellegri, K., Steinbrecher, R., Simpson, D., ten Brink, H., Theloke, J., van der Werf,

G.R., Vautard, R., Vestreng, V., Vlachokostas, C., von Glasow, R., 2009. Atmospheric composition change – global and regional air quality. Atmospheric Environment 43, 5268-5350.

Morakinyo, O., Mokgobu, M., Mukhola, M., Hunter, R., 2016. Health Outcomes of Exposure to Biological and Chemical Components of Inhalable and Respirable Particulate Matter. International Journal of Environmental Research and Public Health 13, 592.

Mukherjee, A., Agrawal, M., 2017. World air particulate matter: sources, distribution and health effects. Environmental Chemistry Letters 15, 283-309.

Phung, V.L.H., Ueda, K., Seposo, X., Takami, A., Sugata, S., Yoshino, A., Michikawa, T., Yamazaki, S., Honda, A., Takano, H., 2020. Hourly association between ambient $PM_{2.5}$ and emergency ambulance dispatches in 11 cities in Japan. Environmental Research 185, 109448.

Pöschl, U., 2005. Atmospheric Aerosols: Composition, Transformation, Climate and Health Effects. Angewandte Chemie International Edition 44, 7520-7540.

Ren, Y., Wei, J., Wu, Z., Ji, Y., Bi, F., Gao, R., Wang, X., Wang, G., Li, H., 2021. Chemical components and source identification of $PM_{2.5}$ in non-heating season in Beijing: The influences of biomass burning and dust. Atmospheric Research 251, 105412.

Seinfeld, J.H., Pandis, S.N., 2006. Atmospheric Chemistry and Physics: From Air Pollution to Climate Change. 2nd Edition, John Wiley & Sons, New York.

Shao, M., Dai, Q., Yu, Z., Zhang, Y., Xie, M., Feng, Y., 2021. Responses in $PM_{2.5}$ and its chemical components to typical unfavorable meteorological events in the suburban area of Tianjin, China. Science of The Total Environment 788, 147814.

Solimini, A., Filipponi, F., Fegatelli, D.A., Caputo, B., De Marco, C.M., Spagnoli, A., Vestri, A.R., 2021. A global association between Covid-19 cases and airborne particulate matter at regional level. Scientific Reports 11.

Švédová, B., Kucbel, M., Raclavská, H., Růžičková, J., Raclavský, K., Sassmanová, V., 2019. Water-soluble ions in dust particles depending on meteorological conditions in urban environment. Journal of Environmental Management 237, 322-331.

Tai, A.Y.C., Chen, L.W.A., Wang, X., Chow, J.C., Watson, J.G., 2017. Atmospheric deposition of particles at a sensitive alpine lake: Size-segregated daily and annual fluxes from passive sampling techniques. Science of The Total Environment 579, 1736-1744.

Tsai, P.J., Young, L.H., Hwang, B.F., Lin, M.Y., Chen, Y.C., Hsu, H.T., 2020. Source and health risk apportionment for $PM_{2.5}$ collected in Sha-Lu area, Taiwan. Atmospheric Pollution Research 11, 851-858.

Wang, Z., Wu, Z., Yue, D., Shang, D., Guo, S., Sun, J., Ding, A., Wang, L., Jiang, J., Guo, H., Gao, J., Cheung, H.C., Morawska, L., Keywood, M., Hu, M., 2017. New particle formation in China: Current knowledge and further directions. The Science of the total environment 577, 258-266.

Wen, J., Wang, X., Zhang, Y., Zhu, H., Chen, Q., Tian, Y., Shi, X., Shi, G., Feng, Y., 2018. $PM_{2.5}$ source profiles and relative heavy metal risk of ship emissions: Source samples from diverse ships, engines, and navigation processes. Atmospheric Environment 191, 55-63.

Zhang, W., Peng, X., Bi, X., Cheng, Y., Liang, D., Wu, J., Tian, Y., Zhang, Y., Feng, Y., 2021. Source apportionment of $PM_{2.5}$ using online and offline measurements of chemical components in Tianjin, China. Atmospheric Environment 244, 117942.

Chapter 2: Sources, species and secondary formation of atmospheric aerosols and gaseous precursors

2.1 Introduction

Atmospheric aerosols are complex pollutants that can be classified as primary aerosols and secondary aerosols and not only affect the radiation budget and climate through cloud formation processes but also cause human health risks due to exposure to toxic components (Kanniah et al., 2016; Pietrogrande et al., 2018; Zhang et al., 2019b). Primary aerosols are directly emitted from natural and anthropogenic sources, while secondary aerosols are formed through gas-to-particle conversion, in a process that can be accomplished by either condensation, which adds mass to pre-existing aerosols, or direct nucleation from gaseous aerosol-forming precursors (Hama et al., 2017; Wang et al., 2017; Kim and Zhang, 2019; Svedova et al., 2019). In Japan, transboundary aerosol pollution can strongly influence air quality, with a large fraction of the primary and secondary aerosols originating from the Asian landmass, where significant emission sources, such as mineral particles from arid or semiarid regions and anthropogenic aerosols and gaseous precursors arising from fossil fuel combustion and vehicle emissions, exist (Khan et al., 2010; Takahashi et al., 2010; Moreno et al., 2012; Kaneyasu et al., 2014; Inomata et al., 2016). In addition, many researchers have clarified that secondary aerosols play a dominant role in severe particle pollution events, now having become an important particle pollution source in Japan and abroad (Khan et al., 2010; Inomata et al., 2016; Kong et al., 2018; Ng et al., 2019; Roger et al., 2019; Wang et al., 2019).

Due to the complex photochemical and aqueous reactions that take place in the atmosphere, the secondary formation process can be influenced by and related to a variety of factors. Wang et al. (2019) showed that SO_4^{2-}, NO_3^-, and NH_4^+ (SNA) contributed to the largest fraction of atmospheric aerosols and had a strong positive relationship with gaseous precursors, especially nitrogen oxides (NOx), sulfur

dioxide (SO_2), and ammonia (NH_3). Wen et al. (2015) investigated the important roles of NH_3 and O_3 on the elevated concentration of fine particulate nitrate. Fu et al. (2015) and Jiang et al. (2019) indicated that aerosol pH is a significant parameter for acidity-dependent heterogeneous reactions on aerosol surfaces, such as the oxidation of SO_2 and the hydrolysis of N_2O_5. Xu et al. (2017) and Svedova et al. (2019) concluded that meteorological conditions play a crucial role in the transformation of atmospheric aerosols. More specifically, variations in wind direction, wind speed, and temperature can drive the horizontal transport and vertical dispersion of atmospheric aerosols and gaseous precursors. Relative humidity also has significant positive correlations with the concentrations of SNA, especially for particles in the size range of 0.606 to 2.48 μm, and a high relative humidity can create conditions that are favorable for aqueous reactions and more easily accelerate the formation of secondary inorganic aerosols (Deshmukh et al., 2011; Svedova et al., 2019). Further, the influence of relative humidity on aerosol liquid water content has been investigated (Xue et al., 2014; Kong et al., 2018; Wang et al., 2019). As the relative humidity increases, the hygroscopic effect from the surrounding environment on aerosols is increased, causing a significant change in the particle size distribution, due to water uptake, and the optical property of the atmospheric aerosols, which affects the scattering and absorption of solar radiation; as a result, the aerosol liquid water content increases accordingly, promoting the dissolution of gaseous precursors and further reactions to form stable aerosol species (McMurry and Wilson, 1983; Kitamori et al., 2009; Tan et al., 2017; Wang et al., 2019). Although many researchers have analyzed the specific relationship between the concentration of SNA and several important factors, few studies have explored secondary aerosol formation with a focus on the comprehensive influence of related factors, even though the inner mechanisms are worth investigating.

In the present study, year-round, daily observation of atmospheric particles and gaseous precursors was carried out in Kitakyushu City on the western edge of Japan by using the filter-pack (FP) method.

The FP method can simultaneously provide useful information regarding atmospheric particles and gaseous precursors (nitric acid (HNO_3), hydrochloric acid (HCl), sulfur dioxide (SO_2), and ammonia (NH_3)), and thus it is frequently used all over the world (Hong et al., 2002; Aikawa et al., 2013; 2016). In contrast, sampling and the following chemical analyses must be carried out manually, which is a time-consuming and laborious process. As a consequence, few datasets based on the FP method and utilizing daily recording for a long period of time, such as one year, have been reported. In this study, by combining precious observational data collected by using the FP method with some statistical and/or thermodynamic model analyses, we set the objectives as follows: (1) to investigate the concentration level of atmospheric particles and gaseous precursors, (2) to quantify the contribution of each pollution source and distinguish the potential pollution source regions, especially for secondary aerosols, and (3) to analyze the factors that drive secondary formation. To achieve these objectives, source diagnosis combined with positive matrix factorization (PMF) and concentration-weighted trajectory (CWT) analysis was applied to evaluate the contribution of secondary sulfates and secondary nitrates, as well as to clarify corresponding transport pathways and potential pollution source regions (Tan et al., 2014; Li et al., 2017; Taghvaee et al., 2018; Zhong et al., 2018; Yamagami et al., 2019). Then, multiple regression analysis was performed to further explore the inner mechanisms of the secondary formation process and their factors of influence (Wang et al., 2019). Among the factors of influence, aerosol liquid water content and aerosol pH were difficult to measure directly; hence, Extended Aerosol Inorganic Model III (E-AIM-III) was employed to estimate these two factors (Silvern et al., 2017; Jia et al., 2018). Simultaneously, ISORROPIA II, a thermodynamic equilibrium model, was also used to assess the gas-to-particle conversion process for the year-round observation dataset (Tang et al., 2016; Tan et al., 2017; Kong et al., 2018; Roig Rodelas et al., 2019). The findings of this work could provide valuable field measurement-based evidence regarding the significant contributions and inner mechanisms of

secondary aerosol pollution, which could be adopted as the important basis for policy-maker to mitigate particle pollution.

2.2 Experimental

2.2.1 Filter-pack method observations

2.2.1.1 Sampling site and period

Air sampling was carried out from the rooftop (18 m above the ground) of the Hibikino Campus of the University of Kitakyushu (33.89° N, 130.71° E) from March 2017 to February 2018. Our sampling site is in the suburb of Kitakyushu City, as illustrated in Fig. 2-1. Kitakyushu City is (1) one of the most urbanized cities in Japan with a population density of more than 961,000 people/492 km^2, (2) one of the largest industrial cities in Japan, which mainly focus on heavy industries such as steel manufacturing and chemical industry, (3) an important transport hub for traffic between Honshu and Kyushu, and (4) on the western edge of Japan, being located on the forefront of transboundary transportation from the Asian landmass. The atmospheric particles around the sampling site were double-influenced by in-country transport and trans-boundary transport, such that their complex emission sources were worth in-depth investigation. In addition, the secondary aerosol studies in a suburban area of Japan are insufficient, and in particular, the available information on the secondary formation process and the potential pollution source regions remains rather limited. Thus, this study has the potential to help policy makers to mitigate particle pollution, especially secondary aerosol pollution.
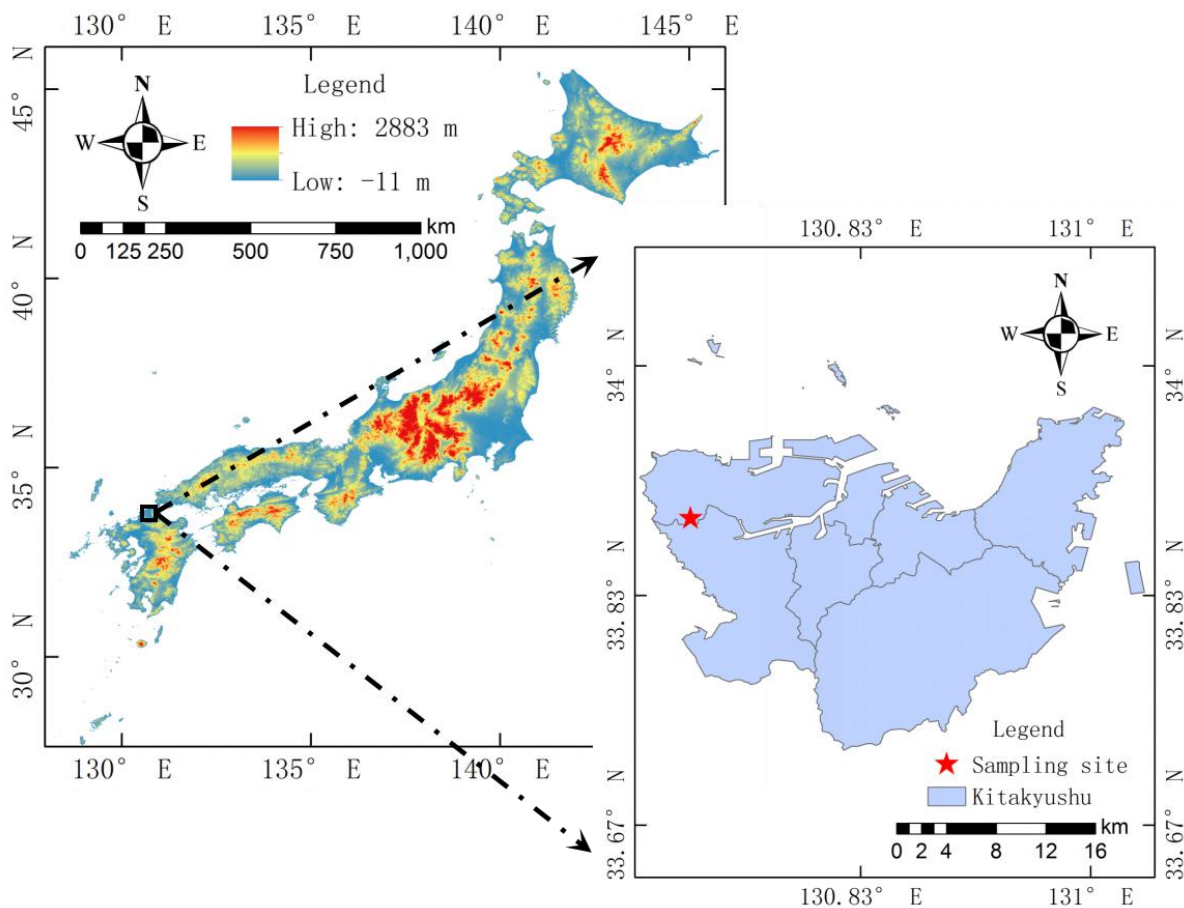
Fig. 2-1 Location of the sampling site.

2.2.1.2 Sample collection and chemical analysis

Atmospheric particles and gaseous compounds (SO_2, HNO_3, HCl, and NH_3) were simultaneously collected on a daily (noon-noon) basis by using the four-stage filter-pack method (1st to 4th stage: PTFE filter, polyamide filter, 6% K_2CO_3/2% glycerin-impregnated filter, and 5% H_3PO_4/2% glycerin-impregnated filter). After sampling, the filters were extracted using 20 mL of ultrapure water and 30 minutes of shaking at room temperature. After filtering, the extracted solutions were used to measure eight water-soluble ions (Na^+, NH_4^+, K^+, Mg^{2+}, Ca^{2+}, Cl^-, NO_3^-, and SO_4^{2-}) by ion chromatography (Thermo Scientific™ Dionex™ Integrion Thermo Fisher Scientific Inc., Waltham, MA, USA). More detailed information regarding the sampling methodology and chemical analysis is given in previous research (Aikawa et al., 2005; 2010; 2013; 2016; 2017a). In addition, the concentrations of other air pollutants (Ox, SO_2, NO_2, SPM, and $PM_{2.5}$) and meteorological data (temperature, relative

16

humidity, wind speed, and wind direction) during the corresponding period were obtained from the monitoring station (ca. 1.5 km from the sampling site) managed by the Kitakyushu City local government.

2.2.1.3 Quality assurance (QA) and quality control (QC)

To ensure the quality of the data, the pretreatment, sampling collection, and subsequent analysis were conducted entirely in accordance with strict QA and QC procedures. The sampling flow was calibrated regularly, and standard curves were constructed during each bath of analysis to retain the correlation coefficients at values greater than 0.995 for every ion. The filter blanks were measured together with samples and subtracted from the results. In addition, the quality of the aerosol components data was assessed by ion balance (R1) and conductivity balance (R2) (Fig. S1). Any sample solutions in which the R1 or R2 was not within the acceptable range were analyzed again by ion chromatography. Moreover, we also compared the gases (SO_2, HNO_3, HCl, and NH_3) collected by four-stage filter-pack method with those obtained from the nearby monitoring station or measured by another device at the same sampling site. The time variation trends of these gaseous precursors measured by different instruments agreed well (Fig. S2), with the R^2 values being larger than 0.8, further confirming the analytical accuracy of the method and data reliability.

2.2.1.4 Calculation of sea-salt and non-sea-salt species

The concentrations of sea-salt and non-sea-salt species were evaluated based on the Na^+ concentration, assuming that only sea salt contributed to Na^+ in the sample (Aikawa et al., 2016; 2017a). The original data were further classified into 16 variables, which included the sea-salt components (Na^+, ss-Cl^-, ss-SO_4^{2-}, ss-K^+, ss-Mg^{2+}, and ss-Ca^{2+}) and non-sea-salt components (nss-SO_4^{2-}, NO_3^-, NH_4^+, nss-K^+, nss-Mg^{2+}, and nss-Ca^{2+}) of the atmospheric particles and their gaseous precursors (HCl, HNO_3, NH_3, and SO_2) (The detailed composition information of seawater was shown in Table S1).

2.2.2 Statistical analysis and model calculation

2.2.2.1 Pearson's correlation analysis

The statistical calculations in this study were performed using IBM SPSS Statistics 20.0. The Pearson's correlation coefficient can be used to show the strength of the linear relationship between two variables (Jiang et al., 2019). The calculations are expressed as follows:

$$P(v_i, v_j) = \frac{Cov(v_i, v_j)}{Std(v_i) \times Std(v_j)}, \qquad (2\text{-}1)$$

where $Cov(vi, vj)$ is the covariance of two variables, and $Std(v_i)$ and $Std(v_j)$ are the standard deviations of the i_{th} and j_{th} variables, respectively.

2.2.2.2 Hierarchical cluster analysis

To identify the sources of the atmospheric particles and gaseous precursors, hierarchical cluster analysis (HCA) was performed using the squared Euclidean distance (SED) as the dissimilarity metric and Ward's distance (WD) as the linkage method. The calculations of SED and WD are expressed as follows:

$$SED(i, j) = \frac{\sum_{k=1}^{n}(X_{ik} - X_{jk})^2}{n}, \qquad (2\text{-}2)$$

$$WD(A, B) = \frac{d(a,b)^2}{n_A^{-1} + n_B^{-1}}, \qquad (2\text{-}3)$$

where X_{ik} denotes the k_{th} sample concentration that is measured for variable i, X_{jk} is the k_{th} sample concentration that is measured for variable j, a and b are the centroids of clusters A and B, respectively, and n_A and n_B are the frequencies of clusters A and B, respectively. The result was depicted in a dendrogram, which can show similarities and potential correlations among the variables. Specifically, the variables with similar properties were classified as a category, and the two categories with the

highest degree of similarity were merged to form a new category. The shorter the distances between the branches, the more significant the association (Chen et al., 2016; Mesquita et al., 2016; Zhong et al., 2016; Pietrogrande et al., 2018; Govender and Sivakumar, 2020).

2.2.2.3 Positive matrix factorization (PMF)

PMF is an effective source apportionment receptor model that does not require the source profiles prior to analysis and has no limitation on source numbers (Tan et al., 2014; Taghvaee et al., 2018; Zhong et al., 2018). In this study, PMF was utilized to quantify not only the proportions of the main pollution sources but also the daily contribution concentration of each source. The input data included the original data matrix, which consisted of the concentrations of 16 variables in each sample, and the uncertainty data matrix, which was calculated as below:

$$U_{ij} = \sqrt{(C_j \times SD)^2 + (0.05 \times X_{ij})^2} \ , \tag{2-4}$$

where U_{ij} is the data uncertainty, C_j is expressed as the uncertainty proportional coefficient of the jth variable, SD is the standard deviation of the dataset of the corresponding variable, and X_{ij} is every particular concentration value in the original data matrix (Prendes et al., 1999; Zhang et al., 2019a).

2.2.2.4 HYSPLIT model and concentration-weighted trajectory (CWT)

The air parcel backward trajectories were computed by the Hybrid Single-Particle Lagrangian Integrated Trajectory (HYSPLIT) model in TrajStat Software based on GDAS data from the National Oceanic and Atmospheric Administration (Li et al., 2017; Zong et al., 2018; Yamagami et al., 2019). In this study, 48-hour backward trajectories were generated, in which the arriving height and start hour were 1000 m and 15:00 (UTC), corresponding to 0:00 (JST (Japan Standard Time)), respectively (Fig. S3). Therefore, a total of 365 backward trajectories were obtained in this study. Adding the daily concentration data of each pollution source identified by PMF to the corresponding daily trajectories, the CWT values can be calculated as follows:

$$C_{ij} = \frac{\sum\limits_{l=1}^{M} C_l \tau_{ijl}}{\sum\limits_{l=1}^{M} \tau_{ijl}}, \tag{2-5}$$

where C_{ij} is the average weighted concentration in the ijth cell, l is the index of the trajectory, M is the total number of trajectories, C_l is the concentration observed on the arrival of trajectory l, and τ_{ijl} is the time spent in the ijth cell by trajectory l. A high value for C_{ij} implies that air parcels traveling over the ijth cell would be, on average, associated with high concentrations at the receptor.

2.2.2.5 Sulfur oxidation rate and nitrogen oxidation rate

The sulfur oxidation rate (SOR) and nitrogen oxidation rate (NOR) are often used to evaluate the degree of secondary formation from SO_2 and NO_2 to SO_4^{2-} and NO_3^- in the atmosphere (Zhou et al., 2016; Xu et al., 2017; Svedova et al., 2019). The calculations are expressed as follows:

$$SOR = \frac{n(SO_4^{2-})}{n(SO_4^{2-}) + n(SO_2)}, \tag{2-6}$$

$$NOR = \frac{n(NO_3^-)}{n(NO_3^-) + n(NO_2)}, \tag{2-7}$$

where *SOR* quantifies the degree of sulfur oxidation and is defined as the ratio of sulfate to total sulfur (sulfate plus sulfur dioxide), *NOR* quantifies the degree of nitrogen oxidation as the ratio of nitrate to total nitrogen (nitrate plus nitrogen dioxide), and n refers to the molar concentration and has a unit of $\mu mol \cdot m^{-3}$.

2.2.2.6 Multiple regression analysis

Multiple regression analysis (MRA) is a widely used method for interpreting the dependence of a response variable on several independent variables to obtain a linear input-output model for a given dataset (Tan et al., 2016; Wang et al., 2019; Yuchi et al., 2019). The MRA model can be expressed as:

$$y = \beta_0 + \beta_1 x_1 + \beta_2 x_2 + ... + \beta_p x_p, \tag{2-8}$$

where y is the concentration of secondary sulfate or secondary nitrate, $x_1, x_2,...x_p$ refer to the relevant

driving factors, β_0 is the constant value of the regression equation, and β_1, β_2,...β_p are regression coefficients.

2.2.2.7 ISORROPIA II model and E-AIM model

ISORROPIA II was used to predict the equilibrium partitioning of the atmospheric inorganic components in the gas phase, the aerosol solid phase, and the aerosol aqueous phase (Tang et al., 2016; Tan et al., 2017; Kong et al., 2018; Nakahara et al., 2019; Roig Rodelas et al., 2019; Wang et al., 2019). According to the agreement level between observed data and simulated data, the forward mode and metastable state were finally chosen in the ISORROPIA II model (Karydis et al., 2010; Sudheer and Rengarajan., 2015). In addition, the Extended Aerosol Inorganic Model (E-AIM)-III was run in open mode to estimate the aerosol pH and aerosol liquid water content (ALWC) with the input data of the concentrations of SO_4^{2-}, NO_3^-, NH_4^+, Na^+, and Cl^- in the aerosol phase and NH_3 in the gas phase (Silvern et al., 2017; Jia et al., 2018).

2.3 Results and discussion

2.3.1 Seasonal variation

During the entire sampling period, the average mass concentration of water-soluble ions (WSIs), i.e., the mean of the sum total of WSI concentrations, was 14.4 μg·m^{-3}, and SNA contributed to 68% of the WSIs, suggesting that secondary formation was the main pollution source of atmospheric particles in suburban Japan. To be specific, the mass concentrations of SO_4^{2-}, NO_3^-, and NH_4^+ were 4.9 μg·m^{-3}, 3.2 μg·m^{-3}, and 1.6 μg·m^{-3}, respectively. The SO_4^{2-} mass concentration presented a seasonal variation similar to that of suspended particulate matter (SPM; 100% cut-off diameter, 10 μm) with a decreasing order of spring > summer > autumn > winter. In contrast, the seasonal variations of the NO_3^- and NH_4^+ mass concentrations were similar to that of the PM$_{2.5}$ mass concentration, and as shown in Fig. 2-2, those contributions were greater in spring and winter and lower in summer and autumn. Pearson's

correlation analysis (Table 2-1) also indicated consistently that the correlation coefficient of SO_4^{2-} with SPM (0.45) was greater than that with $PM_{2.5}$ (0.40), whereas both NO_3^- and NH_4^+ had higher positive correlation coefficients with $PM_{2.5}$ than with SPM ($p < 0.01$). These phenomena revealed that NO_3^- and NH_4^+ were easily concentrated in fine particles, while relatively larger fractions of SO_4^{2-} could be combined with coarse particles, chiefly with the chemical form of $CaSO_4$ in the aerosol solid phase. Sulfates, such as ammonium sulfate (($NH_4)_2SO_4$) and/or ammonium hydrogen sulfate (NH_4HSO_4), are generally understood to exist in the atmosphere as fine particles (Makar et al., 2009; Yin et al., 2018). Our finding regarding the chemical form of sulfates is quite interesting, thus we will discuss these findings quantitively and in more detail in section 2.3.3.3. Combining the seasonal variations in these air pollutants with the meteorological conditions could provide us with a further indication that the winds from the northwest were dominant in spring and had relatively high speeds; hence, transboundary transports occurred easily, and air masses from the Asian landmass could carry high concentrations of air pollutants into the sampling site, causing the most severe pollution in the spring (Hayami, 2005; Khan et al., 2010; Moreno et al., 2012; Inomata et al., 2016; Aikawa et al., 2017a). In addition, three gaseous precursors (SO_2, NO_2, and NH_3) did not show good agreement with the seasonal variation of each corresponding ion in the particles in this study, which revealed that the emitted amounts of SO_2, NO_2, and NH_3 were not the only primary factors that could affect the gas-to-particle conversion process; therefore, mechanisms of secondary formation are worth in-depth investigation.
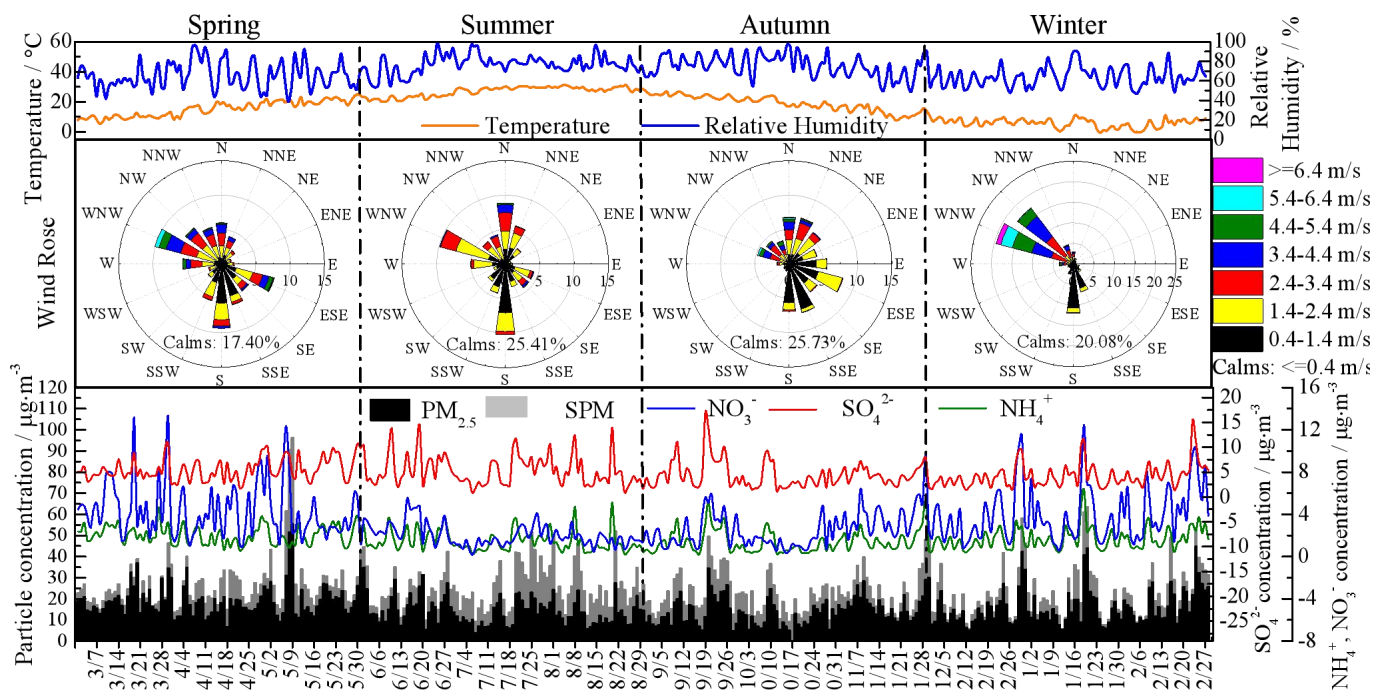
Fig. 2-2 Seasonal variation of air pollutants and meteorological conditions

Table 2-1 Pearson's correlation analysis among PM2.5, SPM, and SNA

Species	SO_4^{2-}	NO_3^-	NH_4^+
$PM_{2.5}$	0.40**	0.42**	0.38**
SPM	0.45**	0.24**	0.32**

Note: **significant level at $p < 0.01$

2.3.2 Source analysis

To better evaluate the interrelationships among particle components and gaseous precursors, hierarchical cluster analysis and Pearson's correlation analysis were combined. As shown in Fig. 2-3, the results indicated that 16 variables were classified and merged into four distinct clusters. The first cluster mainly included sea-salt components (ss-Cl$^-$, ss-SO$_4^{2-}$, Na$^+$, ss-Mg^{2+}, ss-K$^+$, and ss-Ca^{2+}), which can be explained as the influence of marine aerosols. Except for these six components, gaseous HCl was also classified into the first cluster and had the highest Pearson's correlation coefficient (0.42) with ss-Cl$^-$, indicating that most of the gaseous HCl was from a natural source, namely, the release of Cl$^-$ from marine aerosols (Aikawa et al., 2017b; 2018). The second cluster consisted of NO$_3^-$, nss-SO$_4^{2-}$, NH$_4^+$, and nss-K$^+$. Specifically, NO$_3^-$ and nss-SO$_4^{2-}$ were primarily derived from a secondary formation

process, and NH_4^+ had a strong positive correlation with nitrate (0.62) and sulfate (0.82), indicating that NH_4^+ was more easily combined with $nss-SO_4^{2-}$ as a major counter cation. The third cluster was composed of $nss-Mg^{2+}$ and $nss-Ca^{2+}$; these are the basic constituents of soil, rock, and sand and had relatively high correlation coefficients with NO_3^- (0.49 and 0.57, respectively), revealing that these two chemical components were likely from the same transport pathway as NO_3^-. In contrast to the other three clusters, Cluster 4 consisted of three gaseous components (HNO_3, NH_3, and SO_2).
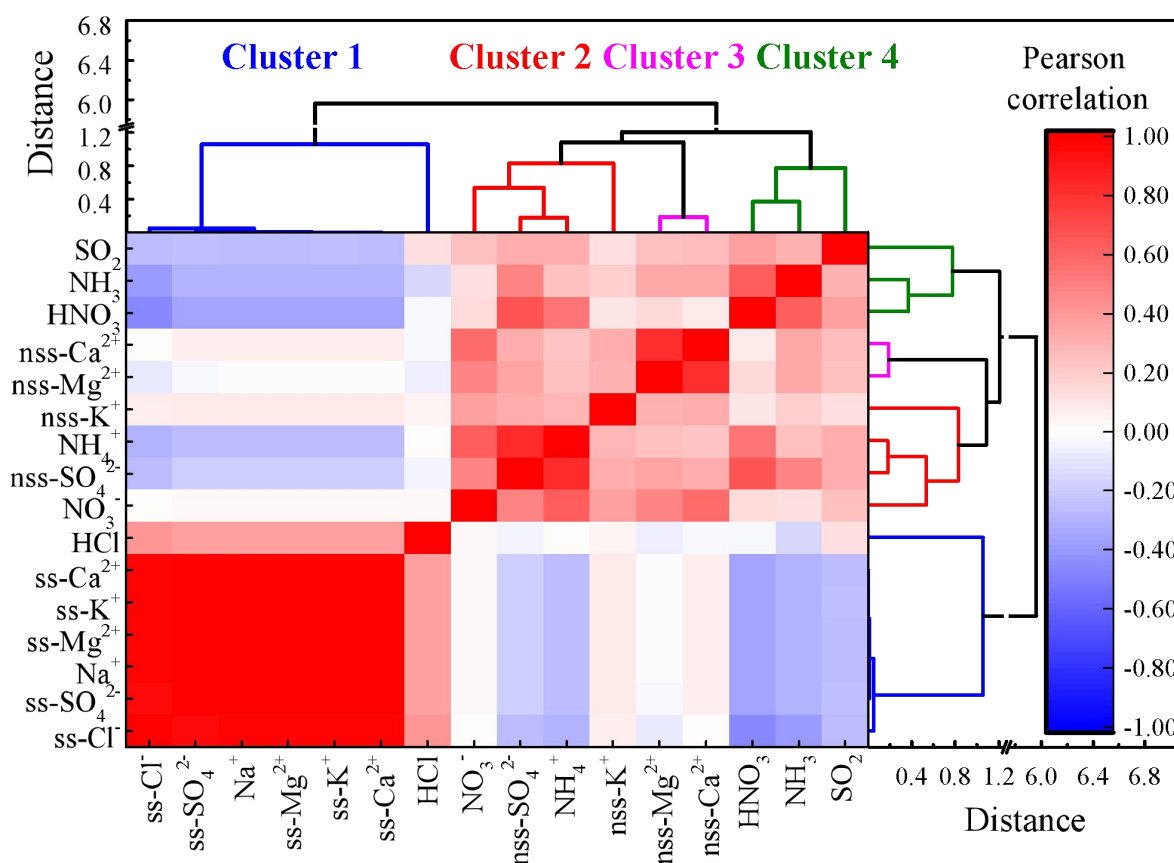
Fig. 2-3 Heatmap with Pearson's correlations between the 16 variables studied throughout the total sampling period

To further quantify the source contributions and identify potential pollution source regions, PMF and CWT analyses were performed (Figs. 2-4 and 2-5). The first source (S1) was characterized by the high loading of SO_2. Coal and oil combustion played a key role in the release of SO_2 into the atmosphere. Moreover, CWT analysis indicated that the potential pollution source regions of S1 were the industrial area around Kyushu, Japan, and some shipping routes between the Kyushu area and the Pacific Ocean (around the western edge of the enclosed sea area (the Seto Inland Sea)). Thus, this source could be

24

explained as a domestic/vicinal pollution source (industrial combustion plus ship emissions). By combining this information with wind roses for the four seasons (Fig. 2-2), it can be seen that wind from the southeast that passed through the potential pollution source regions of S1 had the highest frequency in spring, followed by autumn; hence, S1 had high contribution concentrations in spring (7.3 $\mu g \cdot m^{-3}$) and autumn (5.7 $\mu g \cdot m^{-3}$). The second source (S2) presented secondary sulfates based on high contributions of nss-SO_4^{2-} and NH_4^+. Moreover, gaseous pollutants (HNO_3 and NH_3) were enriched in this source. The origins of the secondary sulfates observed in Japan can be classified as having arrived via in-country transport and transboundary transport. Aikawa et al. (2017a) showed that secondary sulfate from the eruption of Sakurajima volcano and/or Aso volcano in the Kyushu area reached Kobe, Japan (ca. 420 km east of the current study site) by in-country transport, strongly indicating that such in-country loading was observed in this study in addition to the oxidation of SO_2 from the first source (industrial combustion and ship emissions). Meanwhile, the secondary sulfate arriving through transboundary transport originated from the coastal cities of Eastern China, as shown in Fig. 2-5. In addition, S2 had the highest contribution concentration in summer (6.7 $\mu g \cdot m^{-3}$) (Fig. 2-4), which can be attributed to the combination of local SO_2 emissions and more active oxidation to SO_4^{2-} due to the high relative humidity, high temperature, and low wind speed (weak horizontal transport) (shown in Fig. 2-2). The third source (S3) was a mixed source, including secondary nitrates and biomass burning. The potential pollution source region of S3 was northwest of the sampling site, namely, Mongolia and Northern China. The dominant wind directions in spring and winter were mainly from the WNW (west-northwest) and NW (northwest), passing through the potential pollution source regions of S3; thus, this source had the highest contribution in spring and winter (6.3 $\mu g \cdot m^{-3}$), and low influence in summer (2.8 $\mu g \cdot m^{-3}$) and autumn (3.7 $\mu g \cdot m^{-3}$) (Fig. 2-4). The fourth source (S4) was closely associated with sea-salt components (Na^+, ss-Cl^-, ss-SO_4^{2-}, ss-K^+, ss-Mg^{2+}, and ss-Ca^{2+}) and could be interpreted as

marine aerosols. Moreover, the concentration of marine aerosols in autumn (5.9 μg·m^{-3}) was obviously higher than those in the other three seasons. From Fig. 2-2, in autumn, the air masses from the northeast, which passed through the Sea of Japan, and the southeast, which passed through the Pacific Ocean, had the highest frequencies, while the wind speed from the northeast was higher than that from the southeast. Hence, the air masses from the Sea of Japan would be able to carry more marine aerosols to the sampling site, consistent with our CWT results, namely, that the Sea of Japan was the main potential pollution source region of S4 (Fig. 2-5). In particular, on October 22 and 23, under the influence of a typhoon in Japan, the transport pathways of air masses passed through the Sea of Japan, and the wind speeds were high, with maximum momentary wind velocities reaching 19.7 m/s and 16.3 m/s, respectively; thus, marine aerosols became the largest pollution source on these two days, and the concentrations of Na$^+$ and Cl$^-$ in the atmospheric particles accounted for more than 80% of the total water-soluble ions. The last source (S5) was dust (soil dust and desert dust) with typical crustal components, such as nss-Ca^{2+} and nss-Mg^{2+}, and had the same potential pollution source regions as the secondary nitrates (northwest of the sampling site), as shown in Fig. 2-5. The air masses in spring carried the highest concentrations of desert dust from the Asian landmass to the sampling site through a long-distance atmospheric transportation process, which caused severe particle pollution, especially on May 7 and 8. Nitrate was presumably associated with an interaction between dust and anthropogenic air pollution during the transportation process (Li et al., 2012; Klingmüller et al., 2019). Overall, five main sources (S1–S5) were identified in this suburban area of Japan: industrial combustion plus ship emissions, secondary sulfates, secondary nitrates plus biomass burning, marine aerosols, and dust, with average contributions of 26%, 23%, 22%, 19%, and 10%, respectively. Comparing the key variables of the four clusters (Fig. 2-4), we concluded that PMF and HCA produced consistent results, with S1, S4, and S5 corresponding to Cluster 4, Cluster 1, and Cluster 3, respectively. Cluster 2 (secondary aerosols

and biomass burning) was further divided into secondary sulfates (S2) and secondary nitrates plus biomass burning (S3) by PMF.
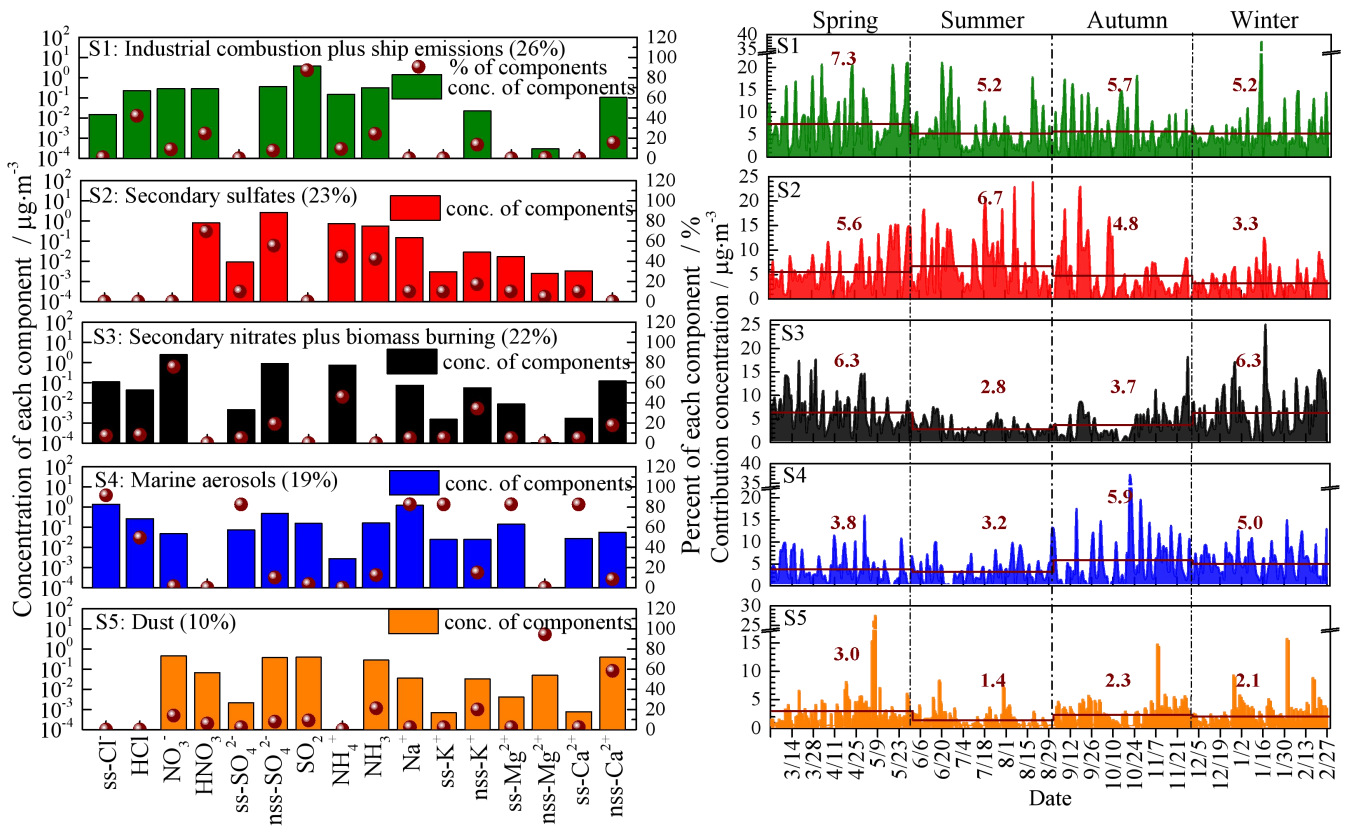
Fig. 2-4 The five source profiles (left) and daily contribution concentrations of each identified source and average values for the four seasons (right)
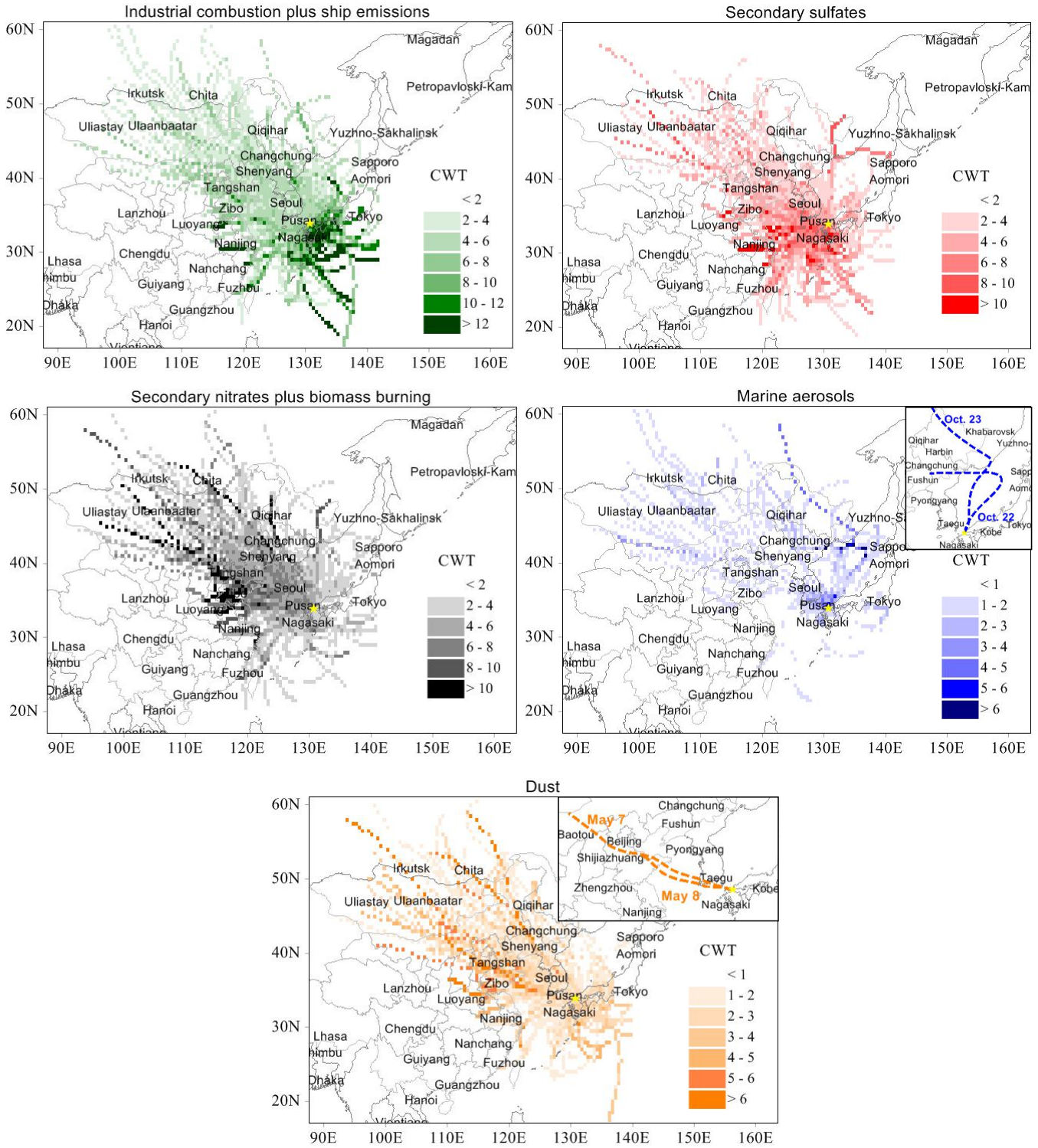
Fig. 2-5 CWT maps of the five sources and transport pathways of air masses in the extreme events (Oct. 22-23 and May 7-8)

by TrajStat software

2.3.3 Secondary formation process

2.3.3.1 SOR and NOR

SOR and NOR are direct parameters for evaluating oxidation and secondary formation events in the

atmosphere. In this study, the SOR and NOR values were larger than those in previous research (Zhou et al., 2016; Xu et al., 2017; Svedova et al., 2019), suggesting that secondary formation is the most significant cause of particle pollution at the sampling site. SOR had the highest value in summer (0.58), followed by autumn (0.50), spring (0.48), and winter (0.42), while NOR did not present any obvious seasonal variations, with values of approximately 0.14. In fact, Eq. (2-6) and Eq. (2-7), which were routinely adopted in previous studies, offered disadvantages for evaluating SOR and NOR. First, the influence of marine aerosols could not be overlooked, especially at our sampling site; thus, the presence of ss-SO_4^{2-} in Eq. (2-6) ($n(SO_4^{2-})$) may cause the overestimation of SOR. For Eq. (2-7), previous research did not take HNO_3 into consideration because HNO_3 determination is generally difficult; however, HNO_3 was also transformed from NO_2, which may cause the underestimation of NOR. In this study, HNO_3 data could be obtained by adopting the four-stage filter-pack method; hence, to evaluate SOR and NOR more accurately, the original calculations were modified as follows:

$$Modified \;\; SOR = \frac{n(nss-SO_4^{2-})}{n(nss-SO_4^{2-})+n(SO_2)}, \tag{2-9}$$

$$Modified \;\; NOR = \frac{n(NO_3^-)+n(HNO_3)}{n(NO_3^-)+n(HNO_3)+n(NO_2)}, \tag{2-10}$$

As expected, the modified SOR was lower than the original SOR; however, the difference was small, and the modified SOR presented a similar seasonal variation with the decreasing order of summer (0.58) > autumn (0.49) > spring (0.47) > winter (0.41). Moreover, the modified SOR was distributed in nearly the same manner as that of the original SOR under the influence of RH and T, as illustrated in Fig. 2-6a and c. The SOR basically increased with the simultaneous growth of the relative humidity and temperature, and the highest value of SOR appeared at a relative humidity that was higher than 70% and a temperature greater than 16°C. For NOR, the modified NOR showed an obvious seasonal variation, with the highest value in summer (0.22), followed by spring (0.19), winter (0.17), and autumn (0.15).

This result was different from the variation of the original NOR, further confirming a clear and significant underestimation of the nitrogen oxidation rate, based on Eq. (2-7), especially at a relative humidity lower than 60% and temperature greater than 16 °C (Fig. 2-6b and d). This phenomenon may be related to gas-particle partitioning among NH_3, HNO_3, and NH_4NO_3; a higher temperature and lower relative humidity generally favor partitioning into the gas phase (Watson, et al., 1994; Schiferl, et al., 2016), ultimately leading to a significant increase of the HNO_3 concentration.
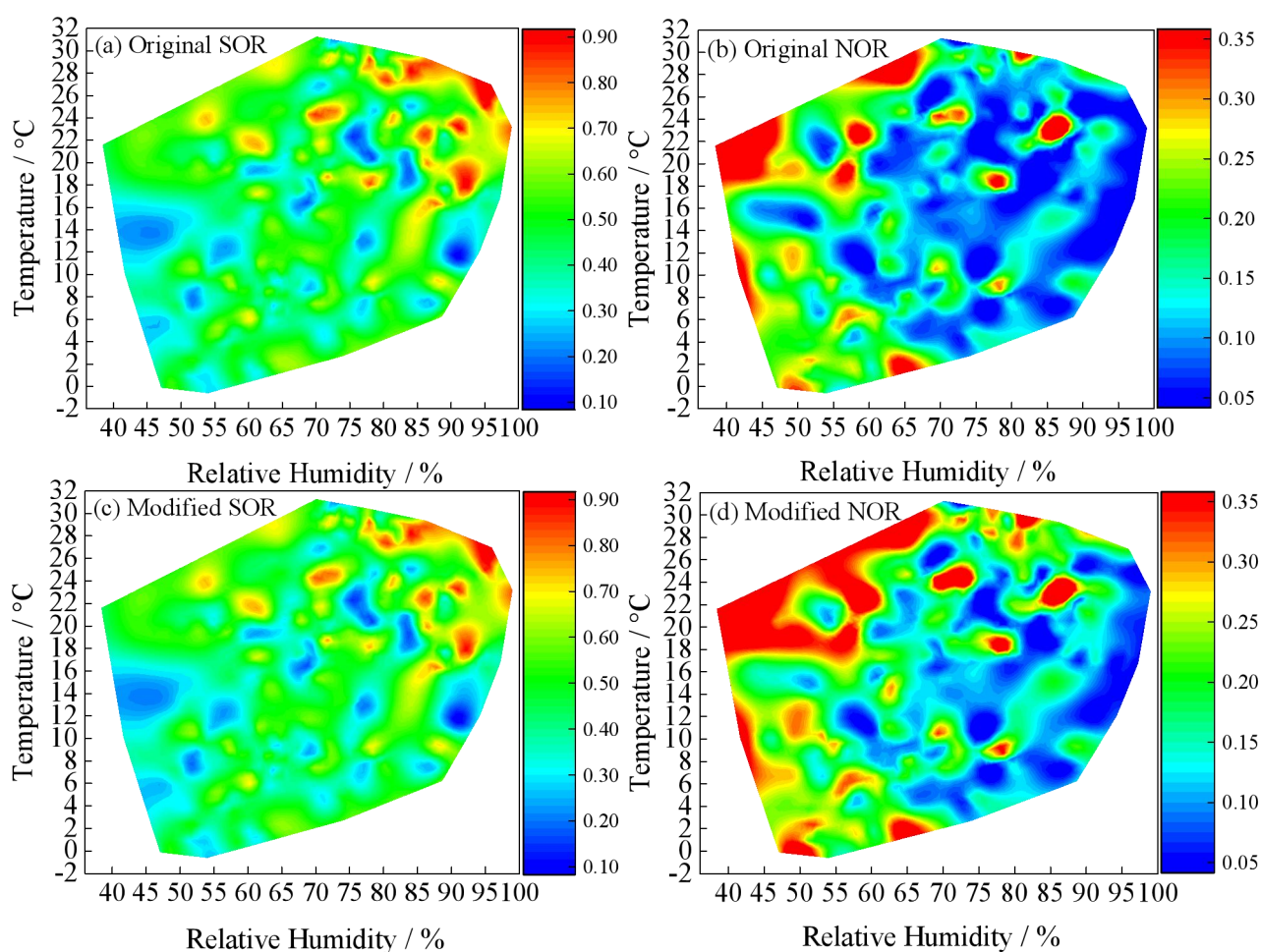
Fig. 2-6 Impacts of temperature and relative humidity on SOR and NOR. The color scale in the legend represents the values of SOR and NOR.

2.3.3.2 Factors of influence

Under complex and variable atmospheric conditions, multiphase chemical reactions are frequently applied between atmospheric particles and gaseous precursors. The formation of secondary aerosols is

significantly influenced by many factors, such as the concentrations of photochemical oxidants and gaseous precursors, ambient temperature, relative humidity, etc. (Biswas et al., 2008; Wen et al., 2015; Jiang et al., 2019; Wang et al., 2019). To investigate the comprehensive impacts of these factors of influence on secondary aerosols, multiple regression analysis was performed by SPSS (Table 2-2), and the functions among the secondary aerosol concentration and factors of influence can be described as follows:

$$[SS] = -9.70 O_x + 0.09 SO_2 - 0.02 NO_2 + 0.15 NH_3 + 3.34 HNO_3 - 1.57 HCl + 0.03T + 0.03RH \quad (R^2 = 0.81, P < 0.01), \quad (2\text{-}11)$$

$$[SN] = 52.77 O_x - 0.08 SO_2 + 0.06 NO_2 + 1.02 NH_3 - 0.26 HNO_3 + 2.44 HCl - 0.24T + 0.04RH \quad (R^2 = 0.72, P < 0.01). \quad (2\text{-}12)$$

where [SS] and [SN] are, respectively, the contributed concentrations ($\mu g \cdot m^{-3}$) of the secondary sulfate and secondary nitrate provided by PMF. The third source estimated by the PMF model was, in fact, a mixed source, including secondary nitrate and biomass burning; however, the influence of biomass burning was ignored in this analysis because of the far lower concentration of nss-K^+ compared with NO_3^- and NH_4^+ (Fig. 2-4). The relationships between the secondary aerosols and eight factors of influence were linear, with high R^2 values. Except for two parameters (NH_3 and RH), the opposite signs in the regression coefficients for the influencing factors in Eqs. (2-11) and (2-12) revealed that the inner formation mechanisms of secondary sulfates and secondary nitrates were distinct. Considering the significant level of each factor of influence (Table 2-2), only three factors of influence would be important driving factors for secondary sulfates. Specifically, HNO_3 and RH presented positive relations, while HCl showed a negative relation with the formation of secondary sulfate (p < 0.01). HNO_3 could accelerate the formation rates of sulfuric acid-ammonia clusters, acting as a "bridge" connecting the smaller and larger clusters (Liu et al., 2018). A high relative humidity could cause a significant size shift in the atmospheric particles and the promotion of aerosol hygroscopic growth, further enhancing secondary formation (Tan et al., 2017; Tian et al., 2018; Wu et al., 2018), while the negative relation of

HCl to secondary sulfate formation was closely related to the aging reactions of marine aerosols. The long-range transport of anthropogenic pollutants (SO_2, NOx, organics, etc.) and their interactions with sea-salt particles often suppress the hygroscopic growth of marine aerosols, which is unfavorable for the secondary formation process (Boreddy and Kawamura, 2016). In addition, SO_2, as an important precursor, was not significantly related to secondary sulfate, which is due to the low oxidation rate of SO_2 to SO_4^{2-}. The formation mechanism of secondary nitrate was different and significantly more complicated compared with that of secondary sulfate. The factors of influence, except SO_2 and HNO_3, significantly impacted the formation of secondary nitrate. Ox, NO_2, NH_3, HCl, and RH had positive relations, while only T had a negative relation ($p < 0.01$), revealing that the secondary nitrate produced via the heterogeneous reaction of N_2O_5 might be significant in this suburban area of Japan. To be specific, NO_2 was first oxidized by O_3, being the main components of Ox (Xu et al., 2018), to form N_2O_5 (Wen et al., 2015; Ge et al., 2017), after which time the heterogeneous hydrolysis of N_2O_5 easily occurred under the low temperature and high relative humidity (Ge et al., 2017). Then the neutralization process of NH_3 and the aging process of marine aerosols (chloride depletion in sea-salt particles) further enhanced the accumulation of NH_4NO_3 and $NaNO_3$ in the aerosol phase (Wen et al., 2015; Li et al., 2016; Ge et al., 2017). In addition, NH_4NO_3 was unstable, causing equilibrium shifts to gaseous HNO_3 and NH_3 under a high temperature and low relative humidity (Wen et al., 2015).

Table 2-2 Multiple regression results for equations (2-11) and (2-12)

Model 1		Unstandardized Coefficients		Standardized Coefficients	t	Sig.
Response variable	Independent factors	β	Std. Error	Beta		
SS[a]/$\mu g \cdot m^{-3}$	Ox[c]/ppm	-9.70	12.07	-0.06	-0.80	0.42
	SO$_2$/$\mu g \cdot m^{-3}$	0.09	0.06	0.08	1.53	0.13
	NO$_2$/$\mu g \cdot m^{-3}$	-0.02	0.02	-0.06	-0.91	0.36
	NH$_3$/$\mu g \cdot m^{-3}$	0.15	0.29	0.04	0.52	0.60
	HNO$_3$/$\mu g \cdot m^{-3}$	3.34	0.20	0.80	16.71	0.00
	HCl/$\mu g \cdot m^{-3}$	-1.57	0.47	-0.22	-3.36	0.00
	T/°C	0.03	0.03	0.09	1.05	0.29
	RH/%	0.03	0.01	0.35	3.13	0.00
SN[b]/$\mu g \cdot m^{-3}$	Ox[c]/ppm	52.77	13.29	0.36	3.97	0.00
	SO$_2$/$\mu g \cdot m^{-3}$	-0.08	0.06	-0.09	-1.35	0.18
	NO$_2$/$\mu g \cdot m^{-3}$	0.06	0.02	0.26	2.98	0.00
	NH$_3$/$\mu g \cdot m^{-3}$	1.02	0.32	0.28	3.21	0.00
	HNO$_3$/$\mu g \cdot m^{-3}$	-0.26	0.22	-0.07	-1.20	0.23
	HCl/$\mu g \cdot m^{-3}$	2.44	0.51	0.37	4.75	0.00
	T/°C	-0.24	0.03	-0.76	-7.31	0.00
	RH/%	0.04	0.01	0.44	3.22	0.00

Note SS[a]: Secondary sulfate; SN[b]: Secondary nitrate; Ox[c]: photochemical oxidants which mainly include ozone and peroxyacetyl nitrate (Xu et al., 2018); The t-value and corresponding p-value are denoted as the "t" and "Sig."

2.3.3.3 Thermodynamic equilibrium model calculation

Gas-particle partitioning significantly influences secondary aerosols and is effectively governed by equilibrium thermodynamics, gas-particle mass transfer kinetics, and heterogeneous chemical reactions (Nakahara et al., 2019). In this study, ISORROPIA II was mainly used to predict the concentrations of existing species in the gas phase, aerosol solid phase, and aerosol aqueous phase at chemical equilibrium with the comprehensive observation data provided by the four-stage filter-pack method.

Few to no studies have predicted the concentrations of chemical forms based on the comprehensive observation of aerosols and their gaseous precursors. As shown in Fig. 2-7, ALWC derived from ISORROPIA II and E-AIM-III agreed well with the R^2 value of 0.97 and the slope of 1.00, revealing that the simulation results of ISORROPIA II/E-AIM-III reliably reinforced each other. The results of gas-particle partitioning (Fig. 2-7) showed that the gaseous NH_3, HCl, and HNO_3 concentrations in this suburban area of Japan were 1.8, 1.1, and 1.1 $\mu g \cdot m^{-3}$, respectively, with the R^2 values between the simulated and observed concentrations of these gases at higher than 0.78. In addition, the total atmospheric particle mass concentration, namely, the total concentration of all components in both the aerosol solid phase and the aerosol aqueous phase, was 32.7 $\mu g \cdot m^{-3}$. In comparison with our observation, the aerosol solid phase only contributed 7% of the total particle mass concentration, being attributed to $CaSO_4$. Furthermore, the aerosol aqueous phase accounted for the largest proportion (93%), and ALWC, as an efficient medium for secondary formation (Wu et al., 2018), had the highest contribution concentration (19.2 $\mu g \cdot m^{-3}$), followed by NO_3^- (3.2 $\mu g \cdot m^{-3}$) and SO_4^{2-} (3.1 $\mu g \cdot m^{-3}$), comprising 59%, 10%, and 9% of the total particle mass concentration, respectively. Moreover, in the aerosol aqueous phase, the molar ratio of ammonia to sulfate ($n(NH_4^+)/n(SO_4^{2-})$), where $n(X)$ is the molar concentration of component (X), was 2.69, and the concentration of HSO_4^- was extremely low, ranging from 0 to 0.1 $\mu g \cdot m^{-3}$ (Fig. 2-7), indicating that aqueous sulfate could be completely neutralized by ammonium with the main chemical form of $(NH_4)_2SO_4$. The particle neutralization ratio ($PNR=n(NH_4^+)/(2n(SO_4^{2-})+n(NO_3^-))$) (0.62) was less than 1, and the aerosol pH determined by E-AIM-III model was approximately 3.3, which revealed that the ammonium could not fully neutralize the nitrate, thus the aerosols were acidic in this suburban area of Japan (Makar et al., 2009; Yin et al., 2018). Moreover, the multiple regression results confirmed that NH_3 had a positive relation with the secondary inorganic aerosols, especially secondary nitrate (Table 2-2); hence, the reductions in NH_3

may result in significant reductions in particulate mass.
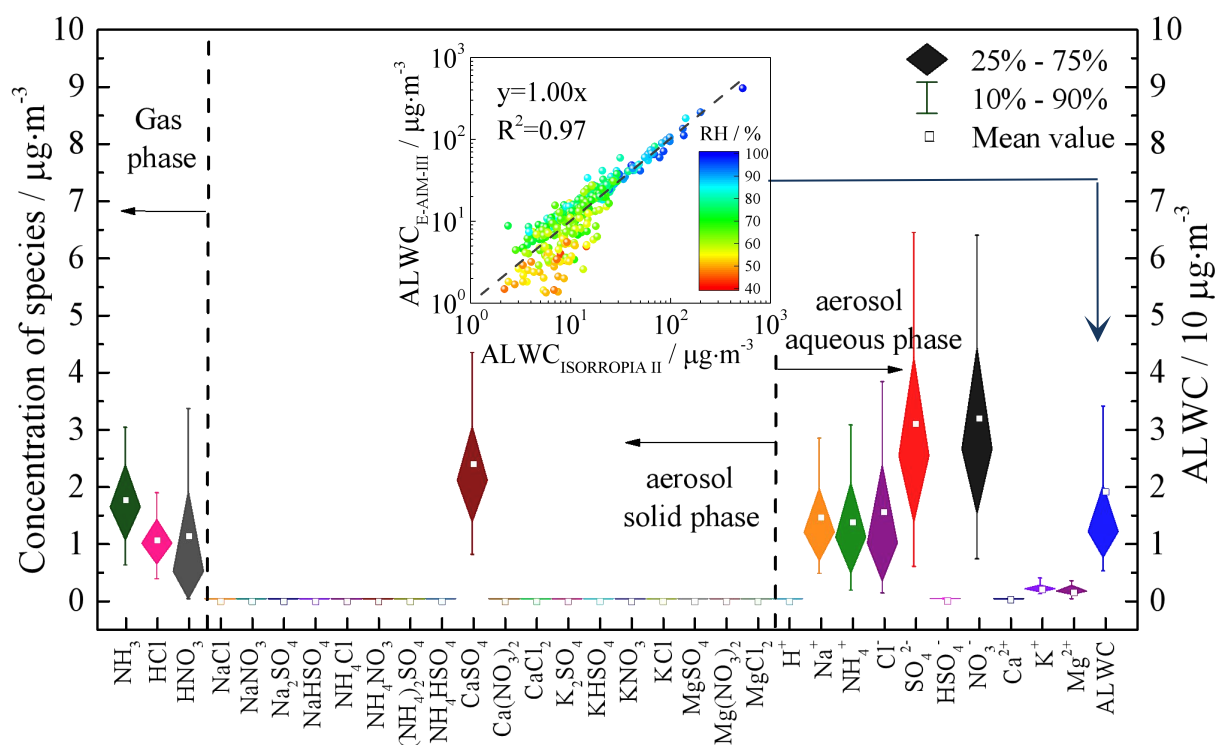
Fig. 2-7 Simulation quality (Top) and chemical forms of aerosol components identified by the ISORROPIA II model

2.4 Conclusions

The simultaneous assessment of source apportionment and secondary formation processes was comprehensively studied in a suburban area located on the western edge of Japan by combining year-round daily observation using a filter-pack method with model calculations. Secondary formation was the most important pollution source, accounting for ca. 45% (23% (secondary sulfates) + 22% (secondary nitrates)) of the sources of total atmospheric aerosol mass. For the secondary aerosol composition at this suburban site in western Japan, the secondary sulfates were mainly derived from volcanic eruptions (Sakurajima volcano and/or Aso volcano), the oxidation of SO_2 from industrial combustion, ship emissions in the Kyushu area, and long-distance transportation from several coastal cities in Eastern China. Multiple regression results further revealed that the secondary sulfate formation process was significantly influenced by and related to HNO_3, HCl, and the relative humidity (RH) ($p <$ 0.01). While the potential pollution source region of secondary nitrates was located in the northwest

region of the sampling site, where air masses pass through Mongolia and Northern China, the formation mechanism of secondary nitrates was more complicated, with the important driving factors being Ox, NO_2, NH_3, HCl, temperature (T), and RH. In addition, if the presence of atmospheric HNO_3 was ignored, the nitrogen oxidation rate (NOR) would be significantly underestimated, especially at relative humidity levels less than 60% and temperatures greater than 16°C. The results of this study clearly demonstrate the source contribution and characteristics of secondary aerosols in the suburban area of western Japan and can be adopted as the important basis to mitigate particle pollution.

References

Aikawa, M., Hiraki, T., Tamaki, M., 2005. Characteristics in Concentration of Chemical Species in Ambient Air Based on Three-Year Monitoring by Filter Pack Method, Water Air & Soil Pollution, 161, 335-352.

Aikawa, M., Ohara, T., Hiraki, T., Oishi, O., Tsuji, A., Yamagami, M., Murano, K., and Mukai, H., 2010. Significant geographic gradients in particulate sulfate over Japan determined from multiple-site measurements and a chemical transport model: Impacts of transboundary pollution from the Asian continent, Atmospheric Environment, 44, 381-391.

Aikawa, M., Hiraki, T., Tomoyose, N., Ohizumi, T., Noguchi, I., Murano, K., and Mukai, H., 2013. Local emission of primary air pollutants and its contribution to wet deposition and concentrations of aerosols and gases in ambient air in Japan, Atmospheric Environment, 79, 317-323.

Aikawa, M., Morino, Y., Kajino, M., Hiraki, T., Horie, Y., Nakatsubo, R., Matsumura, C., and Mukai, H., 2016. Candidates to Provide a Specific Concentration Difference for Ambient Sulfur and Nitrogen Compounds Near the Coastal and Roadside Sites of Japan, Water, Air, & Soil Pollution, 227.

Aikawa, M., Hiraki, T., Horie, Y., Nakatsubo, R., Matsumura, C., and Mukai, H., 2017a. Trans-boundary and in-country transport of air pollutants observed in Kobe, Japan by high frequent filter pack sampling method, Journal of Atmospheric Chemistry, 74, 505-518.

Aikawa, M., Hirokawa, K., and Murakami, T., 2017b. Daily observation of gas/aerosol by FP method in western part of Japan, Proceedings of the 58th Annual Meeting of the Japan Society for Atmospheric Environment, Hyogo, Japan, 6–8 September 2017, 454.

Aikawa, M., Suzuki, M., Murakami, T., and Hirokawa, K., 2018. Daily observation of gas/aerosol by FP method in western part of Japan (2), Proceedings of the 59th Annual Meeting of the Japan Society for Atmospheric Environment, Fukuoka, Japan, 12–14 September 2018, 245.

Bigi, A., Bianchi, F., De Gennaro, G., Di Gilio, A., Fermo, P., Ghermandi, G., Prévôt, A. S. H., Urbani, M., Valli, G., Vecchi, R., and Piazzalunga, A., 2017. Hourly composition of gas and particle phase pollutants at a central urban background site in Milan, Italy, Atmospheric Research, 186, 83-94.

Biswas, K. F., Ghauri, B. M., and Husain, L., 2008. Gaseous and aerosol pollutants during fog and clear episodes in South Asian urban atmosphere, Atmospheric Environment, 42, 7775-7785.

Chen, H. W., Chen, W. Y., Chang, C. N., Chuang, Y. H., and Lin, Y. H., 2016. Identifying airborne metal particles sources near an optoelectronic and semiconductor industrial park, Atmospheric Research, 174-175, 97-105.

Boreddy, S. K., and Kawamura, K., 2016. Hygroscopic growth of water-soluble matter extracted from remote marine aerosols over the western North Pacific: Influence of pollutants transported from East Asia, The Science of the total environment, 557-558, 285-295.

Deshmukh, D., Deb, M., Tsai, Y. I., and Mkoma, S. L., 2011. Water Soluble Ions in $PM_{2.5}$ and PM_1 Aerosols in Durg City, Chhattisgarh, India, Aerosol and Air Quality Research, 11, 696-708.

Fu, X., Guo, H., Wang, X., Ding, X., He, Q., Liu, T., and Zhang, Z., 2015. $PM_{2.5}$ acidity at a background site in the Pearl River Delta region in fall-winter of 2007-2012, Journal of hazardous materials, 286, 484-492.

Ge, X., He, Y., Sun, Y., Xu, J., Wang, J., Shen, Y., and Chen, M., 2017. Characteristics and Formation Mechanisms of Fine Particulate Nitrate in Typical Urban Areas in China, Atmosphere, 8, 62.

Govender, P., and Sivakumar, V., 2020. Application of k-means and hierarchical clustering techniques for analysis of air pollution: A review (1980–2019), Atmospheric Pollution Research, 11, 40-56.

Hama, S. M. L., Cordell, R. L., and Monks, P. S., 2017. Quantifying primary and secondary source contributions to ultrafine particles in the UK urban background, Atmospheric Environment, 166, 62-78.

Hayami, H., 2005. Behavior of secondary inorganic species in gaseous and aerosol phases measured in Fukue Island, Japan, in dust season, Atmospheric Environment, 39, 2243-2248.

Hong, Y. M., Lee, B. K., Park, K. J., Kang, M. H., Jung, Y. R., Lee, D. S., and Kim, M. G., 2002. Atmospheric nitrogen and sulfur containing compounds for three sites of South Korea, Atmospheric Environment, 36, 3485-3494.

Inomata, Y., Ohizumi, T., Take, N., Sato, K., and Nishikawa, M., 2016. Transboundary transport of anthropogenic sulfur in $PM_{2.5}$ at a coastal site in the Sea of Japan as studied by sulfur isotopic ratio measurement, The Science of the total environment, 553, 617-625.

Jia, S., Sarkar, S., Zhang, Q., Wang, X., Wu, L., Chen, W., Huang, M., Zhou, S., Zhang, J., Yuan, L., and Yang, L., 2018. Characterization of diurnal variations of $PM_{2.5}$ acidity using an open thermodynamic system: A case study of Guangzhou, China, Chemosphere, 202, 677-685.

Jiang, F., Liu, F., Lin, Q., Fu, Y., Yang, Y., Peng, L., Lian, X., Zhang, G., Bi, X., Wang, X., and Sheng, G., 2019. Characteristics and Formation Mechanisms of Sulfate and Nitrate in Size-segregated

Atmospheric Particles from Urban Guangzhou, China, Aerosol and Air Quality Research, 19, 1284-1293.

Kaneyasu, N., Yamamoto, S., Sato, K., Takami, A., Hayashi, M., Hara, K., Kawamoto, K., Okuda, T., and Hatakeyama, S., 2014. Impact of long-range transport of aerosols on the PM$_{2.5}$ composition at a major metropolitan area in the northern Kyushu area of Japan, Atmospheric Environment, 97, 416-425.

Kanniah, K. D., Kaskaoutis, D. G., San Lim, H., Latif, M. T., Kamarul Zaman, N. A. F., and Liew, J., 2016. Overview of atmospheric aerosol studies in Malaysia: Known and unknown, Atmospheric Research, 182, 302-318.

Karydis, V. A., Tsimpidi, A. P., Fountoukis, C., Nenes, A., Zavala, M., Lei, W., Molina, L. T., and Pandis, S. N., 2010. Simulating the fine and coarse inorganic particulate matter concentrations in a polluted megacity, Atmospheric Environment, 44, 608-620.

Khan, M. F., Hirano, K., and Masunaga, S., 2010. Quantifying the sources of hazardous elements of suspended particulate matter aerosol collected in Yokohama, Japan, Atmospheric Environment, 44, 2646-2657.

Kim, H., and Zhang, Q., 2019. Chemistry of new particle growth during springtime in the Seoul metropolitan area, Korea, Chemosphere, 225, 713-722.

Kitamori, Y., Mochida, M., and Kawamura, K., 2009. Assessment of the aerosol water content in urban atmospheric particles by the hygroscopic growth measurements in Sapporo, Japan, Atmospheric Environment, 43, 3416-3423.

Klingmüller, K., Lelieveld, J., Karydis, V. A., and Stenchikov, G. L., 2019. Direct radiative effect of dust–pollution interactions, Atmospheric Chemistry and Physics, 19, 7397-7408.

Kong, L., Du, C., Zhanzakova, A., Cheng, T., Yang, X., Wang, L., Fu, H., Chen, J., and Zhang, S., 2018. Trends in heterogeneous aqueous reaction in continuous haze episodes in suburban Shanghai: An in-depth case study, The Science of the total environment, 634, 1192-1204.

Li, J., Wang, Z., Zhuang, G., Luo, G., Sun, Y., and Wang, Q., 2012. Mixing of Asian mineral dust with anthropogenic pollutants over East Asia: a model case study of a super-duststorm in March 2010, Atmospheric Chemistry and Physics, 12, 7591-7607.

Li, T. C., Yuan, C. S., Hung, C. H., Lin, H. Y., Huang, H. C., and Lee, C. L., 2016. Chemical Characteristics of Marine Fine Aerosols over Sea and at Offshore Islands during Three Cruise Sampling Campaigns in the Taiwan Strait-Sea Salts and Anthropogenic Particles, Atmospheric Chemistry and Physics, 1-27.

Li, D., Liu, J., Zhang, J., Gui, H., Peng, D., Yu, T., Wang, J., Lu, Y., and Cheng, Y., 2017. Identification of long-range transport pathways and potential sources of $PM_{2.5}$ and PM_{10} in Beijing from 2014 to 2015, Journal of environmental sciences, 56, 214.

Liu, L., Li, H., Zhang, H., Zhong, J., Bai, Y., Ge, M., Li, Z. S., Chen, Y., and Zhang, X., 2018. The role of nitric acid in atmospheric new particle formation, Physical Chemistry Chemical Physics, 20, 17406-17414.

Makar, P. A., Moran, M. D., Zheng, Q., Cousineau, S., Sassi, M., Duhamel, A., Besner, M., Davignon, D., Crevier, L. P., and Bouchet, V. S., 2009. Modelling the impacts of ammonia emissions reductions on North American air quality, Atmos. Chem. Phys., 9, 7183-7212.

McMurry, P. H., and Wilson, J. C., 1983. Droplet phase (Heterogeneous) and gas phase (homogeneous) contributions to secondary ambient aerosol formation as functions of relative humidity, Journal of Geophysical Research: Oceans, 88, 5101-5108.

Mesquita, S. R., Dachs, J., van Drooge, B. L., Castro-Jimenez, J., Navarro-Martin, L., Barata, C., Vieira, N., Guimaraes, L., and Pina, B., 2016. Toxicity assessment of atmospheric particulate matter in the Mediterranean and Black Seas open waters, The Science of the total environment, 545-546, 163-170.

Moreno, T., Kojima, T., Querol, X., Alastuey, A., Amato, F., and Gibbons, W., 2012. Natural versus anthropogenic inhalable aerosol chemistry of transboundary East Asian atmospheric outflows into western Japan, The Science of the total environment, 424, 182-192.

Nakahara, A., Takagi, K., Sorimachi, A., Katata, G., and Matsuda, K., 2019. Enhancement of dry deposition of $PM_{2.5}$ nitrate in a cool-temperate forest, Atmospheric Environment, 212, 136-141.

Ng, C. F. S., Hashizume, M., Obase, Y., Doi, M., Tamura, K., Tomari, S., Kawano, T., Fukushima, C., Matsuse, H., Chung, Y., Kim, Y., Kunimitsu, K., Kohno, S., and Mukae, H., 2019. Associations of chemical composition and sources of $PM_{2.5}$ with lung function of severe asthmatic adults in a low air pollution environment of urban Nagasaki, Japan, Environmental pollution, 252, 599-606.

Pietrogrande, M. C., Dalpiaz, C., Dell'Anna, R., Lazzeri, P., Manarini, F., Visentin, M., and Tonidandel, G., 2018. Chemical composition and oxidative potential of atmospheric coarse particles at an industrial and urban background site in the alpine region of northern Italy, Atmospheric Environment, 191, 340-350.

Prendes, P., Andrade, J. M., Lopez-Mahia, P., and Prada, D., 1999. Source apportionment of inorganic ions in airborne urban particles from Coruna city (NW of Spain) using positive matrix factorization, Talanta, 49, 165-178.

Roig Rodelas, R., Perdrix, E., Herbin, B., and Riffault, V., 2019. Characterization and variability of inorganic aerosols and their gaseous precursors at a suburban site in northern France over one year (2015–2016), Atmospheric Environment, 200, 142-157.

Schiferl, L. D., Heald, C. L., Van Damme, M., Clarisse, L., Clerbaux, C., Coheur, P.F., Nowak, J. B., Neuman, J. A., Herndon, S. C., Roscioli, J. R., and Eilerman, S. J., 2016. Interannual variability of ammonia concentrations over the United States: sources and implications, Atmospheric Chemistry and Physics, 16, 12305-12328.

Silvern, R. F., Jacob, D. J., Kim, P. S., Marais, E. A., Turner, J. R., Campuzano-Jost, P., and Jimenez, J. L., 2017. Inconsistency of ammonium–sulfate aerosol ratios with thermodynamic models in the eastern US: a possible role of organic aerosol, Atmospheric Chemistry and Physics, 17, 5107-5118.

Sudheer, A. K., and Rengarajan, R., 2015. Time-resolved inorganic chemical composition of fine aerosol and associated precursor gases over an urban environment in western India: Gas-aerosol equilibrium characteristics, Atmospheric Environment, 109, 217-227.

Švédová, B., Kucbel, M., Raclavská, H., Růžičková, J., Raclavský, K., and Sassmanová, V., 2019. Water-soluble ions in dust particles depending on meteorological conditions in urban environment, Journal of environmental management, 237, 322-331.

Taghvaee, S., Sowlat, M. H., Mousavi, A., Hassanvand, M. S., Yunesian, M., Naddafi, K., and Sioutas, C., 2018. Source apportionment of ambient $PM_{2.5}$ in two locations in central Tehran using the Positive Matrix Factorization (PMF) model, The Science of the total environment, 628-629, 672-686.

Takahashi, H., Naoe, H., Igarashi, Y., Inomata, Y., and Sugimoto, N., 2010. Aerosol concentrations observed at Mt. Haruna, Japan, in relation to long-range transport of Asian mineral dust aerosols, Atmospheric Environment, 44, 4638-4644.

Tan, J. h., Duan, J. c., Chai, F. h., He, K. b., and Hao, J. M., 2014. Source apportionment of size segregated fine/ultrafine particle by PMF in Beijing, Atmospheric Research, 139, 90-100.

Tan, K. C., San Lim, H., and Jafri, M. Z. M., 2016. Prediction of column ozone concentrations using multiple regression analysis and principal component analysis techniques: A case study in peninsular Malaysia, Atmospheric Pollution Research, 7, 533-546.

Tan, H., Cai, M., Fan, Q., Liu, L., Li, F., Chan, P. W., Deng, X., and Wu, D., 2017. An analysis of aerosol liquid water content and related impact factors in Pearl River Delta, The Science of the total environment, 579, 1822-1830.

Tang, X., Zhang, X., Ci, Z., Guo, J., and Wang, J., 2016. Speciation of the major inorganic salts in atmospheric aerosols of Beijing, China: Measurements and comparison with model, Atmospheric Environment, 133, 123-134.

Tian, S., Pan, Y., and Wang, Y., 2018. Ion balance and acidity of size-segregated particles during haze episodes in urban Beijing, Atmospheric Research, 201, 159-167.

Wang, Z., Wu, Z., Yue, D., Shang, D., Guo, S., Sun, J., Ding, A., Wang, L., Jiang, J., Guo, H., Gao, J., Cheung, H. C., Morawska, L., Keywood, M., and Hu, M., 2017. New particle formation in China: Current knowledge and further directions, The Science of the total environment, 577, 258-266.

Wang, H., Ding, J., Xu, J., Wen, J., Han, J., Wang, K., Shi, G., Feng, Y., Ivey, C. E., Wang, Y., Nenes, A., Zhao, Q., and Russell, A. G., 2019. Aerosols in an arid environment: The role of aerosol water content, particulate acidity, precursors, and relative humidity on secondary inorganic aerosols, The Science of the total environment, 646, 564-572.

Watson, J. G., Chow, J. C., Lurmann, F. W., and Musarra, S. P., 1994. Ammonium Nitrate, Nitric Acid, and Ammonia Equilibrium in Wintertime Phoenix, Arizona, Air & Waste, 44, 405-412.

Wen, L., Chen, J., Yang, L., Wang, X., Caihong, X., Sui, X., Yao, L., Zhu, Y., Zhang, J., Zhu, T., and Wang, W., 2015. Enhanced formation of fine particulate nitrate at a rural site on the North China

Plain in summer: The important roles of ammonia and ozone, Atmospheric Environment, 101, 294-302.

Wu, Z., Wang, Y., Tan, T., Zhu, Y., Li, M., Shang, D., Wang, H., Lu, K., Guo, S., Zeng, L., and Zhang, Y., 2018. Aerosol Liquid Water Driven by Anthropogenic Inorganic Salts: Implying Its Key Role in Haze Formation over the North China Plain, Environmental Science & Technology Letters, 5, 160-166.

Xu, L., Duan, F., He, K., Ma, Y., Zhu, L., Zheng, Y., Huang, T., Kimoto, T., Ma, T., Li, H., Ye, S., Yang, S., Sun, Z., and Xu, B., 2017. Characteristics of the secondary water-soluble ions in a typical autumn haze in Beijing, Environmental pollution, 227, 296-305.

Xu, X., Zhang, H., Lin, W., Wang, Y., Xu, W., and Jia, S., 2018. First simultaneous measurements of peroxyacetyl nitrate (PAN) and ozone at Nam Co in the central Tibetan Plateau: impacts from the PBL evolution and transport processes, Atmospheric Chemistry and Physics, 18, 5199-5217.

Xue, J., Griffith, S. M., Yu, X., Lau, A. K. H., and Yu, J. Z., 2014. Effect of nitrate and sulfate relative abundance in PM$_{2.5}$ on liquid water content explored through half-hourly observations of inorganic soluble aerosols at a polluted receptor site, Atmospheric Environment, 99, 24-31.

Yamagami, M., Ikemori, F., Nakashima, H., Hisatsune, K., and Osada, K., 2019. Decreasing trend of elemental carbon concentration with changes in major sources at Mega city Nagoya, Central Japan, Atmospheric Environment, 199, 155-163.

Yin, S., Huang, Z., Zheng, J., Huang, X., Chen, D., and Tan, H., 2018. Characteristics of inorganic aerosol formation over ammonia-poor and ammonia-rich areas in the Pearl River Delta region, China, Atmospheric Environment, 177, 120-131.

Yuchi, W., Gombojav, E., Boldbaatar, B., Galsuren, J., Enkhmaa, S., Beejin, B., Naidan, G., Ochir, C., Legtseg, B., Byambaa, T., Barn, P., Henderson, S. B., Janes, C. R., Lanphear, B. P., McCandless, L.

C., Takaro, T. K., Venners, S. A., Webster, G. M., and Allena, R. W., 2019. Evaluation of random forest regression and multiple linear regression for predicting indoor fine particulate matter concentrations in a highly polluted city, Environmental pollution, 245, 746-753.

Zhang, X. X., Yuan, Z. B., Zheng, J. Y., Lin, X. H., Liu, C. H., Yu, Z. J., and Yu, L. Z., 2019a. Establishment of an uncertainty assessment framework for atmospheric pollutant monitoring data and its impact on PMF source apportionment, Acta Scientiae Circumstantiae, 39, 95-104. (in Chinese)

Zhang, X., Zhang, K., Lv, W., Liu, B., Aikawa, M., and Wang, J., 2019b. Characteristics and risk assessments of heavy metals in fine and coarse particles in an industrial area of central China, Ecotoxicology and environmental safety, 179, 1-8.

Zhong, C., Yang, Z., Jiang, W., Hu, B., Hou, Q., Yu, T., and Li, J., 2016. Ecological geochemical assessment and source identification of trace elements in atmospheric deposition of an emerging industrial area: Beibu Gulf economic zone, The Science of the total environment, 573, 1519-1526.

Zhou, M., Qiao, L., Zhu, S., Li, L., Lou, S., Wang, H., Wang, Q., Tao, S., Huang, C., and Chen, C., 2016. Chemical characteristics of fine particles and their impact on visibility impairment in Shanghai based on a 1-year period observation, Journal of environmental sciences, 48, 151-160.

Zong, Z., Wang, X., Tian, C., Chen, Y., Fu, S., Qu, L., Ji, L., Li, J., and Zhang, G., 2018. PMF and PSCF based source apportionment of PM$_{2.5}$ at a regional background site in North China, Atmospheric Research, 203, 207-215.

Chapter 3: Thermodynamic response corresponding to concentration reducing of components in inorganic aerosols

3.1 Introduction

Atmospheric inorganic aerosols are complex mixtures that originate from various pollution sources and have different formation pathways, basically accounting for one third or more of total particulate matters, and main components are sea salts, secondary inorganic ions, crustal materials, and liquid water (Khan et al., 2010; Kong et al., 2018; Yin et al., 2018; Ng et al., 2019; Roger et al., 2019; Zhang et al., 2020, 2021b). The related environmental problems include air quality deterioration, human health risk, climate change, visibility reduction, etc., which are closely related to the loading level of inorganic aerosols in the atmosphere and the physical/chemical characteristics of components (Xue et al., 2011; Carnevale et al., 2012; Tan et al., 2017; Gao et al., 2020). To improve air quality, strict standards for atmospheric particles have been established by individual governments and international organizations (Chen et al., 2016; Wang et al., 2018; Roberts and Wooster, 2021; Zhang et al., 2021a). Controlling particle mass concentration level is necessary and urgent to achieve these environmental standards, especially in the severe pollution regions; moreover, the effective countermeasures are required based on the specific situations of different regions or countries. In previous studies, the thermodynamic inorganic model, ISORROPIA II, was often used to simulate the gas-particle conversion process, providing a simple and effective method of assessing particle-control measures. To be specific, San et al. (2005) modeled the response of inorganic aerosols to changes in sulfate, nitrate, and ammonium concentrations (SNA) in Mexico City; the results indicated that particle behavior was dominated by the abundance of ammonia, and changes in sulfate and nitrate concentrations were expected to have a greater effect on the inorganic aerosol mass concentration (IAM) in an ammonium-rich condition. Zhang et al. (2020) observed that when the atmosphere had an ammonium-rich condition, the reduction

of nitrate emissions was the optimal control measure for fine particle pollution in urban Beijing, followed by controlling sulfate and ammonium concentrations. Ansari and Pandis (1998) simulated the 20% reduction of SNA in two polluted urban areas, showing that reductions in ammonia emissions had the most significant impact on the total particle concentration level in ammonium-poor conditions, although such a reduction would substantially increase atmospheric acidity. Walker et al. (2006) used the same approach to assess the effect of a 50% reduction, clearly illustrating that inorganic fine particles were most sensitive to a reduction in sulfate concentration during warm months and approximately equally sensitive to reductions in sulfate and nitrate concentrations during cold months. It should be noted that these studies focused on the effects of changes in SNA concentrations but not the effects of changes in the amounts of NH_3, SO_2, and NOx emissions on the ambient air quality; moreover, the aerosol liquid water content (ALWC) was the sensitive component, showing its relatively high contribution for the variation of IAM (Lv et al., 2021). However, from the perspective of human health, the mass concentration of ALWC was not the directly influencing factor. Previous researches have shown that the concentration level of ALWC could affect aerosol pH, and low pH could activate particle-bound hazardous materials (e.g., trace metals) (Kong et al., 2018; Zhang et al., 2019; Gao et al., 2020; Song and Osada, 2021). Hence, the mass concentration of dry inorganic aerosols (DIA) and aerosol pH are the most important parameters to evaluate the human health effect of inorganic aerosols.

In the present study, year-round observation of atmospheric particles and gaseous pollutants (HNO_3, HCl, and NH_3) was carried out in the suburbs of western Japan using a four-stage filter-pack method (Hong et al., 2002; Aikawa et al., 2013; 2016). Combining with these field observation data, the sensitive tests for different aerosol components were performed by means of ISORROPIA II model. The main objective was to comprehensively assess how inorganic aerosols respond to concentration reducing of components in the suburbs of Kitakyushu, Japan, to investigate their deep mechanisms and

47

the characteristics of sensitive aerosol components, and, as a consequence, to provide scientific information regarding the mitigation of particle pollution from two perspectives of air quality and human health.

3.2 Materials and Methods

3.2.1 Sampling and chemical analysis

Air sampling was conducted on the roof of the North Building, Hibikino Campus, the University of Kitakyushu (33.89° N, 130.71° E). The four-stage filter-pack method was used to collect total particulate matter (TPM) and gaseous pollutants (SO_2, HNO_3, HCl, and NH_3) simultaneously. The samples were collected on a daily (noon-noon) basis from March 2017 to February 2018. The procedure for determining water-soluble ions (Na^+, NH_4^+, K^+, Mg^{2+}, Ca^{2+}, Cl^-, NO_3^-, and SO_4^{2-}) was described in detail in previous studies (Aikawa et al., 2005; 2010; 2013; 2016; 2017a), and ion chromatography (Thermo Scientific^{TM} Dionex^{TM} Integrion, Thermo Fisher Scientific Inc., Waltham, MA, USA) was used in the determination. More detailed information about the sampling site, experiment methodology, and the process of quality assurance and quality control was shown in Section 2.2.1.

3.2.2 Model calculation

The thermodynamic equilibrium models (ISORROPIA, E-AIM, GFEMN, HETV, MESA and UHAERO) are widely used for investigating the gas-particle conversion process of inorganic aerosols; however, an important limitation of these models is the lack of treatment of crustal species (Ca^{2+}, K^+, and Mg^{2+}) (Karydis et al., 2010). To improve the simulation accuracy, Fountoukis and Nenes (2007) introduced a new thermodynamic model, ISORROPIA II, in which the thermodynamics of the crustal species have been added to the preexisting suite of components of the ISORROPIA model; many studies have adopted this new model to analyze the characteristics of coarse particles (Quan and Zhang, 2008; Karydis et al., 2010; Xue et al., 2011; Carnevale et al., 2012).

In this study, the ISORROPIA II model was run in the forward mode with input data of relative humidity (RH), temperature (T), and the concentrations of sodium (Na^+), chloride ($HCl + Cl^-$), ammonium ($NH_3 + NH_4^+$), sulfate (SO_4^{2-}), nitrate ($HNO_3 + NO_3^-$), magnesium (Mg^{2+}), potassium (K^+), calcium (Ca^{2+}) (abbreviated as TNa^+, TCl^-, TNH_4^+, TSO_4^{2-}, TNO_3^-, TMg^{2+}, TK^+, and TCa^{2+} hereafter) (Sudheer et al., 2015; Kong et al., 2018; Wang et al., 2019; Zhang et al., 2020, 2021b). Then, the stable state or metastable state was selected for inorganic aerosols based on the specific condition of sampling site. For stable condition, salts precipitate once the aqueous phase becomes saturated with respect to a salt, while, for metastable condition, the aerosol is composed only of an aqueous phase regardless of its saturation state (Xue et al., 2011). Finally, this model predicted which species can exist in the gas phase, aerosol solid phase, and aerosol aqueous phase, and calculated their concentration levels at chemical equilibrium, as well as aerosol pH.

3.3 Results and Discussion

3.3.1 Simulation quality of the ISORROPIA II model

To assess the simulation quality of the ISORROPIA II model, the output data of NH_4^+, NO_3^-, and Cl^- in the aerosol phase and NH_3, HNO_3, and HCl in the gas phase were compared with data observed by the four-stage filter-pack method using four statistical parameters, including mean bias (MB), mean error (ME), normalized mean bias (NMB), and normalized mean error (NME) (Karydis et al., 2010; Li et al., 2015; Li et al., 2017a; Sudheer et al., 2015; Zhang et al., 2017; Chen et al., 2018). The statistical analysis of the agreement between observations and model predictions in stable and metastable conditions is shown in Table 3-1. The values of these four parameters in a metastable state were closer to 0 than those in a stable state, which reveals that the metastable condition was the more suitable atmospheric situation in the suburbs of western Japan. In addition, NH_4^+, Cl^-, and HNO_3 showed negative values of MB and NMB under metastable condition, which indicates that the simulation results

slightly underestimate these three species and overestimate NH_3, HCl, and NO_3^-. However, in total, the simulation bias in this study was still within acceptable levels (Karydis et al., 2010; Sudheer et al., 2015). Moreover, the ALWC derived from two different thermodynamic models (ISORROPIA II and E-AIM-III) agreed well, with an R^2 value of 0.97 and a slope of 1.00 (Zhang et al., 2021b). Thus, the simulation results of the ISORROPIA II model in metastable conditions were reliable and can be applicable to the following analysis.

Table 3-1 Statistical evaluation of the simulation results of the ISORROPIA II model

Species	MB / $\mu g \cdot m^{-3}$		ME / $\mu g \cdot m^{-3}$		NMB / %		NME / %	
	Stable	Metastable	Stable	Metastable	Stable	Metastable	Stable	Metastable
NH_4^+	-0.43	-0.34	0.55	0.48	-26.14	-27.75	33.76	39.15
Cl^-	-0.36	-0.28	0.51	0.45	-19.23	-18.23	27.20	29.44
NO_3^-	-0.18	0.02	0.76	0.62	-5.46	0.68	23.43	20.36
NH_3	0.43	0.34	0.55	0.48	29.94	18.08	38.65	25.50
HCl	0.36	0.28	0.51	0.45	45.71	24.02	64.71	38.82
HNO_3	0.18	-0.02	0.76	0.62	15.30	-1.51	65.36	46.58

Note: $MB = \frac{1}{N} \times \sum_{i=1}^{N}(S_i - O_i)$; $ME = \frac{1}{N} \times \sum_{i=1}^{N}|S_i - O_i|$; $NMB = \frac{\sum_{i=1}^{N}(S_i - O_i)}{\sum_{i=1}^{N}O_i} \times 100\%$; $NME = \frac{\sum_{i=1}^{N}|S_i - O_i|}{\sum_{i=1}^{N}O_i} \times 100\%$; where S_i is the simulated value of the pollutant concentration, O_i is the observed value of the corresponding pollutant concentration at the same time, and N is the total number of the samples (365).

3.3.2 Original atmospheric condition (base case)

Table 3-2 shows the initial atmospheric situation in Kitakyushu City, Japan, as simulated by the ISORROPIA II model, which served as the base case for the seven sensitive tests. Specifically, the average mass concentrations of three gaseous pollutants (NH_3, HCl, and HNO_3) were 1.8, 1.1, and 1.1 $\mu g \cdot m^{-3}$, respectively, and the IAM was about 32.7 $\mu g \cdot m^{-3}$, with the aerosol pH of 3.3. Among the inorganic aerosol components, only $CaSO_4$ was in an aerosol solid phase, with an average concentration

of 2.4 $\mu g \cdot m^{-3}$, while other components, including Na^+, Cl^-, NH_4^+, SO_4^{2-}, NO_3^-, K^+, Mg^{2+}, and ALWC, were all in aerosol aqueous phase, and the concentrations were 1.5, 1.6, 1.4, 3.1, 3.2, 0.2, 0.2, and 19.2 $\mu g \cdot m^{-3}$, respectively.

The high loading of the ALWC revealed that inorganic aerosols were highly humid, playing an important role in both visibility impairment and aerosol radiative forcing (Xue et al., 2011). Many studies have proved that the ALWC was principally influenced by the relative humidity (Tan et al., 2017; Xu et al., 2017; Wu et al., 2018; Wang et al., 2019), which was consistent with our result. From Fig. 3-1(a), it can be seen that the ALWC increased exponentially with the increase of the relative humidity. When the relative humidity was lower than 60%, the concentration of aerosol liquid water was approximately 2.11 $\mu g \cdot m^{-3}$ and basically was unchanged, which was because the hygroscopic effect of atmospheric particles was minimal under low-humidity conditions, and the moisture level was too low to be absorbed effectively by particles (Tan et al., 2017). In contrast, when the ambient RH increased from 60% to 85%, the ALWC increased gradually, and this gradual increase could be attributable to the absorption of water by mixed deliquescent salts. Fong et al. (2016) and Wu et al. (2018) actually demonstrated that when the ambient RH reached the lowest deliquescence relative humidity (DRH) of inorganic salts in aerosols (Li et al., 2017b), with increased RH, more and more inorganic salts absorbed water to form saturated solution droplets, until the aerosol system fully deliquesced. Finally, when the relative humidity exceeded approximately 85%, water molecules in the atmosphere started to be adsorbed on aerosol surfaces, forming a water layer, and the thickness of the water layer increased quickly with the humidity (He et al., 2019), causing the obviously higher rate of increase of ALWC.

Table 3-2 The simulated concentrations of related species in the gas phase and the aerosol phase by ISORROPIA II

Phase	Species	Mean value / $\mu g \cdot m^{-3}$
Gas phase	NH_3	1.8
	HNO_3	1.1
	HCl	1.1
Aerosol solid phase	$CaSO_4$	2.4
Aerosol aqueous phase	Na^+	1.5
	Cl^-	1.6
	NH_4^+	1.4
	SO_4^{2-}	3.1
	HSO_4^-	0.0
	NO_3^-	3.2
	K^+	0.2
	Mg^{2+}	0.2
	Ca^{2+}	0.0
	ALWC	19.2

Note: The initial input data (mean value): RH (70%), T (289.9 K), TNa^+ (1.5 $\mu g \cdot m^{-3}$), TCl^- (2.7 $\mu g \cdot m^{-3}$), TNH_4^+ (3.1 $\mu g \cdot m^{-3}$), TSO_4^{2-} (4.9 $\mu g \cdot m^{-3}$), TNO_3^- (4.4 $\mu g \cdot m^{-3}$), TK^+ (0.2 $\mu g \cdot m^{-3}$), TMg^{2+} (0.2 $\mu g \cdot m^{-3}$), and TCa^{2+} (0.8 $\mu g \cdot m^{-3}$).
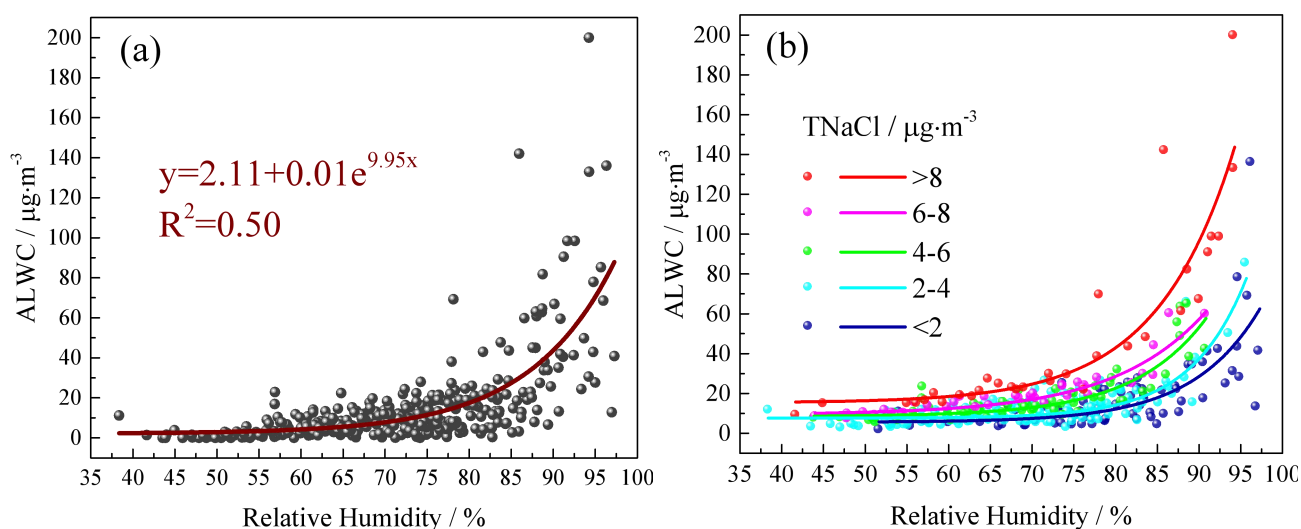

Fig. 3-1 Variation of the ALWC as a function of the relative humidity (a), and the further influence of marine aerosols on the ALWC (b). The samples are grouped according to the concentration level of TNaCl in the atmosphere in Fig. 3-1 (b).

3.3.3 Optimal countermeasure for mitigating particle pollution

To find an effective method of mitigating particle pollution, seven sensitive tests were performed in this study. As shown in Fig. 3-2(a), the IAM changed nonlinearly when we reduced TNH_4^+ and TSO_4^{2-} concentrations (the fitting curves: $y_a = -5.11x - 13.82x^2 + 9.21x^3$ and $y_a = -12.89x + 10.47x^2$, respectively (y_a and x presents IAM variation [$\mu g \cdot m^{-3}$] and concentration reduction ratio (CRR)/100 [dimensionless]). Meanwhile, after reducing $TNaCl$ ($Na^+ + HCl + Cl^-$), TNO_3^-, TMg^{2+}, TK^+, and TCa^{2+} concentrations ($0\% \leq CRR \leq 100\%$, with the exception of 100% in TNaCl), IAM responded linearly with slopes of -13.55, -6.74, -1.78, -0.41, and 1.08, respectively. The largest decrease in the amounts of IAM was basically achieved by the reduction in the TNaCl concentration. However, as TNaCl in the suburbs of western Japan was mainly from marine aerosols (Aikawa et al., 2017b; 2018; Zhang et al., 2021b), its atmospheric concentration was difficult to control artificially and, furthermore, easily varied with changes in the proportion and transport speed of air masses from the Sea of Japan (Zhang et al., 2021b). Hence, limiting the concentration of TSO_4^{2-} (CRR < 35%) or TNH_4^+ (CRR > 35%) in Kitakyushu, Japan was the most effective for particle pollution mitigation from the perspective of air quality.

For human health effect, we should take both DIA mass concentration and inorganic aerosol pH into account; the variations of these two parameters in seven sensitive tests were shown in Fig. 3-2(b and c). Totally speaking, the reduction of TSO_4^{2-} concentration was the most effective, which showed the largest decreasing amount of DIA mass concentration at any CRR and the significant increase of aerosol pH, with corresponding fitting equations of $y_b = -5.55x + 1.76x^2$ and $y_c = 0.97x + 0.54x^2$, respectively (y_b, y_c, and x presents the DIA mass concentration variation [$\mu g \cdot m^{-3}$], inorganic aerosol pH variation [dimensionless], and CRR/100 [dimensionless]). In comparison with TSO_4^{2-}, the decreasing amounts of DIA after controlling $TNaCl$, TNO_3^-, and TNH_4^+ were slightly low, and there was little difference

among these three sensitive tests. However, only the reduction of TNO_3^- could cause the increase of aerosol pH, with the slope of 0.49. The inorganic aerosol pH after controlling TNaCl and TNH_4^+ were obviously lower than that in base case, and the variations of aerosol pH followed the fitting equations of $y_c = -0.49x$ (except for CRR of 100%) and $y_c = -0.35x - 1.50x^2$, respectively. In addition, among seven sensitive tests, the changes of DIA mass concentration under the reductions of TCa^{2+}, TMg^{2+}, and TK^+ concentrations were relatively small, with the linear response slopes of -0.66, -0.47, and -0.25, respectively, revealing that controlling crustal species was not effective measure to mitigate particle pollution in Kitakyushu, Japan. Moreover, these three sensitive tests all caused the decrease of aerosol pH, and the aerosol acidity was the strongest under the reduction of TCa^{2+}, followed by TMg^{2+}, and TK^+ at any CRR.
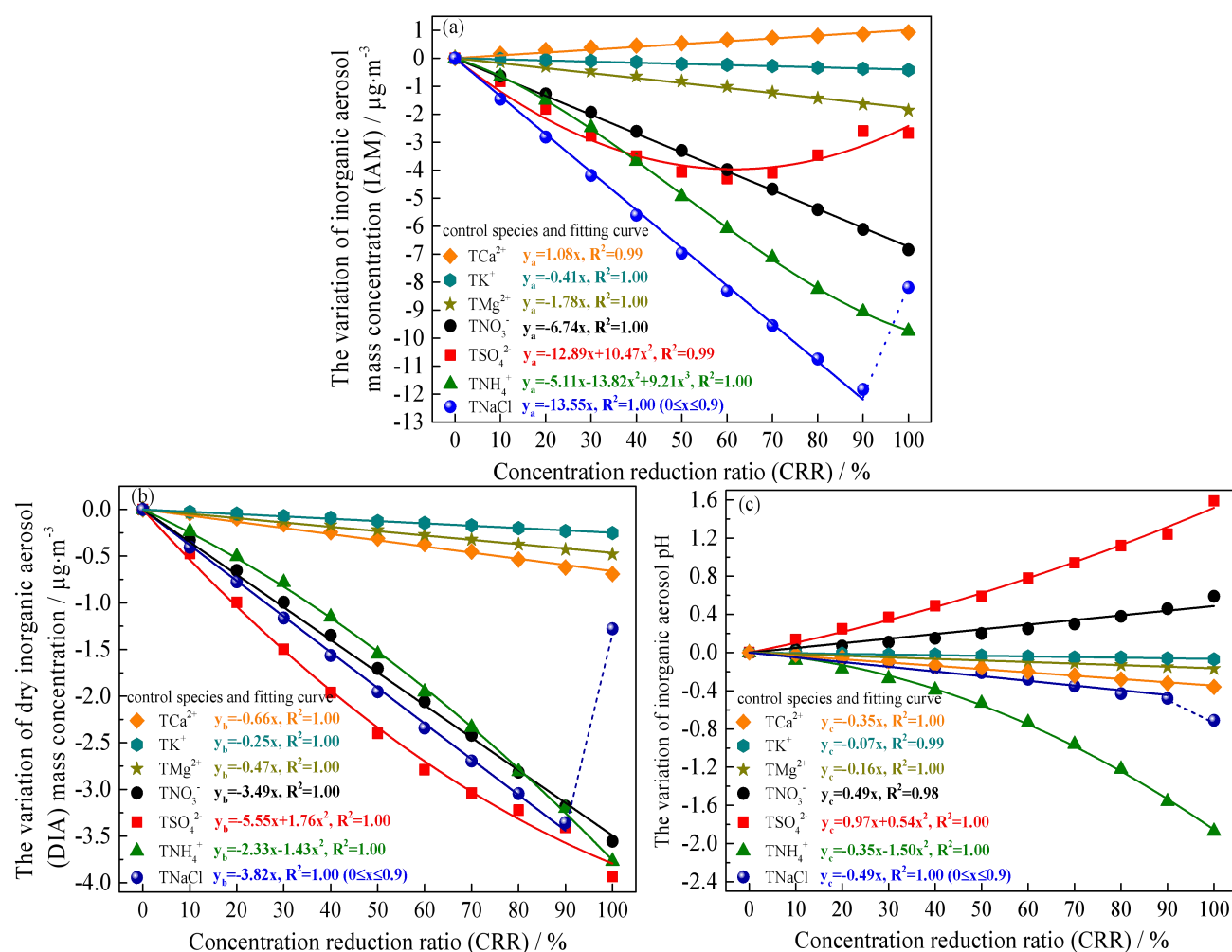

Fig. 3-2 Variations of inorganic aerosol mass concentrations (a), dry inorganic aerosol mass concentrations (without ALWC)

(b), and inorganic aerosol pH (c) in seven sensitive tests (CRR=$\frac{C_0 - C_1}{C_0} \times 100\%$, where C_0 and C_1 represent species

concentrations in cases of without reduction and with reduction, respectively.)

3.3.4 Thermodynamic equilibrium shifts of particle-related species in seven sensitive tests

3.3.4.1 Response to the reduction in TNaCl concentration

To better understand the response of inorganic aerosols, the variations of related species in the gas

phase, aerosol solid phase, and aerosol aqueous phase were investigated. As shown in Fig. 3-3(a), when

TNaCl in the atmosphere decreased from 4.2 $\mu g \cdot m^{-3}$ (0% reduction) to 0.4 $\mu g \cdot m^{-3}$ (90% reduction), the

ALWC was the most sensitive component in the aerosol phase, with the linear slope of 9.7, which could

explain approximately 72% of the total particle concentration variation, followed by the sum of Na$^+$ and

Cl$^-$ (23%). This phenomenon revealed that the concentration level of marine aerosols could also affect

the ALWC, except for the relative humidity. A more-detailed analysis regarding factors involved in the

ALWC is shown in a following section (3.3.4.4). In addition, the slight drop in NO$_3^-$ concentration was

mainly due to the thermodynamic equilibrium shift of aged sea salts from an aerosol aqueous phase

(NaNO$_3$) to a gas phase (HNO$_3$) (Boreddy and Kawamura, 2016; Ge et al., 2017). However, when the

CRR of TNaCl was 100%, the IAM increased by 3.6 $\mu g \cdot m^{-3}$, in which the variation of DIA mass and

ALWC accounted for 58% and 42%, respectively. To understand this sudden increase, we simulated the

gas-particle conversion processes in detail for 91%, 92%, 93%, 94%, 95%, 96%, 97%, 98%, and 99%

reductions of TNaCl (Fig. 3-3(b)). Fig. 3-3(b) indicated that the responses of inorganic aerosols in

conditions of 91%–99% reduction followed the original equation. The sharp variation in the DIA mass

concentration was only observed at 100% reduction, which was due to the changes of NO$_3^-$ and NH$_4^+$ in

the aerosol aqueous phase. The conversion process of nitrate and ammonium from the gas phase to the

aerosol aqueous phase could be enhanced effectively with the extremely low concentration of marine

aerosols; this subsequently influenced the concentration level of the ALWC, finally resulting in the

increase of the IAM and aerosol acidity.

3.3.4.2 Individual response to the reduction for TNH_4^+, TSO_4^{2-}, and TNO_3^- concentrations

As opposed to marine aerosols from natural sources, secondary inorganic aerosols (SIA) are mainly from anthropogenic sources and play a dominant role in severe particle pollution (Sun et al., 2016; Roger et al., 2019; Xu et al., 2019; Zhang et al., 2020). Hence, the reduction of SIA component concentrations could have more practical significance for mitigating particle pollution. Specifically, after reducing the concentration of TNH_4^+ (Fig. 3-3(c)), NH_3 in the gas phase and NH_4^+ in the aerosol aqueous phase decreased simultaneously. With this reducing NH_4^+, the Cl^- and NO_3^-, which had combined with this reduced NH_4^+ (NH_4Cl and NH_4NO_3), were continuously released into the atmosphere in the gaseous form; hence, the concentrations of HCl and HNO_3 in the gas phase increased obviously. In addition, when the CRR of TNH_4^+ was larger than 60%, the remaining NH_4^+ in the aerosol phase was lower than 0.9 $\mu g \cdot m^{-3}$, which was not sufficient for maintaining all SO_4^{2-} with the chemical form of $(NH_4)_2SO_4$; hence, the appearance of HSO_4^- was observed in the aerosol aqueous phase. During the entire process, the ALWC was the most sensitive component, accounting for ca. 64% of the IAM variation. Finally, under the comprehensive influence of NH_4^+, Cl^-, NO_3^-, SO_4^{2-}, HSO_4, and ALWC, the inorganic aerosol pH decreased nonlinearly in the strict sense, and the lowest value (1.4) was observed under 100% reduction of TNH_4^+. As for controlling TSO_4^{2-}, the IAM, DIA mass concentration, and aerosol pH all varied nonlinearly, which was consistent with the findings of a previous study (West et al., 1999); however, the variation trends of these three pollution parameters was obviously different from that of the controlling TNH_4^+ (Fig. 3-2). When the TSO_4^{2-} decreased from 4.9 $\mu g \cdot m^{-3}$ (0% reduction) to 2.5 $\mu g \cdot m^{-3}$ (50% reduction), the concentration of SO_4^{2-} in the aerosol aqueous phase obviously decreased, while the concentration of $CaSO_4$ in the aerosol solid phase had little change (Fig. 3-3(d)). For NH_4^+ that was bound to these reduced SO_4^{2-}, one part could be directly released into the atmosphere,

causing the increase of NH_3 in the gas phase, and the other part could be combined with the Cl^- and NO_3^-, which were transformed from gaseous HCl and HNO_3. When the CRR of TSO_4^{2-} exceeded 50%, $CaSO_4$ also started to decrease significantly, and most of the Ca^{2+} in the aerosol solid phase could enter the aerosol aqueous phase. In addition, during the entire process, the variation of the ALWC was obviously different from that of other components; that is, the ALWC gradually decreased as TSO_4^{2-} decreased, and the amount of the decreased ALWC became smaller and smaller when the CRR was larger than 50%. Hence, if we plan to improve air quality through the reduction of TSO_4^{2-} concentration, the CRR of TSO_4^{2-} should be lower than 60%, because the variation of the ALWC disturbed the decrease of inorganic aerosols in the condition of high TSO_4^{2-} reduction. As for controlling TNO_3^- (Fig. 3-3(e)), NO_3^- in the aerosol aqueous phase and HNO_3 in the gas phase decreased simultaneously. Subsequently, most of NH_4^+ bound to the reduced NO_3^- was directly released into the atmosphere, causing a linear increase of NH_3 in the gas phase, and a small part of NH_4^+ was combined with Cl^-, which was transformed from gaseous HCl. Finally, the ALWC decreased linearly with a slope of -3.2, and the increase of aerosol pH was mainly caused by the variations of Cl^-, NH_4^+, NO_3^-, and ALWC in the aerosol aqueous phase.

3.3.4.3 Clear difference among the response to the reduction in TMg^{2+}, TK^+, and TCa^{2+} concentrations

Among aerosol components, Mg^{2+}, K^+, and Ca^{2+} had relatively low concentrations (Table 3-2), and the reductions in TMg^{2+}, TK^+, and TCa^{2+} concentrations were not as effective as controlling SIA component concentrations for mitigating particle pollution, especially TSO_4^{2-} and TNO_3^- (Fig. 3-2). After controlling TMg^{2+} and TK^+, the inorganic aerosol responses had a similar gas-particle conversion mechanism. As shown in Fig. 3-3(f and g), TMg^{2+} or TK^+ was mainly in the chemical forms of $MgCl_2$ and $Mg(NO_3)_2$ or KCl and KNO_3 in the aerosol aqueous phase. Hence, as the TMg^{2+} or TK^+

concentration was reduced, most of the Cl^- and NO_3^- that had been combined with these reduced Mg^{2+} or K^+ concentrations could be released directly into the atmosphere, resulting in decreased Cl^- and NO_3^- in the aerosol aqueous phase and increased HCl and HNO_3 in the gas phase. A small part of these Cl^- and NO_3^- concentrations could be combined with NH_4^+, which was transformed from gaseous NH_3. In addition, the concentrations of the ALWC decreased slightly under the comprehensive influence of these responsive species, finally resulting in the linear decrease of the IAM and aerosol pH.

As opposed to controlling TMg^{2+} and TK^+, reducing the TCa^{2+} concentration brought the increase of aerosol loading in the atmosphere (Fig. 3-2(a)). As shown in Fig. 3-3(h), after controlling TCa^{2+}, $CaSO_4$ in the aerosol solid phase decreased linearly, but the SO_4^{2-} that had combined with Ca^{2+} in the aerosol solid phase could transfer into the aerosol aqueous phase. Subsequently, a part of the increased SO_4^{2-} in aerosol aqueous phase was combined with the NH_4^+, which was transformed from gaseous NH_3, while another part was abstracted NH_4^+ from existing NH_4Cl and NH_4NO_3 in the aerosol aqueous phase; then Cl^- and NO_3^- were released simultaneously into the gas phase. Moreover, the concentration of the ALWC increased linearly with a slope of 1.67, which was similar to the variation of SO_4^{2-} in the aerosol aqueous phase. Finally, after controlling TCa^{2+}, the IAM and aerosol acidity were higher than that in base case, revealing that the appropriate presence of TCa^{2+} in the atmosphere could facilitate mitigation of particle pollution.
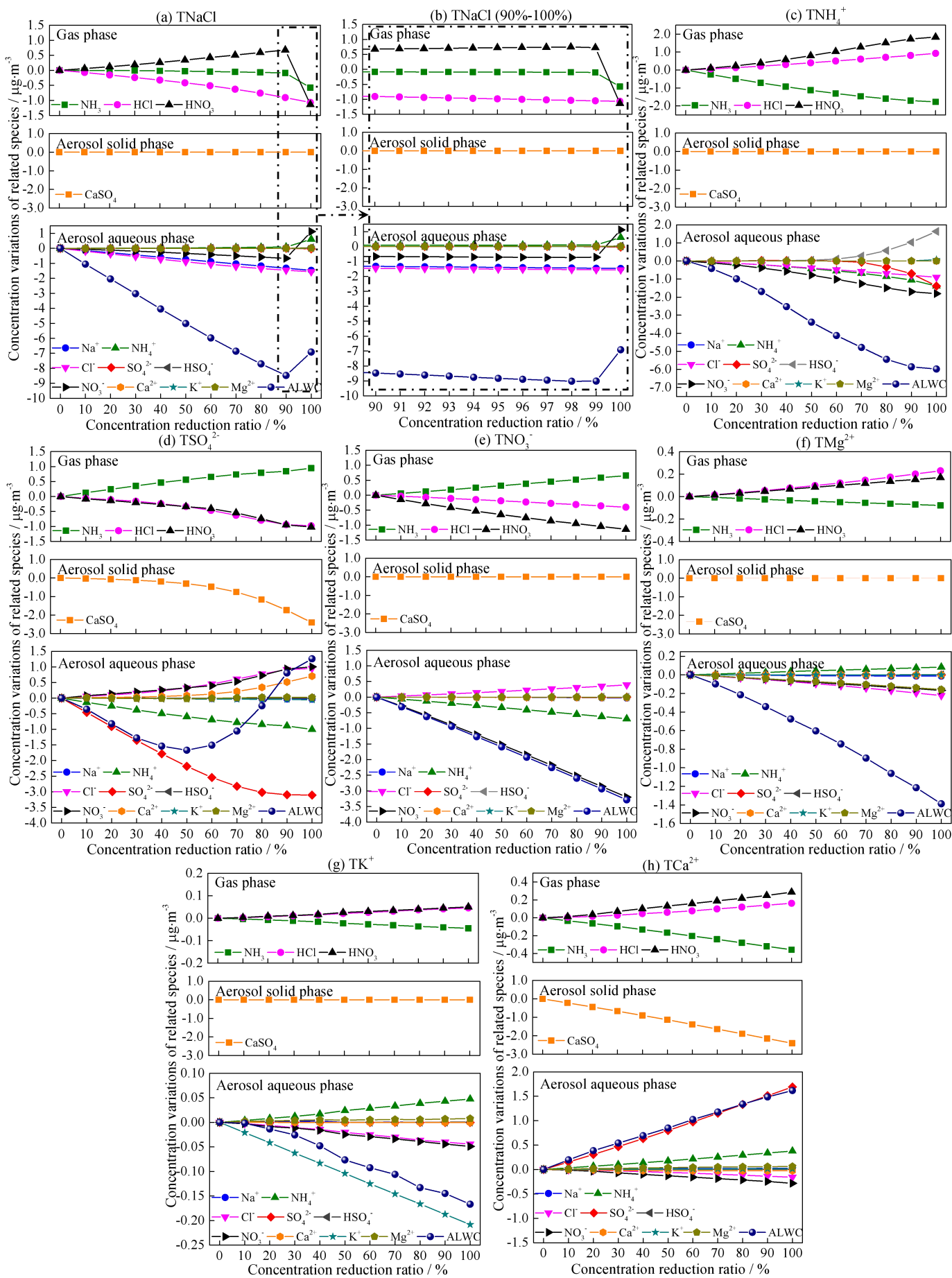
Fig. 3-3 Concentration variations of related species in the gas phase and the aerosol phase in seven sensitive tests

59

3.3.4.4 The characteristics of ALWC

During the gas-particle conversion processes of seven sensitive tests (Fig. 3-3), the ALWC was basically the most sensitive aerosol component. To further investigate the comprehensive influence of related species on the variation of the ALWC, multiple regression analysis (MRA) was performed by SPSS with a forward method (Tan et al., 2016; Wang et al., 2019; Zhang et al., 2021b). Considering significance levels (t-value and p-value) and the variance inflation factor (VIF) of each species in the gas and aerosol phases, only six species were the driving factors of the ALWC, as shown in Table 3-3. The relationship between the concentration variations of the ALWC and the driving factors could be described as follows:

$$[ALWC] = 0.01+1.68[NO_3^-]+5.23[Cl^-]+1.83[SO_4^{2-}]+2.81[HSO_4^-]+0.34[HNO_3]+0.57[NH_3] \ (R^2= 0.99, P < 0.05). \quad (3\text{-}1)$$

where $[x]$ represents the concentration decreasing amount ($\mu g \cdot m^{-3}$) of each species simulated by the ISORROPIA II model. This equation revealed that the variation of Cl^- with a coefficient value of 5.23 ($p < 0.05$) made the largest contribution to the concentration variations of the ALWC in seven sensitive tests. Meng et al. (2021) and Wen et al. (2021) showed that the ALWC was influenced by secondary aerosols, which agreed with our results, while few studies have investigated the influence of Cl^-. In this study, the high coefficient of Cl^- (5.23) proved the key role of sea salts on the concentration variation of the ALWC. Our actual field observations were also consistent with and strongly support the simulation results. Specifically, based on the relationship between the relative humidity and the ALWC in the actual atmospheric conditions (Fig. 3-1(a)), the data points can be divided into five groups according to the concentration level of TNaCl (Fig. 3-1(b)). The concentration of the ALWC associated with the lower concentration of sea salts was much smaller than that associated with higher one at any RH, further proving the significant influence of sea salts on the concentration of the ALWC of inorganic aerosols.

Table 3-3 Multiple regression results

Model 1		Unstandardized Coefficients		Standardized Coefficients			
Response variable	Independent factors	β	Std. Error	Beta	t-value	p-value	VIF
ALWC	Constant	0.01	0.01	-	0.79	0.43	
	NO_3^-	1.68	0.05	0.91	32.02	0.00	4.00
	Cl^-	5.23	0.11	0.87	45.95	0.00	1.80
	SO_4^{2-}	1.83	0.06	0.66	31.86	0.00	2.16
	HSO_4^-	2.81	0.10	0.57	27.64	0.00	2.15
	HNO_3	0.34	0.05	0.17	6.55	0.00	3.48
	NH_3	0.57	0.10	0.12	5.62	0.00	2.33

3.4 Conclusions

In the suburbs of Kitakyushu, Japan, the IAM was about 32.7 $\mu g \cdot m^{-3}$, with the aerosol pH of 3.3. To find an effective method of mitigating particle pollution, seven sensitive tests were performed using the ISORROPIA II model, in which the seven control species—TNaCl, TNH_4^+, TSO_4^{2-}, TNO_3^-, TMg^{2+}, TK^+, and TCa^{2+}—were taken into account. From the perspective of air quality, limiting the concentration of TSO_4^{2-} (CRR < 35%) or TNH_4^+ (CRR > 35%) was the most effective and realistic method, in which the IAM changed nonlinearly, with the fitting equations of $y_a = -5.11x - 13.82x^2 + 9.21x^3$ and $y_a = -12.89x + 10.47x^2$, respectively (y_a and x presents IAM variation [$\mu g \cdot m^{-3}$] and CRR/100 [dimensionless]). For other sensitive tests, IAM responded linearly, and slopes after reducing TNaCl, TNO_3^-, TMg^{2+}, TK^+, and TCa^{2+} were -13.55, -6.74, -1.78, -0.41, and 1.08, respectively ($0\% \leq CRR \leq 100\%$, with the exception of 100% in TNaCl). The ALWC, being the most sensitive aerosol component, was statistically and strongly related to the variations of NO_3^-, Cl^-, SO_4^{2-}, HSO_4^-, HNO_3, and NH_3 ($P < 0.05$), with coefficients of 1.68, 5.23, 1.83, 2.81, 0.34, and 0.57, respectively. The highest coefficient (5.23) was found for Cl^-, revealing that sea salts significantly influenced particle responses. In addition, from the perspective of human health, the reduction of TSO_4^{2-} concentration was the optimal measure;

the DIA mass concentration and aerosol pH followed the fitting equations of $y_b = -5.55x + 1.76x^2$ and $y_c = 0.97x + 0.54x^2$, respectively (y_b, y_c, and x presents the DIA mass concentration variation [$\mu g \cdot m^{-3}$], inorganic aerosol pH variation [dimensionless], and CRR/100 [dimensionless]). Overall, our methodology in using ISORROPIA II is useful for understanding and evaluating the characteristics of aerosol components and the inner response for the reduction of components, conclusively providing basic and effective ideas for mitigating particle pollution.

References

Aikawa, M., Hiraki, T., Horie, Y., Nakatsubo, R., Matsumura, C., Mukai, H., 2017a. Trans-boundary and in-country transport of air pollutants observed in Kobe, Japan by high frequent filter pack sampling method. Journal of Atmospheric Chemistry 74, 505-518.

Aikawa, M., Hiraki, T., Tamaki, M., 2005. Characteristics in Concentration of Chemical Species in Ambient Air Based on Three-Year Monitoring by Filter Pack Method. Water Air & Soil Pollution 161, 335-352.

Aikawa, M., Hiraki, T., Tomoyose, N., Ohizumi, T., Noguchi, I., Murano, K., Mukai, H., 2013. Local emission of primary air pollutants and its contribution to wet deposition and concentrations of aerosols and gases in ambient air in Japan. Atmospheric Environment 79, 317-323.

Aikawa, M., Hirokawa, K., Murakami, T., 2017b. Daily observation of gas/aerosol by FP method in western part of Japan, Proceedings of the 58th Annual Meeting of the Japan Society for Atmospheric Environment, Hyogo, Japan, 6–8 September 2017, 454.

Aikawa, M., Morino, Y., Kajino, M., Hiraki, T., Horie, Y., Nakatsubo, R., Matsumura, C., Mukai, H., 2016. Candidates to Provide a Specific Concentration Difference for Ambient Sulfur and Nitrogen Compounds Near the Coastal and Roadside Sites of Japan. Water, Air, & Soil Pollution 227.

Aikawa, M., Ohara, T., Hiraki, T., Oishi, O., Tsuji, A., Yamagami, M., Murano, K., Mukai, H., 2010. Significant geographic gradients in particulate sulfate over Japan determined from multiple-site measurements and a chemical transport model: Impacts of transboundary pollution from the Asian continent. Atmospheric Environment 44, 381-391.

Aikawa, M., Suzuki, M., Murakami, T., Hirokawa, K., 2018. Daily observation of gas/aerosol by FP method in western part of Japan (2), Proceedings of the 59th Annual Meeting of the Japan Society for Atmospheric Environment, Fukuoka, Japan, 12–14 September 2018, 245.

Ansari, A.S., Pandis, S.N., 1998. Response of Inorganic PM to Precursor Concentrations. Environmental Science & Technology 32, 2706-2714.

Boreddy, S.K., Kawamura, K., 2016. Hygroscopic growth of water-soluble matter extracted from remote marine aerosols over the western North Pacific: Influence of pollutants transported from East Asia. The Science of the total environment 557-558, 285-295.

Carnevale, C., Finzi, G., Pisoni, E., Thunis, P., Volta, M., 2012. The impact of thermodynamic module in the CTM performances. Atmospheric Environment 61, 652-660.

Chen, D., Zhao, N., Lang, J., Zhou, Y., Wang, X., Li, Y., Zhao, Y., Guo, X., 2018. Contribution of ship emissions to the concentration of $PM_{2.5}$: A comprehensive study using AIS data and WRF/Chem model in Bohai Rim Region, China. Science of The Total Environment 610-611, 1476-1486.

Chen, W., Tang, H., Zhao, H., 2016. Urban air quality evaluations under two versions of the national ambient air quality standards of China. Atmospheric Pollution Research 7, 49-57.

Fong, B.N., Kennon, J.T., Ali, H.M., 2016. Mole Ratio Dependence of the Mutual Deliquescence Relative Humidity of Aqueous Salts of Atmospheric Importance. The journal of physical chemistry. A 120, 3596-3601.

Fountoukis, C., Nenes, A., 2007. ISORROPIA II: a computationally efficient thermodynamic equilibrium model for K^+–Ca^{2+}–Mg^{2+}–NH_4^+–Na^+–SO_4^{2-}–NO_3^-–Cl^-–H_2O aerosols. Atmospheric Chemistry and Physics 7, 4639–4659.

Gao, J., Wei, Y., Shi, G., Yu, H., Zhang, Z., Song, S., Wang, W., Liang, D., Feng, Y., 2020. Roles of RH, aerosol pH and sources in concentrations of secondary inorganic aerosols, during different pollution periods. Atmospheric Environment 241, 117770.

Ge, X., He, Y., Sun, Y., Xu, J., Wang, J., Shen, Y., Chen, M., 2017. Characteristics and Formation Mechanisms of Fine Particulate Nitrate in Typical Urban Areas in China. Atmosphere 8, 62.

He, Y., Gu, Z., Lu, W., Zhang, L., Okuda, T., Fujioka, K., Luo, H., Yu, C.W., 2019. Atmospheric humidity and particle charging state on agglomeration of aerosol particles. Atmospheric Environment 197, 141-149.

Karydis, V.A., Tsimpidi, A.P., Fountoukis, C., Nenes, A., Zavala, M., Lei, W., Molina, L.T., Pandis, S.N., 2010. Simulating the fine and coarse inorganic particulate matter concentrations in a polluted megacity. Atmospheric Environment 44, 608-620.

Khan, M.F., Hirano, K., Masunaga, S., 2010. Quantifying the sources of hazardous elements of suspended particulate matter aerosol collected in Yokohama, Japan. Atmospheric Environment 44, 2646-2657.

Kong, L., Du, C., Zhanzakova, A., Cheng, T., Yang, X., Wang, L., Fu, H., Chen, J., Zhang, S., 2018. Trends in heterogeneous aqueous reaction in continuous haze episodes in suburban Shanghai: An in-depth case study. The Science of the total environment 634, 1192-1204.

Li, X., Zhang, Q., Zhang, Y., Zhang, L., Wang, Y., Zhang, Q., Li, M., Zheng, Y., Geng, G., Wallington, T.J., Han, W., Shen, W., He, K., 2017a. Attribution of $PM_{2.5}$ exposure in Beijing–Tianjin–Hebei region to emissions: implication to control strategies. Science Bulletin 62, 957-964.

Li, X., Zhang, Q., Zhang, Y., Zheng, B., Wang, K., Chen, Y., Wallington, T.J., Han, W., Shen, W., Zhang, X., He, K., 2015. Source contributions of urban $PM_{2.5}$ in the Beijing–Tianjin–Hebei region: Changes between 2006 and 2013 and relative impacts of emissions and meteorology. Atmospheric Environment 123, 229-239.

Li, Y.J., Liu, P.F., Bergoend, C., Bateman, A.P., Martin, S.T., 2017b. Rebounding hygroscopic inorganic aerosol particles: Liquids, gels, and hydrates. Aerosol Science and Technology 51, 388-396.

Lv, W.L., Zhang, K., Zhi, M.K.Cao, Q., Luo, Y.Q., Liu, H.Q., 2021. Influences of NH_3 and AWC on the Formation of SNA in $PM_{2.5}$ in Winter and Sensitivity Analysis.Research of Environmental Sciences, 34(5),1053-1062. (in Chinese)

Meng, J., Li, Z., Zhou, R., Chen, M., Li, Y., Yi, Y., Ding, Z., Li, H., Yan, L., Hou, Z., Wang, G., 2021. Enhanced photochemical formation of secondary organic aerosols during the COVID-19 lockdown in Northern China. Science of The Total Environment 758, 143709.

Ng, C.F.S., Hashizume, M., Obase, Y., Doi, M., Tamura, K., Tomari, S., Kawano, T., Fukushima, C., Matsuse, H., Chung, Y., Kim, Y., Kunimitsu, K., Kohno, S., Mukae, H., 2019. Associations of chemical composition and sources of $PM_{2.5}$ with lung function of severe asthmatic adults in a low air pollution environment of urban Nagasaki, Japan. Environmental pollution 252, 599-606.

Quan, J., Zhang, X., 2008. Assessing the role of ammonia in sulfur transformation and deposition in China. Atmospheric Research 88, 78-88.

Roberts, G., Wooster, M.J., 2021. Global impact of landscape fire emissions on surface level $PM_{2.5}$ concentrations, air quality exposure and population mortality. Atmospheric Environment 252, 118210.

Roig Rodelas, R., Perdrix, E., Herbin, B., Riffault, V., 2019. Characterization and variability of inorganic aerosols and their gaseous precursors at a suburban site in northern France over one year (2015–2016). Atmospheric Environment 200, 142-157.

San Martini, F.M., West, J.J., de Foy, B., Molina, L.T., Molina, M.J., Sosa, G., McRae, G.J., 2005. Modeling inorganic aerosols and their response to changes in precursor concentration in Mexico City. Journal of the Air & Waste Management Association 55, 803-815.

Song, Q., Osada, K., 2021. Direct measurement of aerosol acidity using pH testing paper and hygroscopic equilibrium under high relative humidity. Atmospheric Environment 261, 118605.

Sudheer, A.K., Rengarajan, R., 2015. Time-resolved inorganic chemical composition of fine aerosol and associated precursor gases over an urban environment in western India: Gas-aerosol equilibrium characteristics. Atmospheric Environment 109, 217-227.

Sun, Y., Wang, Z., Wild, O., Xu, W., Chen, C., Fu, P., Du, W., Zhou, L., Zhang, Q., Han, T., Wang, Q., Pan, X., Zheng, H., Li, J., Guo, X., Liu, J., Worsnop, D.R., 2016. "APEC Blue": Secondary Aerosol Reductions from Emission Controls in Beijing. Scientific reports 6, 20668.

Tan, H., Cai, M., Fan, Q., Liu, L., Li, F., Chan, P.W., Deng, X., Wu, D., 2017. An analysis of aerosol liquid water content and related impact factors in Pearl River Delta. The Science of the total environment 579, 1822-1830.

Tan, K.C., San Lim, H., Jafri, M.Z.M., 2016. Prediction of column ozone concentrations using multiple regression analysis and principal component analysis techniques: A case study in peninsular Malaysia. Atmospheric Pollution Research 7, 533-546.

Walker, J.T., Robarge, W.P., Shendrikar, A., Kimball, H., 2006. Inorganic $PM_{2.5}$ at a U.S. agricultural site. Environmental pollution 139, 258-271.

Wang, H., Ding, J., Xu, J., Wen, J., Han, J., Wang, K., Shi, G., Feng, Y., Ivey, C.E., Wang, Y., Nenes, A., Zhao, Q., Russell, A.G., 2019. Aerosols in an arid environment: The role of aerosol water content, particulate acidity, precursors, and relative humidity on secondary inorganic aerosols. The Science of the total environment 646, 564-572.

Wang, J., Zhang, X., Zhang, K., Zheng, Z., 2018. Characterization of size distribution and concentration of atmospheric particles during summer in Zhuzhou, China. Polish Journal of Environmental Studies 27, 2793-2800.

Wen, Z., Xu, W., Pan, X., Han, M., Wang, C., Benedict, K., Tang, A., Collett Jr, J.L., Liu, X., 2021. Effects of reactive nitrogen gases on the aerosol formation in Beijing from late autumn to early spring. Environmental Research Letters. https://doi.org/10.1088/1748-9326/abd973.

West, J.J., Ansari, A.S., Pandis, S.N., 1999. Marginal $PM_{2.5}$: Nonlinear Aerosol Mass Response to Sulfate Reductions in the Eastern United States. Journal of the Air & Waste Management Association 49, 1415-1424.

Wu, Z., Wang, Y., Tan, T., Zhu, Y., Li, M., Shang, D., Wang, H., Lu, K., Guo, S., Zeng, L., Zhang, Y., 2018. Aerosol Liquid Water Driven by Anthropogenic Inorganic Salts: Implying Its Key Role in Haze Formation over the North China Plain. Environmental Science & Technology Letters 5, 160-166.

Xu, L., Duan, F., He, K., Ma, Y., Zhu, L., Zheng, Y., Huang, T., Kimoto, T., Ma, T., Li, H., Ye, S., Yang, S., Sun, Z., Xu, B., 2017. Characteristics of the secondary water-soluble ions in a typical autumn haze in Beijing. Environmental pollution 227, 296-305.

Xu, Z., Liu, M., Zhang, M., Song, Y., Wang, S., Zhang, L., Xu, T., Wang, T., Yan, C., Zhou, T., Sun, Y., Pan, Y., Hu, M., Zheng, M., Zhu, T., 2019. High efficiency of livestock ammonia emission controls

in alleviating particulate nitrate during a severe winter haze episode in northern China. Atmos. Chem. Phys. 19, 5605-5613.

Xue, M., Ma, J., Yan, P., Pan, X., 2011. Impacts of pollution and dust aerosols on the atmospheric optical properties over a polluted rural area near Beijing city. Atmospheric Research 101, 835-843.

Yin, S., Huang, Z., Zheng, J., Huang, X., Chen, D., Tan, H., 2018. Characteristics of inorganic aerosol formation over ammonia-poor and ammonia-rich areas in the Pearl River Delta region, China. Atmospheric Environment 177, 120-131.

Zhang, X., Eto, Y., Aikawa, M., 2021a. Risk assessment and management of $PM_{2.5}$-bound heavy metals in the urban area of Kitakyushu, Japan. Science of The Total Environment 795, 148748.

Zhang, X., Murakami, T., Wang, J., Aikawa, M., 2021b. Sources, species and secondary formation of atmospheric aerosols and gaseous precursors in the suburb of Kitakyushu, Japan. Science of The Total Environment 763, 143001.

Zhang, X., Zhang, K., Liu, H., Lv, W., Aikawa, M., Liu, B., Wang, J., 2020. Pollution sources of atmospheric fine particles and secondary aerosol characteristics in Beijing. Journal of Environmental Sciences 95, 91-98.

Zhang, X., Zhang, K., Lv, W., Liu, B., Aikawa, M., Wang, J., 2019. Characteristics and risk assessments of heavy metals in fine and coarse particles in an industrial area of central China. Ecotoxicology and environmental safety 179, 1-8.

Zhang, Z., Wang, W., Cheng, M., Liu, S., Xu, J., He, Y., Meng, F., 2017. The contribution of residential coal combustion to $PM_{2.5}$ pollution over China's Beijing-Tianjin-Hebei region in winter. Atmospheric Environment 159, 147-161.

Chapter 4: Risk assessment and management of PM$_{2.5}$-bound heavy metals

4.1 Introduction

Over the past few decades, atmospheric particle pollution has become one of the most serious environmental problems on a global scale (Onishi et al., 2012; Molepo et al., 2019; Eck et al., 2020; Kasimov et al., 2020; Zhang et al., 2020). How dangerous an atmospheric particle is for the environment and living organisms largely depends on its size distribution and inner chemical components (Behrooz et al., 2021). As compared with coarse-mode particles, fine-mode particles (PM$_{2.5}$) are characterized by higher surface/mass ratio; thus, their ability to adsorb harmful substances is relatively strong, which can cause greater risk for the ecological system (Li et al., 2019; Tsai et al., 2020; Xie et al., 2020). PM$_{2.5}$ mainly includes organic matter, secondary inorganic ions, element carbon, heavy metals, and liquid water (Kasimov et al., 2020; Fan et al., 2021), among which heavy metals have induced great interest due to their high toxicity, persistence, biological accumulation, and complicated sources (Ali et al., 2019; Duan et al., 2020; Moryani et al., 2020; Tsai et al., 2020). Many toxicological experiments have confirmed that excessive exposure to PM$_{2.5}$-bound heavy metals could threaten human health, causing respiratory irritation and inflammation, lung disease, cardiovascular disease, heart disease, and even cancer (Roy et al., 2019; Tsai et al., 2020; Xie et al., 2020; Xu et al., 2020). The main pathways of exposure to PM$_{2.5}$-bound heavy metals are oral ingestion, inhalation, and dermal contact (Hu et al., 2012; Jiang et al., 2018; Liu and Ren, 2019; Xu et al., 2020). At present, the risk assessment of heavy metals is focused mainly on cities and regions with severe particle pollution and large quantities of industrial emissions, especially in China (Hu et al., 2012; Jiang et al., 2018; Wang et al., 2018b; Cui et al., 2019; Li et al., 2019; Duan et al., 2020; Hao et al., 2020; Xie et al., 2020). By comparison, the concentration level of PM$_{2.5}$ in Japan was relatively low (Khan et al., 2010; Inomata et al., 2016; Phung et al., 2020; Ikemori et al., 2021), and domestic research has given priority to the

physical/chemical characteristics, spatiotemporal variation, and source apportionment of particle-bound heavy metals, rather than risk assessment (Wang et al., 2005; Wang et al., 2006; Moreno et al., 2012; Hidemori et al., 2014; Nakatsubo et al., 2020; Suzuki et al., 2021). However, a low concentration of $PM_{2.5}$ does not signify a lower health risk (Chen et al., 2021); hence, it is necessary and important to renew the analysis about the potential ecological risk and human health risk of $PM_{2.5}$-bound heavy metals in Japan.

Kitakyushu City is a well-known urbanized and industrial area in Japan with about one million inhabitants; the atmospheric particles in this area could be double influenced by local emissions from the Kyushu area of Japan and trans-boundary transport from the Asian continent (Zhang et al., 2021). Hence, heavy metals loaded in atmospheric particles have complex sources (crustal dust, vehicle exhaust, ship emissions, coal combustion, industrial production and mining, municipal waste incineration, construction activities, etc. (Kaneyasu et al., 2014; Wen et al., 2018; Duan et al., 2020; Tsai et al., 2020; Zhi et al., 2021)), and their risk levels are worthy of in-depth investigation. In this study, $PM_{2.5}$ samples were collected in the coastal urban area of Kitakyushu City from May 2013 to February 2019, with the main objectives as follows: (1) to investigate the specific concentration levels and inner relationship of 29 heavy metals; (2) to evaluate the integrated environmental risk around the sampling site; (3) to assess the non-carcinogenic and carcinogenic risk posed to adults and children via oral ingestion, inhalation, and dermal contact; and (4) to identify the high-risk metal sources and their potential pollution source regions. Our comprehensive study about $PM_{2.5}$-bound heavy metals could provide scientific reference for the formulation of targeted risk-mitigation and pollution-control strategies to improve the ambient air quality of the urban area of Kitakyushu, Japan.

4.2 Materials and Methods

4.2.1 Sampling

The PM$_{2.5}$ sampling campaign was carried out at Kitakyushu's monitoring station (33.89° N, 130.85° E), as shown in Fig. 4-1. This sampling site is located in the coastal urban area of Kitakyushu City, which is (1) one of the largest industrial cities in Japan, (2) an important transport hub between Kyushu and Honshu, and (3) on the western edge of Japan, being located on the forefront of transboundary transportation from the Asian landmass (Zhang et al., 2021). The whole sampling period lasted six years (from May 2013 to February 2019), during which time particle samplings were conducted for two weeks in each season using a low-volume air sampler (Model LV-250R, Sibata Scientific Technology Ltd., Japan) with a flow rate of 16.7 L·min^{-1}. The duration of collection for each particle sample was about 23 h (starting at 11:00 a.m. (Japan Standard Time) and ending at 10:00 a.m. the next day); hence, a total of 336 samples were collected.
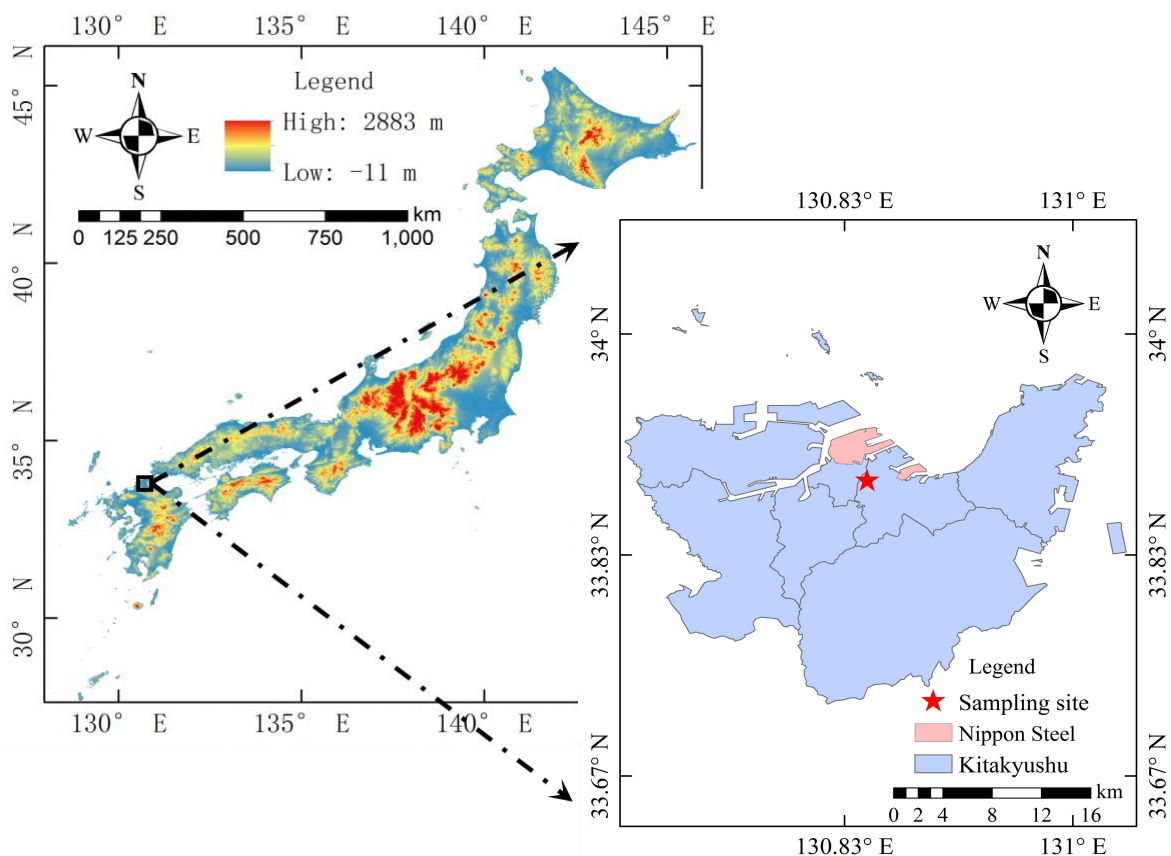

Fig. 4-1 Location of sampling site

4.2.2 Chemical analysis

After sampling, each polytetrafluoroethylene (PTFE) filter was put in plastic case and kept in Lamizip (AL-9, Seisannipponsha, Ltd., Fukuoka, Japan). These samples were then stored in the freezer at a temperature of -30 °C. During pretreatment processes, each loaded filter was cut off and put into a Teflon vessel, and 5 mL of HNO_3, 2 mL of HF, and 1 mL of H_2O_2 were added; subsequently, the collected $PM_{2.5}$ was digested by means of a microwave digestion system (MARS 5Plus, CEM Japan K.K., Tokyo, Japan). After cooling, these solutions were diluted to 5 mL with 5% HNO_3 for use in the following chemical analysis. In this study, 29 heavy metals (Na, Fe, Zn, Al, Ca, K, Ti, Ni, Cu, Cr, Pb, Mn, Ba, Mo, Sb, W, Co, V, Sc, Se, As, Rb, Ce, Ta, Hf, La, Cs, Sm, and Th) were measured by inductively coupled plasma mass spectrometry (Agilent 7800 ICP-MS, Agilent Technologies, Santa Clara, CA, USA), with corresponding detection limits of 11.0, 11.0, 7.5, 7.1, 7.0, 4.1, 4.0, 2.3, 0.6, 0.6, 0.4, 0.4, 0.2, 0.1, 0.1, 0.1, 0.04, 0.03, 0.02, 0.01, 0.01, 0.01, 0.01, 0.01, 0.01, 0.01, 0.004, 0.003, 0.003 $ng \cdot m^{-3}$, respectively, and the recoveries of these metals were all within the target range (85%-115%). In addition, the mass concentrations of $PM_{2.5}$ during the corresponding period were determined by $PM_{2.5}$ monitor (PM-712, Kimoto Electric Co., Ltd., Osaka, Japan). The methods for sampling and analyzing $PM_{2.5}$ and heavy metals, as well as the quality assurance (QA) and quality control (QC) measures, were in accordance with the $PM_{2.5}$ component measurement manual established by the Ministry of the Environment of Japan (2019).

4.2.3 Statistical analysis and model calculation

4.2.3.1 Pearson's correlation analysis and hierarchical cluster analysis

Pearson's correlation analysis was performed by using IBM SPSS Statistics 20.0. The correlation coefficient in this study showed the strength of the linear relationship between two heavy metals in $PM_{2.5}$. Then, hierarchical cluster analysis (HCA) was run using Ward as the cluster method and the

Pearson's correlation coefficient (r) as the distance type (Pietrogrande et al., 2018; Govender and Sivakumar, 2020). Heavy metals with relatively high correlations were classified as one category; subsequently, two categories with the highest similarity were merged into a new category. Finally, the results were shown in a dendrogram, where the shorter the distance between the branches, the more significant the association (Zhong et al., 2016; Zhang et al., 2021).

4.2.3.2 Enrichment factor and geo-accumulation index

To assess the contamination level of each heavy metal in PM$_{2.5}$ and identify whether it was mainly from a natural or anthropogenic source, the enrichment factors (EF) and geo-accumulation index (Igeo) were calculated and are expressed as follows:

$$EF = (\frac{C_{sample}^{i}}{C_{sample}^{ref}})/(\frac{C_{crust}^{i}}{C_{crust}^{ref}}), \tag{4-1}$$

$$I_{geo} = \log_2 \frac{C_{sample}^{i}}{1.5 \times C_{crust}^{i}}, \tag{4-2}$$

where C_{sample}^{i} and C_{crust}^{i} stand for the concentration of the i$_{th}$ metal in PM$_{2.5}$ and the earth crust, respectively; C_{sample}^{ref} and C_{crust}^{ref} represent the reference concentration in PM$_{2.5}$ and the earth crust, respectively. In this study, Ti was selected as the reference element (Zhang et al., 2019) (Fig. S4), and the specific concentration values of 29 heavy metals in the earth crust were obtained from Lide (2008).

4.2.3.3 Ecological risk index

The high enrichment of heavy metals in the environment not only breaks the balance of natural ecosystems but also has toxic effects on microorganisms, plants, animals, and humans (Wang et al., 2018a; Chen et al., 2020). The ecological risk index (RI) has been used extensively to evaluate the degree of particle-bound heavy metal pollution (Bai et al., 2019; Alves et al., 2020; Zhi et al., 2021). This parameter considers the specific concentrations of heavy metals and their toxicity responses and is expressed as follows:

$$RI = \sum_{i=1}^{m} E_r^i,$$ (4-3)

$$E_r^i = T_r^i \times \frac{C_{sample}^i}{C_{crust}^i},$$ (4-4)

where E_r^i is the potential ecological risk coefficient of the i_{th} metal, and T_r^i is the i_{th} metal's toxic response factor, which was related to its release capability and the relative abundance in different media (igneous rock, soil, fresh water, terrestrial plant, terrestrial animal, etc.) (Liu et al., 2018; Wang et al., 2018a; Chen et al., 2020; Liu et al., 2021). The detailed information about T_r^i for the anthropogenic metals identified in this study can be seen in Table S2. According to previous research, if RI<150, there is low ecological risk around the sampling site; 150≤RI<300, 300≤ RI<600, and RI≥600 indicate moderate ecological risk, considerable ecological risk, and very high ecological risk, respectively. For individual metals, the potential ecological risk can be divided into five levels based on their E_r^i values, namely, low risk (E_r^i <40), moderate risk (40≤ E_r^i <80), considerable risk (80≤ E_r^i <160), high risk (160≤ E_r^i <320), and extremely high risk (E_r^i ≥320) (Li et al., 2018; Zhi et al., 2021).

4.2.3.4 Health risk assessment

Residents living in Kitakyushu, Japan are potential receptors of heavy metals in PM$_{2.5}$. Due to the difference on their behaviors and respiratory systems, we divided the subjects into two groups: children (0-15 years) and adults (Hu et al., 2012; Behrooz et al., 2021). The chemical daily intake through oral ingestion (CDI$_{ing}$, mg·(kg·day)$^{-1}$), exposure concentration through inhalation (EC$_{inh}$, μg·m^{-3}), and dermal absorption dose through dermal contact (DAD$_{der}$, mg·(kg·day)$^{-1}$) were calculated as follows:

$$CDI_{ing} = C_{95\%} \times \frac{\text{IngR} \times \text{EF} \times \text{ED} \times \text{CF}}{\text{BW} \times \text{AT}},$$ (4-5)

$$EC_{inh} = C_{95\%} \times \frac{\text{ET} \times \text{EF} \times \text{ED}}{\text{AT}_n},$$ (4-6)

$$DAD_{der} = C_{95\%} \times \frac{\text{SA} \times \text{AF} \times \text{ABS} \times \text{EF} \times \text{ED} \times \text{CF}}{\text{BW} \times \text{AT}},$$ (4-7)

$$C_{95\%} = \exp(\overline{\ln X} + 0.5 \times S_{\ln X}^2 + \frac{S_{\ln X} \times H_{0.95}}{\sqrt{n-1}}),$$ (4-8)

where $C_{95\%}$ means the reasonable maximum exposure (95% upper confidence limit) in the urban area of Kitakyushu, Japan. In Eq. (4-8), $\overline{\ln X}$ and $S_{\ln X}$ are the arithmetic mean and standard deviation of the log-transformed concentration data, respectively; n is the number of samples; and $H_{0.95}$ values depend on $S_{\ln X}$, n, and the chosen confidence level (0.05), which could be obtained from Gilbert (1987). The description and specific values of other parameters in Eqs. (4-5~4-7) are shown in Table S3. The corresponding hazard quotient (HQ) and carcinogenic risk (CR) of toxic metals through the three pathways were further evaluated based on Eqs. (9–14).

$$HQ_{ing} = \frac{CDI_{ing}}{RfD_o}, \quad HQ_{inh} = \frac{EC_{inh}}{RfCi \times 1000}, \quad HQ_{der} = \frac{DAD_{der}}{RfD_o \times GIABS}, \qquad (4\text{-}9\sim4\text{-}11)$$

$$CR_{ing} = CDI_{ing} \times SF_o, \quad CR_{inh} = EC_{inh} \times IUR, \quad CR_{der} = \frac{DAD_{der} \times SF_o}{GIABS}, \qquad (4\text{-}12\sim4\text{-}14)$$

where RfDo, RfCi, GIABS, SFo, and IUR are the oral reference doses $(mg \cdot (kg \cdot day)^{-1})$, inhalation reference concentration $(mg \cdot m^{-3})$, gastrointestinal absorption factor, oral slope factor $((mg \cdot (kg \cdot day)^{-1})^{-1})$, and inhalation unit risk $((\mu g \cdot m^{-3})^{-1})$, respectively (Table S2). A hazard index (HI), i.e., the sum of the HQ, is used to assess the non-carcinogenic risks (chronic effects). When both HQs≤1.0 and HI≤1.0, there is no significant risk of chronic effects. Conversely, HQ>1 or HI>1 indicates that there is a chance that chronic effects will occur. The CR value reveals the probability that an individual will develop any type of cancer from a lifetime of exposure to carcinogenic metals, which can be categorized as very low $(CR \leq 10^{-6})$, low $(10^{-6} \leq CR < 10^{-4})$, moderate $(10^{-4} \leq CR < 10^{-3})$, high $(10^{-3} \leq CR < 10^{-1})$, and very high $(CR \geq 10^{-1})$ (Hu et al., 2012; Roy et al., 2019; Behrooz et al., 2021).

4.2.3.5 Concentration-weighted trajectory analysis (CWT)

TrajStat software was used to generate air mass trajectory in this study, with the arriving height, start hour, and backward time setting as 1500 m, 14:00 (UTC), and 72 h, respectively. Hence, 336 backward trajectories were obtained. Then we added the daily concentration data of high-risk metals to the corresponding trajectories. Finally, the CWT value of each grid was calculated, and the areas with high

CWT values could be explained as potential pollution source regions. More detailed information was shown in our previous research (Zhang et al., 2021).

4.3 Results and discussion

4.3.1 Characteristics of heavy metals

During the whole sampling period, $PM_{2.5}$ mass concentration in the urban area of Kitakyushu, Japan, ranged from 6.3 $\mu g \cdot m^{-3}$ to 57.5 $\mu g \cdot m^{-3}$, with a median value of 21.3 $\mu g \cdot m^{-3}$. About 76% of the daily $PM_{2.5}$ concentration exceeded the annual National Ambient Air Quality Standards of the United State Environmental Protection Agency (15 $\mu g \cdot m^{-3}$), while 94% in respect of the air quality guidelines of the World Health Organization (10 $\mu g \cdot m^{-3}$). The sum concentration of 29 heavy metals identified in this study was about 628.4 $ng \cdot m^{-3}$, accounting for 3% of $PM_{2.5}$. Compared with the typical cities of China (Table S4), the mass concentration of $PM_{2.5}$ in this sampling site was obviously low, however, the proportion of loaded heavy metals still showed medium level. To be specific, Na, Fe, K, Al, Ca, Zn, and Pb showed relatively high loading concentrations in $PM_{2.5}$, with median values of 144.9, 140.0, 101.1, 41.5, 30.7, 29.5, and 10.5 $ng \cdot m^{-3}$, respectively, and their sum concentration could occupy approximately 91% of the total concentration of heavy metals (Table S5). In comparison, Mn, V, Ti, Cu, Ni, Cr, Ba, Mo, As, and Se exhibited medium loading levels, and their concentrations were 8.3, 5.7, 4.4, 3.6, 3.3, 3.0, 2.1, 1.5, 1.4, and 1.0 $ng \cdot m^{-3}$, respectively. With the exception of the metals mentioned above, other metals had extremely low contributions (only accounting for 0.4% of the total concentration of heavy metals), and the concentration levels ranked in the deceasing order of Sb>Rb>W>La>Co>Ce>Cs>Hf>Sc>Th>Ta>Sm.

To better understand the relationship among 29 heavy metals and further identify their sources, the HCA, enrichment factor, and geo-accumulation index were combined. From Fig. 4-2, it can be seen that the first cluster (C1) included Al, Th, Ce, Sm, and Ca, among which there were strong correlations, with

the r values larger than 0.59. Of these five metals, only Al and Ca had high loading levels in $PM_{2.5}$, and their concentrations in spring (132.6 ng·m^{-3} and 77.3 ng·m^{-3}) were obviously higher than those in the other three seasons. Moreover, the EF values of Al and Ca were 0.6 and 1.0, and their Igeo values were -5.2 and -4.5, respectively (Fig. 4-3). Zhang et al. (2021) has confirmed that dust was one of the important pollution sources for atmospheric particles in Kitakyushu, Japan, and the air masses in spring carried the highest concentrations of dust from the Asian landmass to the sampling site. In our study, the Al and Ca, as the typical crustal elements (Hu et al., 2014; Zhang et al., 2018; Gaonkar et al., 2019), also had the highest concentrations in spring, which revealed that the source of heavy metals in the first cluster was crustal dust from the Asian landmass. The second cluster (C2) consisted of Fe, Mn, Zn, K, Pb, As, Se, Rb, and Cs. Of these nine heavy metals, Zn, Pb, As, Se, and Cs were important anthropogenic metals, with corresponding EF values of 509.8, 818.5, 788.0, 23339.2, and 28.6; and Igeo values of 4.5, 5.2, 5.3, 10.1, and 0.5; respectively. Zn and Pb were derived from traffic sources (Lin et al., 2015; Han and Lu, 2017; Shi and Lu, 2018); moreover, these two heavy metals had high correlations with As (0.58 and 0.60, respectively), Se (0.58 and 0.69, respectively), and Cs (0.38 and 0.60, respectively) in this study, therefore revealing that vehicle exhaust was the main source of the anthropogenic metals in C2. In addition, the other four metals (Fe, Mn, K, and Rb) were identified as natural metals, which had EF values lower than 10 and Igeo values lower than 0. The source of Fe was generally considered to be industrial emissions in Kitakyushu, Japan, because the Nippon Steel Corporation, one of the largest steel company, was located near our sampling site (Fig. 4-1). In contrast, our results likely suggest Fe came from a natural source (road dust), taking the previous studies (Yang et al., 2016; Juda-Rezler et al., 2020) into account. However, as Ti was selected as the reference element in this study and further both Fe and Ti are the indicator for road dust and steel industry, the discrimination and correct determination for industrial emission from steel company had some difficulty; therefore, the

possibility on the influence from industrial emission (steel company) also still remains. The third cluster (C3) was composed of six natural metals (Na, Ba, Ti, Ta, La, and Co) and seven anthropogenic metals (Cu, V, Sb, Ni, Cr, Mo, and W). Of the natural metals in C3, Na had the highest concentration, which was about 21.8 times higher than the sum of concentrations of the other five metals. Taking the geographic location of our sampling site into consideration, the Na observed in this study was mainly from sea salts and was carried by the air mass from the Sea of Japan or the Pacific Ocean. Among anthropogenic metals in C3, V is a key marker for heavy fuel oil (HFO) combustion, and the V/Ni ratio herein was approximately 2.9, which is consistent with that for typical shipping emissions (Hadley, 2017; Tsai et al., 2020). Zhang et al. (2021) also observed the influence of ship emissions in Kitakyushu, Japan, which can also support our consideration that ship emissions played an important role for seven (Cu, V, Sb, Ni, Cr, Mo, and W) metals. The last cluster (C4) only consisted of Hf and Sc; these two metals basically had extremely low concentration levels during the whole sampling period, with a median value of 0.01 ng·m^{-3}, but simultaneously reached the highest concentrations (10.0 ng·m^{-3} and 2.5 ng·m^{-3}, respectively) on November 1, 2017. This demonstrated that the influence of this source was very low and not stable, having great uncertainty; hence we excluded this source in this study.
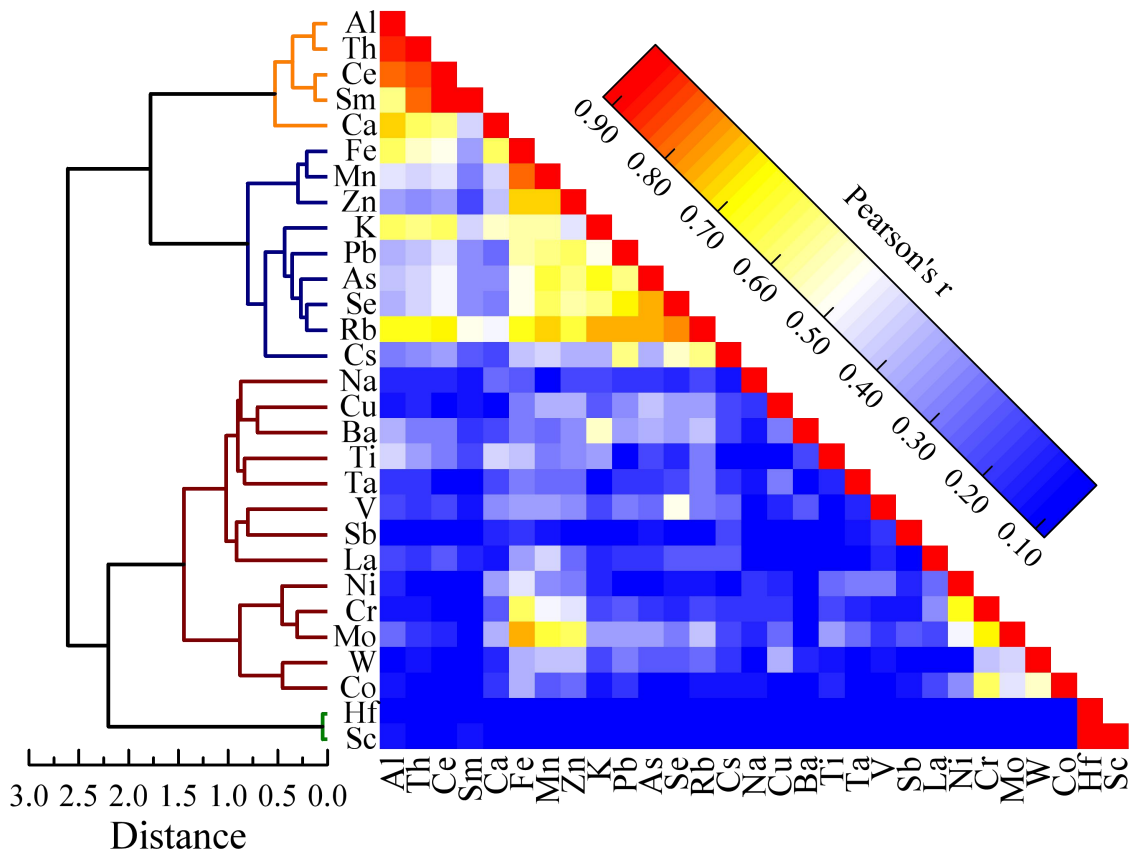
Fig. 4-2 Pearson's correlation matrix coupled with hierarchical clustering results for 29 heavy metals in PM$_{2.5}$.
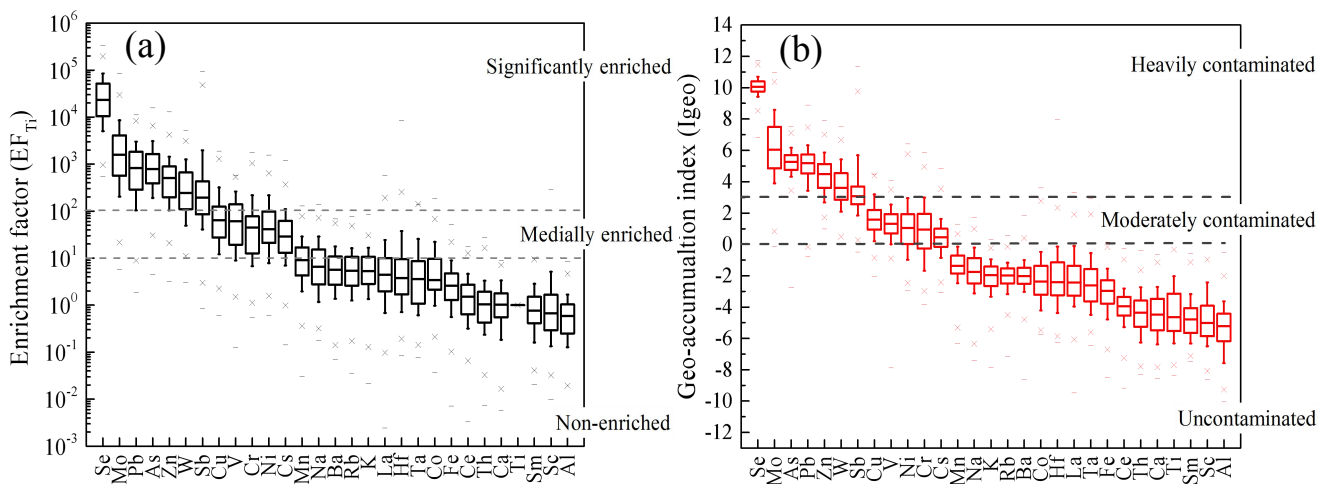
Fig. 4-3 Enrichment factors (a) and Geo-accumulation indexes (b) of 29 heavy metals in PM$_{2.5}$.

4.3.2 Risk assessment

4.3.2.1 Environmental risk

As compared with emissions from natural sources, those from anthropogenic sources must be significantly controlled as much as possible. The comprehensive evaluation of the risk levels of

anthropogenic metals can provide information for risk management around the sampling site that is more valuable than that for metals from natural sources. In this study, Se, Mo, Pb, As, Zn, W, Sb, Cu, V, Cr, Ni, and Cs were identified as anthropogenic metals that had EF values larger than 10 and Igeo values larger than 0 (Fig. 4-3); thus, the following analysis regarding environmental risk assessment mainly focused on these 12 metals.

From Fig. 4-4, it can be clearly seen that Mo, Se, and As were the top risk contributors, with median E_r^i values of 1079.5, 992.2, and 364.4, respectively. Correspondingly, the statistical percentage of each risk level for all samples further showed that Mo, Se, and As, respectively, had extremely high risk with 83%, 98%, and 59% probability; high risk with 8%, 1%, and 31% probability; considerable risk with 5%, 1%, and 8% probability; and moderate risk with 2%, 0%, and 1% probability. In addition, Pb showed high risk (E_r^i: 177.7), and Sb showed considerable risk (E_r^i: 105.9) for the environment at the sampling site. To be specific, the proportions of the samples with extremely high risk, high risk, considerable risk, and moderate risk were 14%, 40%, 25%, and 10% for Pb; and 14%, 11%, 43%, and 23% for Sb, respectively. Meanwhile, the environmental risks caused by Zn, Cu, Ni, V, and Cr were slight, and their contributions could be neglected, with corresponding E_r^i values of 20.1, 13.1, 9.6, 4.5, and 3.2, respectively, which were all obviously lower than 40. Overall, the comprehensive ecological risk index for 12 anthropogenic metals, i.e., the sum of each E_r^i, was far greater than 600, revealing that there was severe metal pollution and very high ecological risk in the urban area of Kitakyushu, Japan, which merits serious attention, especially for Mo, Se, As, Pb, and Sb.
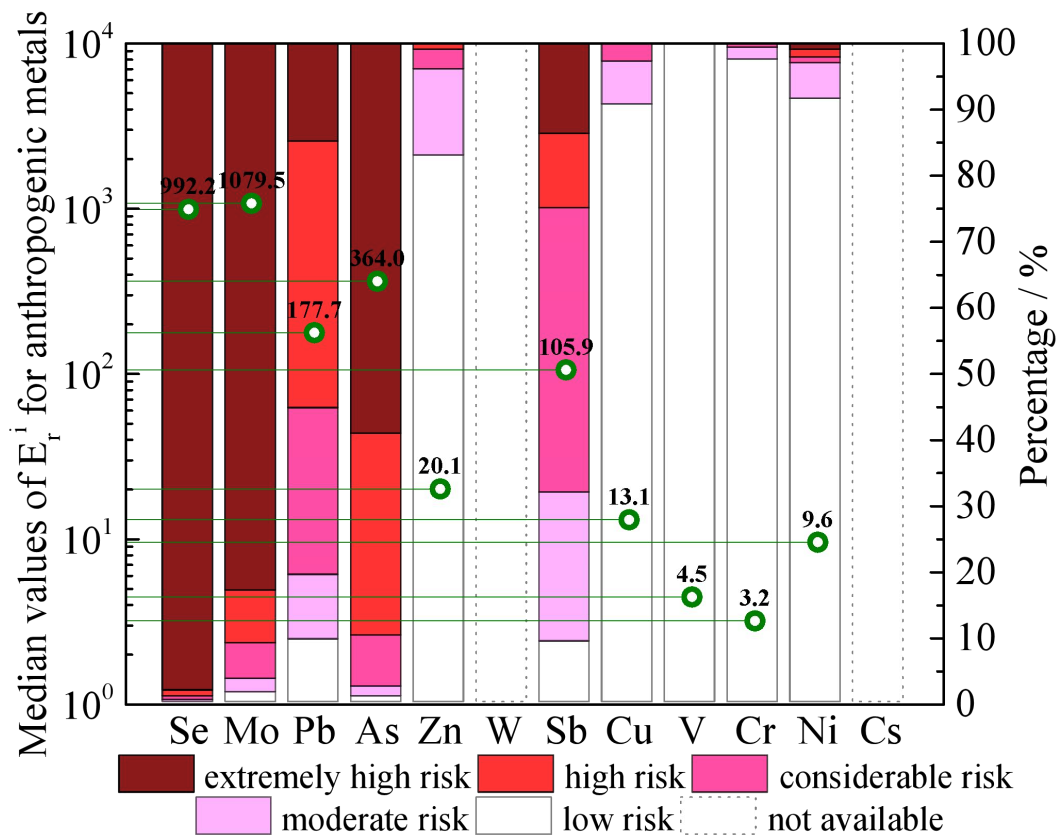
Fig. 4-4 Median E_r^i values of anthropogenic metals in PM$_{2.5}$ and statistical percentage of each risk level for 336 samples.

4.3.2.2 Human health risk

The harm of heavy metals to humans is an important part of the total environmental risk, which has attracted public attention in recent years (Guo et al., 2010; Jiang et al., 2018; Hu et al., 2012; Liu and Ren, 2019; Chen et al, 2020; Xu et al., 2020). The human health risk through different exposure pathways in the urban area of Kitakyushu, Japan, is worth in-depth investigation. Table 4-1 further shows the health risks caused by these 12 anthropogenic metals in PM$_{2.5}$. For adults, the contributions of the studied metals decreased in the following order: As>Pb>Sb>V>Ni>Mo>Cr(VI)>W>Se>Zn>Cu>Cs, and the total HI value of 1.0 for these 12 metals revealed that the integrated effects of multi-metal exposure in the urban area of Kitakyushu, Japan, might not result in severe non-carcinogenic risk. HI$_{Ing}$, HI$_{Inh}$, and HI$_{Der}$ were 0.7, 0.2, and 0.2, respectively, indicating that oral ingestion was the primary exposure pathway, followed by dermal contact and inhalation. This phenomenon was related to the differences of heavy metal accumulation amounts in human body through three exposure pathways and

the sensitivities of heavy metals for their target organs (Tchounwou et al., 2012; Sah et al., 2019); our result is consistent with previous research (Fang et al., 2013; MohseniBandpi et al., 2018; Wang et al., 2018b; Zhang et al., 2019). In addition, among these 12 heavy metals, Cr(VI), As, Pb, and Ni were the carcinogens (IARC, 2016; Megido et al., 2017), and their CR values were 3.6×10^{-5}, 3.5×10^{-5}, 2.4×10^{-6}, and 2.8×10^{-7}, respectively. The most important exposure pathway for Cr(VI) and Ni was inhalation, while that for As and Pb was oral ingestion. In total, the integrated carcinogenic risk for adults (7.3×10^{-5}) was also within the acceptable/tolerable limits (Hu et al., 2012; Xu et al., 2020), and CR_{Ing}, CR_{Inh}, and CR_{Der} accounted for 53%, 26%, and 21%, respectively.

As compared with adults, the particle exposure to children is relatively high because of their playing activities, hand to mouth habit and licking objects which may be contaminated (Ali et al., 2017). Mostly children are more susceptible to adsorption of heavy metal from the digestion system, and the hemoglobin sensitivity to heavy metals are much higher than those of adults due to children's body at early ages and lower body weight (Sah et al., 2019). Hence, children living in the urban area of Kitakyushu, Japan, faced significantly higher health risks than adults. To be specific, the total HI for children (7.8) was obviously higher than the safe level, and the HQ_{ing} had the highest proportion (78%), which was similar to the result (79%) of Fan et al. (2021) in Beijing, China. The high non-carcinogenic risk in this study was mainly caused by As, Pb, and Sb, with corresponding HI values of 2.0, 1.9, and 1.9, respectively. Moreover, for these three heavy metals, the HQ values through different exposure pathways had the same trends—oral ingestion>dermal contact>inhalation—and the proportion of non-carcinogenic risk posed by oral ingestion could reach 84% (ranging from 78% to 89%); hence, countermeasures for reducing the particle exposure risk caused by oral ingestion are most effective for the children around our study area (the specific suggestions are shown in section 4.3.4). For children's carcinogenic risk, the total CR value for multi-metal exposure was 1.2×10^{-4}, which was obviously lower

than that in typical cities of China (Table S6). However, the risk level in this study was still above the safe level (1.0×10^{-4}), revealing a moderate carcinogenic risk for children living in the urban area of Kitakyushu, Japan. Among four carcinogens, the contribution of As to the total CR for children was highest (7.6×10^{-5}, 63%), and those of CR_{Ing}, CR_{Inh}, and CR_{Der} were 92%, 0.5%, and 8%, respectively. In addition, the contribution of Cr(VI) was also relatively high (4.0×10^{-5}, 33%), and dermal contact was the most important exposure pathway for Cr(VI), accounting for 47%, followed by oral ingestion (42%) and inhalation (11%). In contrast, the contributions of Pb and Ni were relatively low and could be neglected (4.9×10^{-6} and 6.9×10^{-8}, only occupying 4% and 0.1%, respectively).

Table 4-1 Health risks for adults and children due to the exposure of anthropogenic metals (Bold: Value above the safe level).

Resident	Metal	Non-Carcinogenic risk							Carcinogenic risk						
		CDI	EC	DAD	HQ$_{ing}$	HQ$_{inh}$	HQ$_{der}$	HI	CDI	EC	DAD	CR$_{ing}$	CR$_{inh}$	CR$_{der}$	CR
Adults	Se	4.0×10^{-5}	6.7×10^{-4}	1.6×10^{-6}	0.0	0.0	0.0	0.0	1.4×10^{-5}	2.3×10^{-4}	5.4×10^{-7}				
	Mo	1.8×10^{-4}	2.6×10^{-3}	7.0×10^{-6}	0.0	0.0	0.0	0.0	6.0×10^{-5}	8.8×10^{-4}	2.4×10^{-6}				
	Pb	5.7×10^{-4}	9.8×10^{-3}	2.3×10^{-4}	0.2	0.0	0.1	0.2	1.9×10^{-4}	3.4×10^{-3}	7.8×10^{-5}	1.7×10^{-6}	4.0×10^{-8}	6.6×10^{-7}	2.4×10^{-6}
	As	5.8×10^{-5}	9.5×10^{-4}	6.9×10^{-6}	0.2	0.1	0.0	0.3	2.0×10^{-5}	3.3×10^{-4}	2.4×10^{-6}	3.0×10^{-5}	1.4×10^{-6}	3.6×10^{-6}	3.5×10^{-5}
	Zn	1.5×10^{-3}	2.3×10^{-2}	5.9×10^{-5}	0.0	0.0	0.0	0.0	5.1×10^{-4}	8.0×10^{-3}	2.0×10^{-5}				
	W	1.7×10^{-5}	2.6×10^{-4}	6.6×10^{-7}	0.0		0.0	0.0	5.7×10^{-6}	8.8×10^{-5}	2.3×10^{-7}				
	Sb	6.7×10^{-5}	1.1×10^{-3}	2.7×10^{-6}	0.2	0.0	0.0	0.2	2.3×10^{-5}	3.8×10^{-4}	9.2×10^{-7}				
	Cu	1.8×10^{-4}	2.7×10^{-3}	7.1×10^{-6}	0.0	0.0	0.0	0.0	6.1×10^{-5}	9.3×10^{-4}	2.4×10^{-6}				
	V	2.6×10^{-4}	4.1×10^{-3}	1.0×10^{-5}	0.0	0.0	0.1	0.1	8.9×10^{-5}	1.4×10^{-3}	3.6×10^{-6}				
	Cr(VI)	4.2×10^{-5}	6.0×10^{-4}	1.7×10^{-6}	0.0	0.0	0.0	0.0	1.4×10^{-5}	2.1×10^{-4}	5.7×10^{-7}	7.2×10^{-6}	1.7×10^{-5}	1.1×10^{-5}	3.6×10^{-5}
	Ni	2.3×10^{-4}	3.1×10^{-3}	9.1×10^{-6}	0.0	0.0	0.0	0.1	7.8×10^{-5}	1.1×10^{-3}	3.1×10^{-6}		2.8×10^{-7}		2.8×10^{-7}
	Cs	3.7×10^{-6}	6.3×10^{-5}	1.5×10^{-7}					1.3×10^{-6}	2.2×10^{-5}	5.1×10^{-8}				
	SUM	3.1×10^{-3}	4.9×10^{-2}	3.3×10^{-4}	0.7	0.2	0.2	1.0	1.1×10^{-3}	1.7×10^{-2}	1.1×10^{-4}	3.9×10^{-5}	1.9×10^{-5}	1.6×10^{-5}	7.3×10^{-5}
	Se	3.7×10^{-4}	6.7×10^{-4}	1.0×10^{-5}	0.1	0.0	0.0	0.1	3.2×10^{-5}	5.8×10^{-5}	8.9×10^{-7}				
	Mo	1.6×10^{-3}	2.6×10^{-3}	4.6×10^{-5}	0.3	0.0	0.0	0.3	1.4×10^{-4}	2.2×10^{-4}	3.9×10^{-6}				
	Pb	5.3×10^{-3}	9.8×10^{-3}	1.5×10^{-3}	**1.5**	0.0	0.4	**1.9**	4.5×10^{-4}	8.4×10^{-4}	1.3×10^{-4}	3.9×10^{-6}	1.0×10^{-8}	1.1×10^{-6}	4.9×10^{-6}
	As	5.4×10^{-4}	9.5×10^{-4}	4.5×10^{-5}	**1.8**	0.1	0.2	**2.0**	4.6×10^{-5}	8.2×10^{-5}	3.9×10^{-6}	6.9×10^{-5}	3.5×10^{-7}	5.8×10^{-6}	7.6×10^{-5}
	Zn	1.4×10^{-2}	2.3×10^{-2}	3.9×10^{-4}	0.0	0.0	0.0	0.0	1.2×10^{-3}	2.0×10^{-3}	3.3×10^{-5}				
	W	1.5×10^{-4}	2.6×10^{-4}	4.3×10^{-6}	0.2		0.0	0.2	1.3×10^{-5}	2.2×10^{-5}	3.7×10^{-7}				
Children	Sb	6.3×10^{-4}	1.1×10^{-3}	1.8×10^{-5}	**1.6**	0.0	0.3	**1.9**	5.4×10^{-5}	9.4×10^{-5}	1.5×10^{-6}				
	Cu	1.7×10^{-3}	2.7×10^{-3}	4.6×10^{-5}	0.0	0.0	0.0	0.0	1.4×10^{-4}	2.3×10^{-4}	4.0×10^{-6}				
	V	2.4×10^{-3}	4.1×10^{-3}	6.8×10^{-5}	0.4	0.0	0.4	0.8	2.1×10^{-4}	3.5×10^{-4}	5.8×10^{-6}				
	Cr(VI)	3.9×10^{-4}	6.0×10^{-4}	1.1×10^{-5}	0.1	0.0	0.2	0.3	3.3×10^{-5}	5.2×10^{-5}	9.4×10^{-7}	1.7×10^{-5}	4.4×10^{-6}	1.9×10^{-5}	4.0×10^{-5}
	Ni	2.1×10^{-3}	3.1×10^{-3}	5.9×10^{-5}	0.1	0.0	0.1	0.2	1.8×10^{-4}	2.7×10^{-4}	5.1×10^{-6}		6.9×10^{-8}		6.9×10^{-8}
	Cs	3.5×10^{-5}	6.3×10^{-5}	9.8×10^{-7}					3.0×10^{-6}	5.4×10^{-6}	8.4×10^{-8}				
	SUM	2.9×10^{-2}	4.9×10^{-2}	2.2×10^{-3}	**6.2**	0.2	**1.5**	**7.8**	2.5×10^{-3}	4.2×10^{-3}	1.9×10^{-4}	9.0×10^{-5}	4.8×10^{-6}	2.6×10^{-5}	**1.2×10^{-4}**

4.3.3 Potential pollution source regions of high-risk metals

Based on the risk-assessment results, it can be clearly seen that exposure to $PM_{2.5}$ in the urban area of Kitakyushu, Japan, could exert significant influences on the ecological environment and children's health, and the high-risk metals loaded in $PM_{2.5}$ included Mo, Se, As, Pb, Sb, and Cr. CWT analysis was used to further identify the pollution source regions of these important metals. To be specific, heavy fuel oil was commonly composed of Mo, Sb, and Cr (Corbin et al., 2018; Sugiyama et al., 2020; Suzuki et al., 2021); some shipping routes in the Pacific Ocean or the Sea of Japan were identified as the potential pollution regions of these three high-risk metals (Fig. 4-5), revealing the significant influence of ship emissions around the sampling site. This was consistent with our HCA results (Mo, Sb, and Cr were in the same cluster with V and Ni). During the whole sampling period, the loading concentrations of Mo, Sb, and Cr in $PM_{2.5}$ varied obviously, ranging from 0.01 ng·m⁻³ to 67.8 ng·m⁻³, 0.1 ng·m⁻³ to 132.4 ng·m⁻³, and 0.3 ng·m⁻³ to 112.5 ng·m⁻³, respectively (Fig. S5). Extremely high concentration events for these three heavy metals could be observed when the air masses originated from shipping routes on the sea.

In comparison, three other metals (Se, As, and Pb) had different pollution source regions, which were mainly distributed northwest of the sampling site, especially Shandong Province, Hebei Province, and Shanxi Province, China. These regions are characterized by rapid economic development, high population density, and heavy traffic. Moreover, to meet increased traffic demand, the number of urban roads and motor vehicles are increasing obviously, and many previous studies showed that the influence of traffic emissions on particle pollution has become increasingly significant in China (Song et al., 2019; Wang et al., 2019). Hence, the transboundary transport from the Asian landmass was the important origin of these three metals, and more strict control of traffic emissions in these identified pollution

regions in China will be helpful for reducing the risk level of particle exposure around our sampling site.

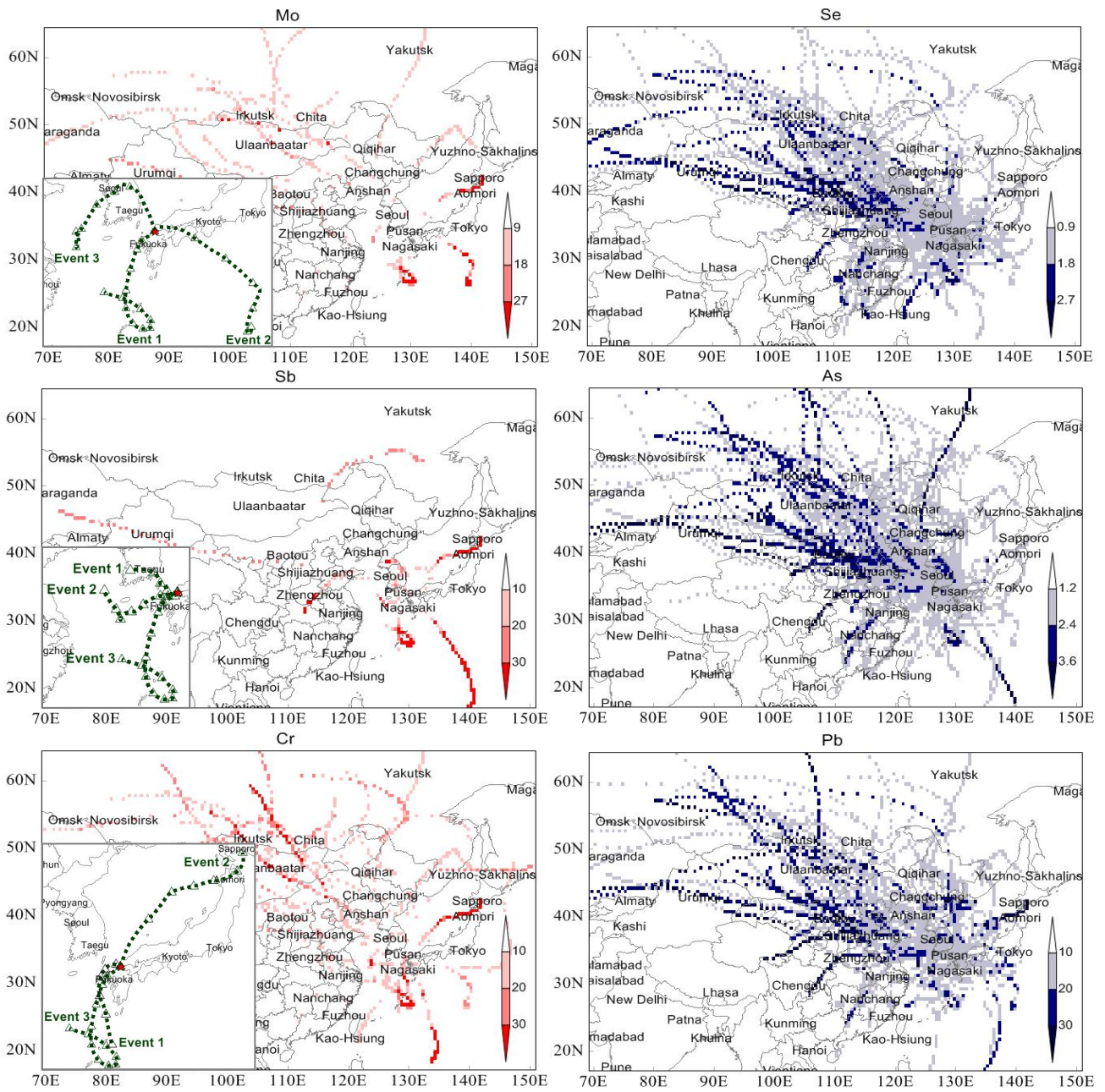Fig. 4-5 CWT analysis of high risk metals in the urban area of Kitakyushu, Japan, and the trajectories of extremely high concentration (top three) events for Mo, Sb and Cr.

4.3.4 Risk management

According to the identified priority control regions and heavy metals, several pertinent countermeasures and suggestions for risk management in the urban area of Kitakyushu, Japan, are put forward as

follows:

(1) Strengthen source control. Focus should be first on ship emissions, as the local source. Two practical approaches are suggested to mitigate the risk caused by ship emissions: using clean fuels, such as methanol and liquefied natural gas (Lee et al., 2020; Zhu et al., 2020), and installing scrubbers to collect primary particles emitted by the combustion of heavy fuel oil. Presently, the control of ship emissions in the waters near our sampling site mainly concentrates on sulfur emissions. The International Maritime Organization (IMO)'s regulation limiting ship fuel's sulfur content to 0.5% became effective on January 1, 2020 (Solakivi et al., 2019). Although this control policy is not aimed at heavy metal pollution, the countermeasures that could be adopted by ship operators are similar, such as installing a cleaning system in a ship and switching to lower sulfur fuel oil or a clean energy source (Zhou and Yuen, 2021). Therefore, the risk of heavy metals loaded in ship-emitted particles may also be reduced under the IMO's sulfur regulation, which is worth in-depth investigation in the future. Second, for traffic emissions, internationally collaborative efforts are essential. It is recommended to encourage the consumers in China to buy and use vehicles with clean energy by increasing relevant preferential policies. In addition, it is of great importance to encourage more people to use clean automobiles by improving their quality, convenience, and appearance.

(2) Raise public protection awareness. It is necessary to reinforce education about the environmental risks and self-environmental exposure protection. The relevant department should establish or perfect a real-time health risk information-sharing system based on integrated geographic modeling and visualization. The public can utilize this system to plan activities, such as reducing physical exertion outdoors near pollution sources, wearing masks in appropriate circumstances, and using air cleaners fitted with high-efficiency filters to reduce particle exposure in the indoor environment during high-risk

days. In addition, for families with children, parents should pay more attention to the condition of the living environment, especially places children could contact easily, such as the surfaces of floors, tables, toys, etc. On the other hand, it is necessary and important to cultivate good health habits in children, such as reminders not to eat or drink things that are exposed to the air for a long time; to store unfinished food in fresh-keeping bags; and to avoid touching the face, mouth, eyes, or nose before washing hands. Moreover, hand washing needs to be done in the proper way, namely, carefully wash all skin surfaces of the hands and fingers for at least 20 seconds by using hand sanitizer. If hand washing is not immediately possible in some situations, we can use disinfectant wipes on our hands.

4.4 Conclusions

The sampling campaign of $PM_{2.5}$ was carried out in Kitakyushu City on the western edge of Japan from 2013 to 2019, and 29 heavy metals loaded in $PM_{2.5}$ were measured in this study. During the whole sampling period, the $PM_{2.5}$ mass concentration ranged from 6.3 $\mu g \cdot m^{-3}$ to 57.5 $\mu g \cdot m^{-3}$, with a median value of 21.3 $\mu g \cdot m^{-3}$, and the sum concentration of heavy metals only accounted for 3%. According to the enrichment factor (EF) and geo-accumulation index (Igeo) analysis, it can be known that Se, Mo, Pb, As, Zn, W, Sb, Cu, V, Cr, Ni, and Cs were mainly from anthropogenic sources, which had EF values larger than 10 and Igeo values larger than 0. The comprehensive ecological risk index for these 12 anthropogenic metals was far greater than 600. This large index showed severe metal pollution and very high ecological risk in the urban area of Kitakyushu, Japan, which should be paid great attention. The human health assessment result further revealed that children living at the sampling site faced severe non-carcinogenic risk (HI=7.8) and moderate carcinogenic risk (CR=1.2×10^{-4}), and oral ingestion was basically the most important exposure pathway, followed by dermal contact and inhalation. The priority control metals included Mo, Se, As, Pb, Sb, and Cr; moreover, the concentration-weighted trajectory

analysis (CWT) indicated that Mo, Sb, and Cr were from ship emissions because some shipping routes around the Kyushu area were identified as their potential pollution source regions, while Se, As, and Pb were carried by the air masses from the Asian landmass. Overall, although the $PM_{2.5}$ concentration in the urban area of Kitakyushu, Japan was not high, the heavy metal risk cannot be overlooked; it is necessary to strengthen the source control of high-risk metals and raise public protection awareness.

References

Ali, H., Khan, E., Ilahi, I., 2019. Environmental Chemistry and Ecotoxicology of Hazardous Heavy Metals: Environmental Persistence, Toxicity, and Bioaccumulation. Journal of Chemistry 2019, 1-14.

Ali, M.U., Liu, G., Yousaf, B., Abbas, Q., Ullah, H., Munir, M.A.M., Fu, B., 2017. Pollution characteristics and human health risks of potentially (eco)toxic elements (PTEs) in road dust from metropolitan area of Hefei, China. Chemosphere 181, 111-121.

Alves, C.A., Vicente, E.D., Vicente, A.M.P., Rienda, I.C., Tomé, M., Querol, X., Amato, F., 2020. Loadings, chemical patterns and risks of inhalable road dust particles in an Atlantic city in the north of Portugal. Science of The Total Environment 737, 139596.

Bai, L., He, Z., Ni, S., Chen, W., Li, N., Sun, S., 2019. Investigation of $PM_{2.5}$ absorbed with heavy metal elements, source apportionment and their health impacts in residential houses in the North-east region of China. Sustainable Cities and Society 51, 101690.

Behrooz, R.D., Kaskaoutis, D.G., Grivas, G., Mihalopoulos, N., 2021. Human health risk assessment for toxic elements in the extreme ambient dust conditions observed in Sistan, Iran. Chemosphere 262, 127835.

Chen, C.R., Lai, H.C., Liao, M.I., Hsiao, M.C., Ma, H.w., 2021. Health risk assessment of trace elements of ambient $PM_{2.5}$ under monsoon patterns. Chemosphere 264, 128462.

Chen, H., Chen, Z., Chen, Z., Ou, X., Chen, J., 2020. Calculation of Toxicity Coefficient of Potential Ecological Risk Assessment of Rare Earth Elements. Bulletin of Environmental Contamination and Toxicology 104, 582-587.

Corbin, J.C., Mensah, A.A., Pieber, S.M., Orasche, J., Michalke, B., Zanatta, M., Czech, H., Massabò, D., Buatier de Mongeot, F., Mennucci, C., El Haddad, I., Kumar, N.K., Stengel, B., Huang, Y., Zimmermann, R., Prévôt, A.S.H., Gysel, M., 2018. Trace Metals in Soot and $PM_{2.5}$ from Heavy-Fuel-Oil Combustion in a Marine Engine. Environmental Science & Technology 52, 6714-6722.

Cui, L., Wu, Z., Han, P., Taira, Y., Wang, H., Meng, Q., Feng, Z., Zhai, S., Yu, J., Zhu, W., Kong, Y., Wang, H., Zhang, H., Bai, B., Lou, Y., Ma, Y., 2019. Chemical content and source apportionment of 36 heavy metal analysis and health risk assessment in aerosol of Beijing. Environmental Science and Pollution Research 27, 7005-7014.

Duan, X., Yan, Y., Li, R., Deng, M., Hu, D., Peng, L., 2020. Seasonal variations, source apportionment, and health risk assessment of trace metals in $PM_{2.5}$ in the typical industrial city of changzhi, China. Atmospheric Pollution Research, https://doi.org/10.1016/j.apr.2020.09.017.

Eck, T.F., Holben, B.N., Kim, J., Beyersdorf, A.J., Choi, M., Lee, S., Koo, J.H., Giles, D.M., Schafer, J.S., Sinyuk, A., Peterson, D.A., Reid, J.S., Arola, A., Slutsker, I., Smirnov, A., Sorokin, M., Kraft, J., Crawford, J.H., Anderson, B.E., Thornhill, K.L., Diskin, G., Kim, S.W., Park, S., 2020. Influence of cloud, fog, and high relative humidity during pollution transport events in South Korea: Aerosol properties and $PM_{2.5}$ variability. Atmospheric Environment 232, 117530.

Fan, M.Y., Zhang, Y.L., Lin, Y.C., Cao, F., Sun, Y., Qiu, Y., Xing, G., Dao, X., Fu, P., 2021. Specific sources of health risks induced by metallic elements in $PM_{2.5}$ during the wintertime in Beijing, China. Atmospheric Environment 246, 118112.

Fang, W., Yang, Y., Xu, Z., 2013. PM_{10} and $PM_{2.5}$ and Health Risk Assessment for Heavy Metals in a Typical Factory for Cathode Ray Tube Television Recycling. Environmental Science & Technology 47, 12469-12476.

Gaonkar, C.V., Kumar, A., Matta, V.M., Kurian, S., 2019. Assessment of crustal element and trace metal concentrations in atmospheric particulate matter over a coastal city in the Eastern Arabian Sea. Journal of the Air & Waste Management Association 70, 78-92.

Gilbert, R.O., 1987. Statistical Methods for Environmental Pollution Monitoring. John Wiley & Sons, Inc., New York, pp. 177-185.

Govender, P., Sivakumar, V., 2020. Application of k-means and hierarchical clustering techniques for analysis of air pollution: A review (1980–2019). Atmospheric Pollution Research 11, 40-56.

Guo, W., Liu, X., Liu, Z., Li, G., 2010. Pollution and Potential Ecological Risk Evaluation of Heavy Metals in the Sediments around Dongjiang Harbor, Tianjin. Procedia Environmental Sciences 2, 729-736.

Hadley, O.L., 2017. Background $PM_{2.5}$ source apportionment in the remote Northwestern United States. Atmospheric Environment 167, 298-308.

Han, X., Lu, X., 2017. Spatial distribution, environmental risk and source of heavy metals in street dust from an industrial city in semi-arid area of China. Archives of Environmental Protection 43, 10-19.

Hao, Y., Luo, B., Simayi, M., Zhang, W., Jiang, Y., He, J., Xie, S., 2020. Spatiotemporal patterns of PM$_{2.5}$ elemental composition over China and associated health risks. Environmental Pollution 265, 114910.

Hidemori, T., Nakayama, T., Matsumi, Y., Kinugawa, T., Yabushita, A., Ohashi, M., Miyoshi, T., Irei, S., Takami, A., Kaneyasu, N., Yoshino, A., Suzuki, R., Yumoto, Y., Hatakeyama, S., 2014. Characteristics of atmospheric aerosols containing heavy metals measured on Fukue Island, Japan. Atmospheric Environment 97, 447-455.

Hu, X., Zhang, Y., Ding, Z., Wang, T., Lian, H., Sun, Y., Wu, J., 2012. Bioaccessibility and health risk of arsenic and heavy metals (Cd, Co, Cr, Cu, Ni, Pb, Zn and Mn) in TSP and PM$_{2.5}$ in Nanjing, China. Atmospheric Environment 57, 146-152.

Hu, Z., Wang, J., Chen, Y., Chen, Z., Xu, S., 2014. Concentrations and source apportionment of particulate matter in different functional areas of Shanghai, China. Atmospheric Pollution Research 5, 138-144.

IARC, 2016. Agents Classified by the IARC (International Agency for Research on Cancer) Monographs, http://monographs.iarc.fr/ENG/Classification/ (last access 17.04.2021)

Ikemori, F., Uranishi, K., Sato, T., Fujihara, M., Hasegawa, H., Sugata, S., 2021. Time-resolved characterization of organic compounds in PM$_{2.5}$ collected at Oki Island, Japan, affected by transboundary pollution of biomass and non-biomass burning from Northeast China. Science of The Total Environment 750, 142183.

Inomata, Y., Ohizumi, T., Take, N., Sato, K., Nishikawa, M., 2016. Transboundary transport of anthropogenic sulfur in PM$_{2.5}$ at a coastal site in the Sea of Japan as studied by sulfur isotopic ratio measurement. Science of The Total Environment 553, 617-625.

Japan Ministry of the Environment, 2019. $PM_{2.5}$ components measurement manual, https://www.env.go.jp/air/osen/pm/ca/manual.html (last access 09.02.2021).

Jiang, N., Yin, S., Guo, Y., Li, J., Kang, P., Zhang, R., Tang, X., 2018. Characteristics of mass concentration, chemical composition, source apportionment of $PM_{2.5}$ and PM_{10} and health risk assessment in the emerging megacity in China. Atmospheric Pollution Research 9, 309-321.

Juda-Rezler, K., Reizer, M., Maciejewska, K., Błaszczak, B., Klejnowski, K., 2020. Characterization of atmospheric $PM_{2.5}$ sources at a Central European urban background site. Science of The Total Environment 713, 136729.

Kaneyasu, N., Yamamoto, S., Sato, K., Takami, A., Hayashi, M., Hara, K., Kawamoto, K., Okuda, T., Hatakeyama, S., 2014. Impact of long-range transport of aerosols on the $PM_{2.5}$ composition at a major metropolitan area in the northern Kyushu area of Japan. Atmospheric Environment 97, 416-425.

Kasimov, N.S., Vlasov, D.V., Kosheleva, N.E., 2020. Enrichment of road dust particles and adjacent environments with metals and metalloids in eastern Moscow. Urban Climate 32, 100638.

Khan, M.F., Shirasuna, Y., Hirano, K., Masunaga, S., 2010. Characterization of $PM_{2.5}$, $PM_{2.5-10}$ and $PM_{>10}$ in ambient air, Yokohama, Japan. Atmospheric Research 96, 159-172.

Lee, H.J., Yoo, S.H., Huh, S.Y., 2020. Economic benefits of introducing LNG-fuelled ships for imported flour in South Korea. Transportation Research Part D: Transport and Environment 78, 102220.

Li, H., Yang, J., Ye, B., Jiang, D., 2018. Pollution characteristics and ecological risk assessment of 11 unheeded metals in sediments of the Chinese Xiangjiang River. Environmental Geochemistry and Health 41, 1459-1472.

Li, P.h., Yu, J., Bi, C.l., Yue, J.j., Li, Q.q., Wang, L., Liu, J., Xiao, Z., Guo, L., Huang, B.j., 2019. Health risk assessment for highway toll station workers exposed to $PM_{2.5}$-bound heavy metals. Atmospheric Pollution Research 10, 1024-1030.

Lide, D.R., 2008. CRC Handbook of Chemistry and Physics, 88th edition. Boca Raton, Florida, pp. 14-17.

Lin, Y.C., Tsai, C.J., Wu, Y.C., Zhang, R., Chi, K.H., Huang, Y.T., Lin, S.H., Hsu, S.C., 2015. Characteristics of trace metals in traffic-derived particles in Hsuehshan Tunnel, Taiwan: size distribution, potential source, and fingerprinting metal ratio. Atmospheric Chemistry and Physics 15, 4117-4130.

Liu, B., Xu, M., Wang, J., Wang, Z., Zhao, L., 2021. Ecological risk assessment and heavy metal contamination in the surface sediments of Haizhou Bay, China. Marine Pollution Bulletin 163, 111954.

Liu, K., Ren, J., 2019. Characteristics, sources and health risks of $PM_{2.5}$-bound potentially toxic elements in the northern rural China. Atmospheric Pollution Research 10, 1621-1626.

Liu, Y., Wang, Q., Zhuang, W., Yuan, Y., Yuan, Y., Jiao, K., Wang, M., Chen, Q., 2018. Calculation of Thallium's toxicity coefficient in the evaluation of potential ecological risk index: A case study. Chemosphere 194, 562-569.

Megido, L., Suárez-Peña, B., Negral, L., Castrillón, L., Fernández-Nava, Y., 2017. Suburban air quality: Human health hazard assessment of potentially toxic elements in PM_{10}. Chemosphere 177, 284-291.

MohseniBandpi, A., Eslami, A., Ghaderpoori, M., Shahsavani, A., Jeihooni, A.K., Ghaderpoury, A., Alinejad, A., 2018. Health risk assessment of heavy metals on $PM_{2.5}$ in Tehran air, Iran. Data in Brief 17, 347-355.

Molepo, K.M., Abiodun, B.J., Magoba, R.N., 2019. The transport of PM_{10} over Cape Town during high pollution episodes. Atmospheric Environment 213, 116-132.

Moreno, T., Kojima, T., Querol, X., Alastuey, A., Amato, F., Gibbons, W., 2012. Natural versus anthropogenic inhalable aerosol chemistry of transboundary East Asian atmospheric outflows into western Japan. Science of The Total Environment 424, 182-192.

Moryani, H.T., Kong, S., Du, J., Bao, J., 2020. Health Risk Assessment of Heavy Metals Accumulated on $PM_{2.5}$ Fractioned Road Dust from Two Cities of Pakistan. International Journal of Environmental Research and Public Health 17, 7124.

Nakatsubo, R., Oshita, Y., Aikawa, M., Takimoto, M., Kubo, T., Matsumura, C., Takaishi, Y., Hiraki, T., 2020. Influence of marine vessel emissions on the atmospheric $PM_{2.5}$ in Japan's around the congested sea areas. Science of The Total Environment 702, 134744.

Onishi, K., Kurosaki, Y., Otani, S., Yoshida, A., Sugimoto, N., Kurozawa, Y., 2012. Atmospheric transport route determines components of Asian dust and health effects in Japan. Atmospheric Environment 49, 94-102.

Phung, V.L.H., Ueda, K., Seposo, X., Takami, A., Sugata, S., Yoshino, A., Michikawa, T., Yamazaki, S., Honda, A., Takano, H., 2020. Hourly association between ambient $PM_{2.5}$ and emergency ambulance dispatches in 11 cities in Japan. Environmental Research 185, 109448.

Pietrogrande, M.C., Dalpiaz, C., Dell'Anna, R., Lazzeri, P., Manarini, F., Visentin, M., Tonidandel, G., 2018. Chemical composition and oxidative potential of atmospheric coarse particles at an industrial

and urban background site in the alpine region of northern Italy. Atmospheric Environment 191, 340-350.

Roy, D., Singh, G., Seo, Y.C., 2019. Carcinogenic and non-carcinogenic risks from PM_{10}-and $PM_{2.5}$-Bound metals in a critically polluted coal mining area. Atmospheric Pollution Research 10, 1964-1975.

Sah, D., Verma, P.K., Kandikonda, M.K., Lakhani, A., 2019. Pollution characteristics, human health risk through multiple exposure pathways, and source apportionment of heavy metals in PM_{10} at Indo-Gangetic site. Urban Climate 27, 149-162.

Shi, D., Lu, X., 2018. Accumulation degree and source apportionment of trace metals in smaller than 63 μm road dust from the areas with different land uses: A case study of Xi'an, China. Science of The Total Environment 636, 1211-1218.

Solakivi, T., Laari, S., Kiiski, T., Töyli, J., Ojala, L., 2019. How shipowners have adapted to sulphur regulations – Evidence from Finnish seaborne trade. Case Studies on Transport Policy 7, 338-345.

Song, X., Hao, Y., Zhu, X., 2019. Air Pollutant Emissions from Vehicles and Their Abatement Scenarios: A Case Study of Chengdu-Chongqing Urban Agglomeration, China. Sustainability 11, 6503.

Sugiyama, T., Ueda, K., Seposo, X.T., Nakashima, A., Kinoshita, M., Matsumoto, H., Ikemori, F., Honda, A., Takano, H., Michikawa, T., Nitta, H., 2020. Health effects of $PM_{2.5}$ sources on children's allergic and respiratory symptoms in Fukuoka, Japan. Science of The Total Environment 709, 136023.

Suzuki, Y., Matsunaga, K., Yamashita, Y., 2021. Assignment of $PM_{2.5}$ sources in western Japan by non-negative matrix factorization of concentration-weighted trajectories of GED-ICP-MS/MS element concentrations. Environmental Pollution 270, 116054.

Tchounwou, P.B., Yedjou, C.G., Patlolla, A.K., Sutton, D.J., 2012. Heavy Metal Toxicity and the Environment. 101, 133-164.

Tsai, P.J., Young, L.H., Hwang, B.F., Lin, M.Y., Chen, Y.C., Hsu, H.T., 2020. Source and health risk apportionment for PM$_{2.5}$ collected in Sha-Lu area, Taiwan. Atmospheric Pollution Research 11, 851-858.

Wang, J., Wu, Q., Liu, J., Yang, H., Yin, M., Chen, S., Guo, P., Ren, J., Luo, X., Linghu, W., Huang, Q., 2019. Vehicle emission and atmospheric pollution in China: problems, progress, and prospects. PeerJ 7, e6932.

Wang, N., Wang, A., Kong, L., He, M., 2018a. Calculation and application of Sb toxicity coefficient for potential ecological risk assessment. Science of The Total Environment 610-611, 167-174.

Wang, X., He, S., Chen, S., Zhang, Y., Wang, A., Luo, J., Ye, X., Mo, Z., Wu, L., Xu, P., Cai, G., Chen, Z., Lou, X., 2018b. Spatiotemporal Characteristics and Health Risk Assessment of Heavy Metals in PM$_{2.5}$ in Zhejiang Province. International Journal of Environmental Research and Public Health 15, 583.

Wang, X., Sato, T., Xing, B., 2006. Size distribution and anthropogenic sources apportionment of airborne trace metals in Kanazawa, Japan. Chemosphere 65, 2440-2448.

Wang, X., Sato, T., Xing, B., Tamamura, S., Tao, S., 2005. Source identification, size distribution and indicator screening of airborne trace metals in Kanazawa, Japan. Journal of Aerosol Science 36, 197-210.

Wen, J., Wang, X., Zhang, Y., Zhu, H., Chen, Q., Tian, Y., Shi, X., Shi, G., Feng, Y., 2018. PM$_{2.5}$ source profiles and relative heavy metal risk of ship emissions: Source samples from diverse ships, engines, and navigation processes. Atmospheric Environment 191, 55-63.

Xie, J., Jin, L., Cui, J., Luo, X., Li, J., Zhang, G., Li, X., 2020. Health risk-oriented source apportionment of $PM_{2.5}$-associated trace metals. Environmental Pollution 262, 114655.

Xu, P., Chen, Y., He, S., Chen, W., Wu, L., Xu, D., Chen, Z., Wang, X., Lou, X., 2020. A follow-up study on the characterization and health risk assessment of heavy metals in ambient air particles emitted from a municipal waste incinerator in Zhejiang, China. Chemosphere 246, 125777.

Yang, J., Teng, Y., Song, L., Zuo, R., 2016. Tracing Sources and Contamination Assessments of Heavy Metals in Road and Foliar Dusts in a Typical Mining City, China. Plos One 11, e0168528.

Zhang, J., Wei, E., Wu, L., Fang, X., Li, F., Yang, Z., Wang, T., Mao, H., 2018. Elemental Composition and Health Risk Assessment of PM_{10} and $PM_{2.5}$ in the Roadside Microenvironment in Tianjin, China. Aerosol and Air Quality Research 18, 1817-1827.

Zhang, X., Murakami, T., Wang, J., Aikawa, M., 2021. Sources, species and secondary formation of atmospheric aerosols and gaseous precursors in the suburb of Kitakyushu, Japan. Science of The Total Environment 763, 143001.

Zhang, X., Zhang, K., Liu, H., Lv, W., Aikawa, M., Liu, B., Wang, J., 2020. Pollution sources of atmospheric fine particles and secondary aerosol characteristics in Beijing. Journal of Environmental Sciences 95, 91-98.

Zhang, X., Zhang, K., Lv, W., Liu, B., Aikawa, M., Wang, J., 2019. Characteristics and risk assessments of heavy metals in fine and coarse particles in an industrial area of central China. Ecotoxicology and Environmental Safety 179, 1-8.

Zhi, M., Zhang, X., Zhang, K., Ussher, S.J., Lv, W., Li, J., Gao, J., Luo, Y., Meng, F., 2021. The characteristics of atmospheric particles and metal elements during winter in Beijing: Size

distribution, source analysis, and environmental risk assessment. Ecotoxicology and environmental safety 211, 111937.

Zhong, C., Yang, Z., Jiang, W., Hu, B., Hou, Q., Yu, T., Li, J., 2016. Ecological geochemical assessment and source identification of trace elements in atmospheric deposition of an emerging industrial area: Beibu Gulf economic zone. Sci Total Environ 573, 1519-1526.

Zhou, Q., Yuen, K.F., 2021. Low-sulfur fuel consumption: Marine policy implications based on game theory. Marine Policy 124, 104304.

Zhu, M., Li, K.X., Lin, K.C., Shi, W., Yang, J., 2020. How can shipowners comply with the 2020 global sulphur limit economically? Transportation Research Part D: Transport and Environment 79, 102234.

Chapter 5: Summary and future prospect

5.1 Summary

The long-term monitoring of atmospheric particles (total particles and $PM_{2.5}$) was conducted in Kitakyushu, Japan. We investigated particle characteristics from sources, secondary formation, reduction mechanism, and risk assessment. The major conclusions are summarized as follows:

• The main sources of total particles in Kitakyushu, Japan included industrial combustion plus ship emissions, secondary sulfates, secondary nitrates plus biomass burning, marine aerosols, and dust, accounting for 26 %, 23 %, 22 %, 19 %, and 10 %, respectively.

• The high concentration of total particles was mainly caused by local emissions around the Kyushu area and long-range transport from the Asian landmass. The transboundary transport of air pollutants significantly influenced the particle characteristics, especially during spring.

• The secondary formation process of total particles is significantly influenced by Ox, NO_2, NH_3, HNO_3, HCl, T, and RH. In addition, ALWC acted as an efficient medium of secondary formation, comprising 59 % of the total particle mass concentration.

• Of the seven sensitive tests, the largest decreasing amounts of the IAM were basically achieved by reducing TNaCl, followed by SIA components, TMg^{2+}, TK^+, and TCa^{2+}; however, inorganic aerosol pH increased only after controlling TSO_4^{2-} and TNO_3^-.

• The ALWC made the greatest contribution to the variations of the IAM for five control species (TNaCl, TNH_4^+, TNO_3^-, TMg^{2+}, and TCa^{2+}) except two (TSO_4^{2-} and TK^+) among seven species, and the ALWC in inorganic aerosols was significantly restrained by sea salts.

• The process of converting nitrate and ammonium from the gas phase to the aerosol phase could be enhanced effectively under extremely low concentration level of marine aerosols in the atmosphere.

• The appropriate presence of TCa^{2+} in the atmosphere could facilitate the mitigation of particle pollution related to the transfer process of SO$_4$$^{2-}$ between the aerosol solid phase and the aerosol aqueous phase.

• The PM$_{2.5}$ mass concentration was about 21.3 μg·m^{-3} at the sampling site; the heavy metals loaded in it only accounted for 3%. Among 29 metals, Na, Fe, K, Al, Ca, Zn, and Pb were present in high concentrations (>10 ng·m^{-3}), and Mn, V, Ti, Cu, Ni, Cr, Ba, Mo, As, and Se were present in medium concentrations (>1 ng·m^{-3}).

• For the environment, Mo, Se, and As were extremely high risk with median E_r^i values of 1079.5, 992.2, and 364.4, respectively, moreover, Pb showed high risk (177.7), and Sb showed considerable risk (105.9). These five metals caused severe ecological risk around the sampling site, which should be the focus of great attention.

• For human beings, As, Pb, and Sb showed severe non-carcinogenic risks for children, with HI values of 2.0, 1.9, and 1.9, respectively. In addition, exposure to As and Cr(VI) could cause slight carcinogenic risk for children, with CR values of 7.6×10^{-5} and 4.0×10^{-5}, respectively.

• Reducing the PM$_{2.5}$ exposure risk by oral ingestion is the most effective strategy for children around our study area, followed by reducing the risks of dermal contact and inhalation. Parents should pay more attention to the condition of their living environment and cultivate good health habits in their children.

• As priority control metals, Se, As, and Pb originated from traffic emissions through transboundary transport, while Mo, Sb, and Cr were from local sources, namely ship emissions in the Pacific Ocean/Sea of Japan.

In this research, we comprehensively investigated and studied the characteristics of atmospheric

aerosols in Kitakyushu City from emission sources to risk level of receptor site, clarified the contribution of each apportionment on aerosol pollution, and validated its chemical mechanism from the viewpoint of thermodynamics. Our outcomes including risk assessment on aerosol pollution could totally provide useful/fruitful/optical/basic scientific reference/information/knowledge to formulate countermeasures for air pollution issue on aerosol.

5.2 Future Prospect

A low particle concentration does not signify low risk for the environment and human health, and the pollution of $PM_{2.5}$-bound heavy metals in Kitakyushu, Japan, should not be neglected, especially for metals from traffic and ship emissions. Regarding traffic emissions from transboundary transport, the Chinese government's Three-year Action Plan to Win the Battle for a Blue-Sky (from 2018) emphasized special action regarding $PM_{2.5}$ pollution control in 2 + 26 Cities, in which traffic has been one important control source for the mitigation of $PM_{2.5}$ pollution in recent years. As for ship emissions, stricter limitations on ship fuel oil by the IMO have been executed in waters near the sampling site since January 1, 2020. Thus, these high-risk sources will be controlled, and the heavy metal risk in the urban area of Kitakyushu, Japan, may be significantly reduced. In future work, we can analyze the annual variations of traffic-emitted and ship-emitted metals and the reduction of $PM_{2.5}$ exposure risk at the sampling site after obtaining data from recent years (May, 2019 to the present). In addition, combining the data of multiple monitoring stations, we can further investigate the spatiotemporal distribution of $PM_{2.5}$-bound heavy metals in Japan and identify control cities of primary and secondary priorities and, correspondingly, prioritize controlling heavy metals based on risk levels of different regions, which can help in making cost-effective risk management policies under limited national/local budgets.

The other research direction is about organic aerosols. In the present study, we only focused on the

water-soluble ions and heavy metals in atmospheric aerosols. However, the organic components also make a high contribution for the particle mass concentration, and their formation process are more complex. The organic components of atmospheric aerosols mainly include *n*-alkanes, branched alkanes, *n*-alkanoic acids, *n*-alkanals, aromatic polycarboxylic acids, polycyclic aromatic hydrocarbons (PAHs), heterocyclic aromatic hydrocarbons, dicarboxylic acids, ketones, etc. PAHs make a relatively low contribution for organic aerosols, but a majority of PAHs have carcinogenic, teratogenic, and mutagenic effects., playing an important destructive role in heritable, immune or pulmonary toxicity (The detail information is shown in Table S7). Hence, the concentration levels, pollution sources, secondary formation processes, and human health risks of organic aerosols (PAHs for particular) are worth in-depth investigation.

Publication List

[1] **Zhang, X.**, Eto, Y., and Aikawa, M., 2021. Risk assessment and management of $PM_{2.5}$-bound heavy metals in the urban area of Kitakyushu, Japan, Science of The Total Environment, 795, 148748, 10.1016/j.scitotenv.2021.148748.

[2] **Zhang, X.**, Murakami, T., Wang, J., and Aikawa, M., 2021. Sources, species and secondary formation of atmospheric aerosols and gaseous precursors in the suburb of Kitakyushu, Japan, Science of The Total Environment, 763, 143001, 10.1016/j.scitotenv.2020.143001.

[3] **Zhang, X.**, Wang, J., Zhang, K., Shang, X., Aikawa, M., Zhou, G., Li, J., and Li, H., 2021. Year-round observation of atmospheric inorganic aerosols in urban Beijing: Size distribution, source analysis, and reduction mechanism, Journal of Environmental Sciences, (accepted on September 15, 2021).

[4] **Zhang, X.**, Zhang, K., Liu, H., Lv, W., Aikawa, M., Liu, B., and Wang, J., 2020. Pollution sources of atmospheric fine particles and secondary aerosol characteristics in Beijing, Journal of Environmental Sciences, 95, 91-98, 10.1016/j.jes.2020.04.002.

[5] **Zhang, X.**, Zhang, K., Lv, W., Liu, B., Aikawa, M., and Wang, J., 2019. Characteristics and risk assessments of heavy metals in fine and coarse particles in an industrial area of central China, Ecotoxicology and Environmental Safety, 179, 1-8, 10.1016/j.ecoenv.2019.04.024.

[6] Zhi, M., **Zhang, X.**, Zhang, K., Ussher, S. J., Lv, W., Li, J., Gao, J., Luo, Y., and Meng, F., 2021. The characteristics of atmospheric particles and metal elements during winter in Beijing: Size distribution, source analysis, and environmental risk assessment, Ecotoxicology and Environmental Safety, 211, 111937, 10.1016/j.ecoenv.2021.111937.

[7] Wang, J., **Zhang, X.**, Yang, Q., Zhang, K., Zheng, Y., and Zhou, G., 2018. Pollution characteristics

of atmospheric dustfall and heavy metals in a typical inland heavy industry city in China, Journal of Environmental Sciences, 71, 283-291, 10.1016/j.jes.2018.05.031.

[8] Wang, J., **Zhang, X.**, Zhang, K., and Zheng, Z., 2018. Characterization of Size Distribution and Concentration of Atmospheric Particles During Summer in Zhuzhou, China, Polish Journal of Environmental Studies, 27, 2793-2800, 10.15244/pjoes/80714.

[9] Li, J., Zhang, K., **Zhang, X.**, Lv, W., Guo, Y., Zhi, M., and Li, J., 2021. Analysis on the influence and cause of a heavy pollution process on air quality in Baoding during COVID-19, Polish Journal of Environmental Studies, (accepted on July 27, 2021).

[10] Zhi, M., Zhang, K., **Zhang, X.**, Herrmann, H., Gao, J., Fomba, K.W., Tang, W., Luo, Y., Li, H., and Meng, F., 2021. A statistic comparison of multielement analysis of low atmospheric fine particles (PM$_{2.5}$) using different spectroscopy techniques, Journal of Environmental Sciences, (accepted on August 17, 2021).

[11] Peng, Y., Suzuki, M., Nguyen, L.K., **Zhang, X.**, Aikawa, M., 2021. Presence and Source Attribution of Airborne Anthropogenic/Non-Sea-Salt Inorganic Chloride Determined by Filter-Pack Method at Eastern Edge in East Asia. Water, Air, & Soil Pollution, 232, 238, 10.1007/s11270-021-05186-0.

Acknowledgment

This doctoral research has been supported by many people, and I would like to express my heartfelt thanks to them.

Kitakyushu, Japan

September, 2021

Xi ZHANG

Supplementary data

Table S1 The ion amount in 1kg seawater.

Ions	Na^+	K^+	Mg^{2+}	Ca^{2+}	Sr^{2+}	Cl^-	Br^-	SO_4^{2-}	HCO_3^-	BO_3^{3-}
g	10.56	0.38	1.27	0.4	0.013	18.98	0.065	2.65	0.14	0.026
mmol	455	9.2	52.5	10.2	0.15	535.1	0.81	27.6	2.35	0.44

Table S2 The values of T_r, RfD_o, $RfCi$, GIABS, SF_o, and IUR for the anthropogenic metals.

Parameter	Se	Mo	Pb	As	Zn	W	Sb	Cu	V	Cr or Cr(VI)	Ni	Cs
T_r	1	18	5	10	1	-	13	5	2	2	5	-
RfD_o	5.00×10^{-3}	5.00×10^{-3}	3.50×10^{-3}	3.00×10^{-4}	3.00×10^{-1}	8.00×10^{-4}	4.00×10^{-4}	4.00×10^{-2}	7.00×10^{-3}	3.00×10^{-3}	2.00×10^{-2}	-
$RfCi$	2.00×10^{-2}	4.00×10^{-4}	3.52×10^{-3}	1.50×10^{-5}	3.01×10^{-1}	-	3.00×10^{-4}	4.02×10^{-2}	1.00×10^{-4}	1.00×10^{-4}	9.00×10^{-5}	-
GIABS	1	1	1	1	1	1	0.15	1	0.026	0.025	0.04	-
SF_o	-	-	0.0085	1.5	-	-	-	-	-	0.5	-	-
IUR	-	-	0.000012	0.0043	-	-	-	-	-	0.084	0.00026	-

Note: For health risk, the Cr(VI) concentration was calculated as one seventh of the total Cr (Behrooz et al., 2021).

Table S3 Input parameters and abbreviations for cancer and non-cancer exposure assessment.

Parameter	Notation	Unit	Value	
			Children	Adults
Ingestion rate	IngR	$mg \cdot day^{-1}$	200	100
Exposure frequency	EF	$days \cdot year^{-1}$	180	180
Exposure duration	ED	year	6	24
Unit conversion factor	CF	$kg \cdot mg^{-1}$	1.0×10^{-6}	1.0×10^{-6}
Body weight	BW	kg	15	70
Averaging lifetime	AT	days	ED × 365 (for non-carcinogens) 70 × 365 (for carcinogens)	ED × 365 (for non-carcinogens) 70 × 365 (for carcinogens)
Exposure time	ET	$h \cdot day^{-1}$	24	24
Average lifetime	AT_n	hours	ED × 365 × 24 (non-carcinogens) 70 × 365 × 24 (carcinogens)	ED × 365 × 24 (non-carcinogens) 70 × 365 × 24 (carcinogens)
Skin surface area	SA	cm^2	2800	5700
Skin adherence factor	AF	$mg \cdot cm^{-2}$	0.2	0.07
Dermal absorption factor	ABS	-	0.03 (As), 0.1 (Pb), 0.001 (Cd), 0.01 (other metals)	

Table S4 Comparison of concentration of PM$_{2.5}$ and total heavy metals (THM) between Kitakyushu and other regions

City	Sampling period	PM$_{2.5}$ ($\mu g \cdot m^{-3}$)	THM ($ng \cdot m^{-3}$)	THM/PM$_{2.5}$	Reference
Kitakyushu, Japan	May, 2013-February, 2019	21.3	628.4	3%	This study
Xiamen, China	April, 2017-January, 2019	44.9	320.0	1%	(Wang et al., 2021)
Baoding, China	Oct, 2016-Auggust, 2017	132	789.7	1%	(Xie et al., 2019)
Guangzhou, China	March, 2016-February, 2017	55.0	702.5	1%	(Xie et al., 2020a)
Nanjing, China	March, 2016-February, 2017	61.1	816.3	1%	(Xie et al., 2020a)
Taiyuan, China	April-December, 2016	180	1142	1%	(Liu et al., 2019)
Tangshan, China	October, 2017-October, 2018	89.7	2670	3%	(Fang et al., 2021)
Changsha, China	March-April, 2013	100	3211	3%	(Zhai et al., 2014)
Chengdu, China	October 2014-July, 2015	67.7	2100	3%	(Wang et al., 2018a)
Chongqing, China	October 2014-July, 2015	70.0	2800	4%	(Wang et al., 2018a)
Hangzhou, China	December, 2014-December, 2015	80.0	3100	4%	(Xu et al., 2021)
Qingdao, China	January-February, 2015	72.2	3630	5%	(Gao et al., 2017)
Beijing, China	November-December, 2018	69.3	3482	5%	(Fan et al., 2021)
Ningbo, China	December, 2014-December, 2015	54.3	2920	5%	(Xu et al., 2021)
Zhengzhou, China	October, 2014-July, 2015	118	6926	6%	(Jiang et al., 2018)

Table S5 Statistical evaluation (min., max. and each percentile) of $PM_{2.5}$ ($\mu g \cdot m^{-3}$) and 29 heavy metal concentrations ($ng \cdot m^{-3}$) during whole sampling period.

Item	Min.	25th	50th	75th	Max.
$PM_{2.5}$	6.3	15.8	21.3	29.4	57.5
Na	1.7	95.7	144.9	210.0	770.0
Fe	2.3	78.9	140.0	240.5	1745.7
K	1.1	62.1	101.1	166.0	640.0
Al	2.4	20.0	41.5	85.8	1600.0
Ca	2.0	15.0	30.7	65.4	660.0
Zn	1.5	12.3	29.5	51.8	319.3
Pb	0.1	5.1	10.5	17.6	57.6
Mn	0.2	4.2	8.3	13.2	56.1
V	0.0	3.3	5.7	9.8	38.8
Ti	0.7	2.0	4.4	11.5	123.0
Cu	0.2	2.0	3.6	5.8	33.3
Ni	0.3	1.4	3.3	6.2	123.5
Cr	0.3	1.9	3.0	9.4	112.5
Ba	0.0	1.3	2.1	3.1	34.3
Mo	0.0	0.7	1.5	4.0	67.8
As	0.0	0.7	1.4	2.2	6.1
Se	0.1	0.6	1.0	1.7	5.5
Sb	0.1	0.4	0.8	1.4	132.4
Rb	0.0	0.2	0.4	0.7	3.0
W	0.0	0.2	0.3	0.6	5.1
La	0.0	0.1	0.2	0.3	8.1
Co	0.0	0.1	0.1	0.2	6.8
Ce	0.0	0.0	0.1	0.2	1.5
Cs	0.0	0.0	0.1	0.1	1.2
Hf	0.0	0.0	0.0	0.0	10.0
Sc	0.0	0.0	0.0	0.0	2.5
Th	0.0	0.0	0.0	0.0	0.2
Ta	0.0	0.0	0.0	0.0	0.2
Sm	0.0	0.0	0.0	0.0	0.1

Table S6 Carcinogenic risk for children living in Kitakyushu and other regions

City	Sampling period	Pb	As	Cr(VI)	Ni	Total CR	Reference
Kitakyushu, Japan	May, 2013-February, 2019	3.9×10^{-6}	7.6×10^{-5}	4.0×10^{-5}	6.9×10^{-8}	1.2×10^{-4}	This study
Xiamen, China	April, 2017-January, 2019	-	-	1.2×10^{-4}	4.8×10^{-8}	1.2×10^{-4}	(Wang et al., 2021)
Baoding, China	December, 2017	1.5×10^{-5}	-	1.1×10^{-4}	-	1.3×10^{-4}	(Xie et al., 2020b)
Guangzhou, China	January, 2013-February, 2019	-	4.6×10^{-5}	9.3×10^{-5}	1.4×10^{-6}	1.4×10^{-4}	(Li et al., 2021)
Chongqing, China	October 2014-July, 2015	-	2.5×10^{-5}	1.2×10^{-4}	1.5×10^{-6}	1.5×10^{-4}	(Li et al., 2021)
Chengdu, China	October 2014-July, 2015	-	1.0×10^{-4}	6.2×10^{-5}	1.7×10^{-6}	1.7×10^{-4}	(Li et al., 2021)
Zhengzhou, China	October, 2014-July, 2015	-	2.2×10^{-4}	-	-	2.2×10^{-4}	(Jiang et al., 2018)
Beijing, China	November-December, 2018	4.8×10^{-6}	7.2×10^{-5}	2.1×10^{-5}	1.6×10^{-4}	2.6×10^{-4}	(Fan et al., 2021)
Nanjing, China	April-September, 2010	2.1×10^{-4}	6.5×10^{-5}	1.1×10^{-4}	1.8×10^{-7}	3.9×10^{-4}	(Hu et al., 2012)
Zhejiang, China	January-December, 2015	3.0×10^{-4}	1.5×10^{-4}	1.9×10^{-5}	-	4.7×10^{-4}	(Wang et al., 2018b)
Taiyuan, China	April-December, 2016	2.0×10^{-4}	2.0×10^{-5}	3.0×10^{-4}	1.5×10^{-5}	5.4×10^{-4}	(Liu et al., 2019)
Hangzhou, China	December, 2014-December, 2015	3.8×10^{-6}	5.6×10^{-4}	1.6×10^{-4}	4.3×10^{-6}	7.3×10^{-4}	(Xu et al., 2021)
Qingdao, China	March, 2006-February, 2007	2.0×10^{-3}	7.2×10^{-5}	9.8×10^{-6}	4.1×10^{-8}	2.1×10^{-3}	(Zhang et al., 2018)
Jinan, China	March, 2006-February, 2007	2.8×10^{-3}	1.2×10^{-4}	1.5×10^{-5}	5.9×10^{-8}	2.9×10^{-3}	(Zhang et al., 2018)
Zaozhuang, China	March, 2006-February, 2007	3.2×10^{-3}	9.3×10^{-5}	1.2×10^{-5}	6.5×10^{-8}	3.3×10^{-3}	(Zhang et al., 2018)
Zibo, China	March, 2006-February, 2007	3.2×10^{-3}	1.4×10^{-4}	1.3×10^{-5}	6.9×10^{-8}	3.4×10^{-3}	(Zhang et al., 2018)

Table S7 The information about PAHs.

Species	Abbreviation	Chemical formula (Benzene rings)	TEF	MEF	RfD
Naphthalene	Nap	$C_{10}H_8$ (2)	0.001		0.02
Acenaphthylene	Acy	$C_{12}H_8$ (3)	0.001		
Acenaphthene	Ace	$C_{12}H_{10}$ (3)	0.001		0.06
Fluorene	Flu	$C_{13}H_{10}$ (3)	0.001		0.04
Phenanthrene	Phe	$C_{14}H_{10}$ (3)	0.001		0.015
Anthracene	Ant	$C_{14}H_{10}$ (3)	0.01		0.3
Fluoranthene	Fla	$C_{16}H_{10}$ (4)	0.001		0.04
Pyrene	Pyr	$C_{16}H_{10}$ (4)	0.001		0.015
Benzo(a)anthracene	BaA	$C_{18}H_{12}$ (4)	0.1	0.082	
Chrysene	Chr	$C_{18}H_{12}$ (4)	0.01	0.017	
Benzo(b)Fluoranthene	BbF	$C_{20}H_{12}$ (5)	0.1	0.25	
Benzo(k)Fluoranthene	BkF	$C_{20}H_{12}$ (5)	0.1	0.11	
Benzo(a)Pyrene	BaP	$C_{20}H_{12}$ (5)	1	1	0.0003
Dibenzo(a, h)anthracene	DBA	$C_{22}H_{14}$ (5)	1	0.29	
Indeno(123-c, d)Pyrene	IDP	$C_{22}H_{12}$ (6)	0.1	0.31	
Benzo(g, h, i)perylene	BghiP	$C_{22}H_{12}$ (6)	0.01	0.19	0.015
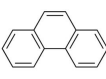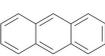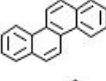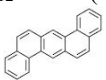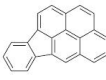
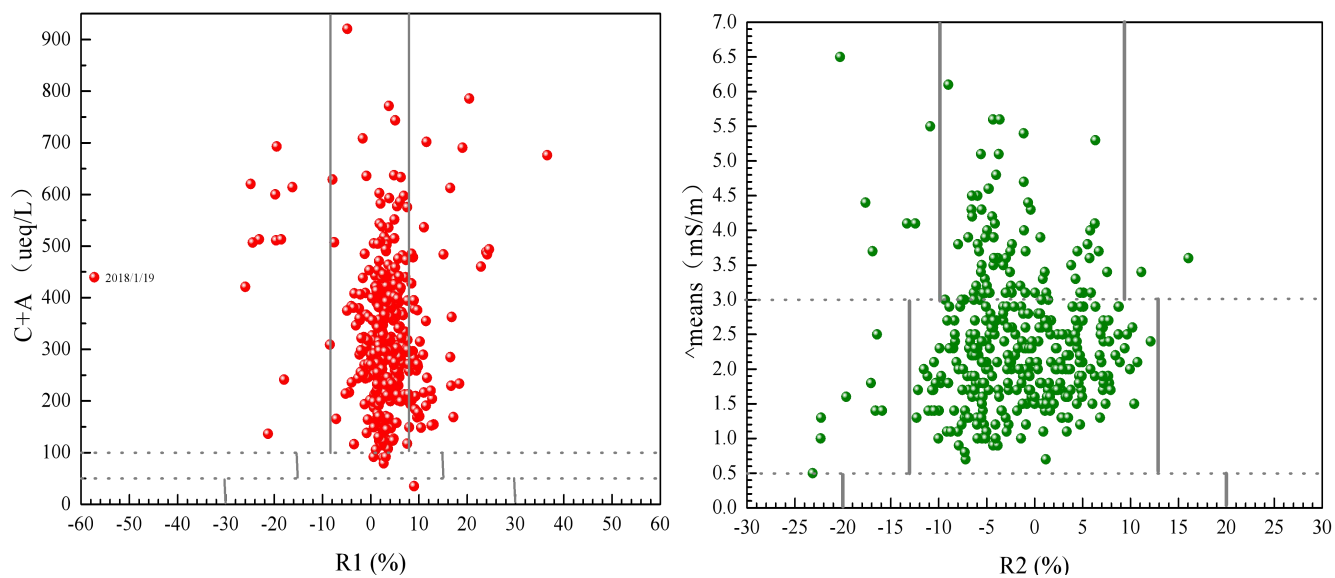Note: TEF: Toxic equivalent factor; MEF: Mutagenic potency factor.

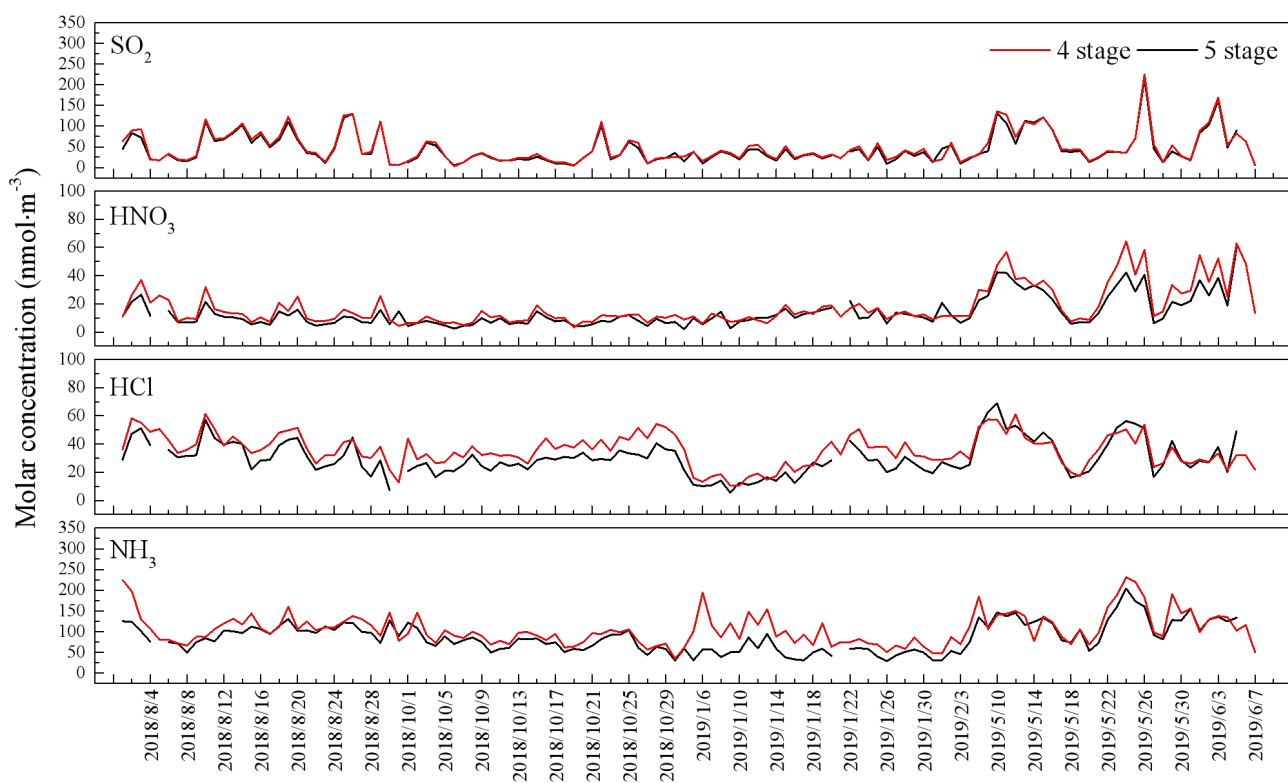Fig. S1 Ion balance and conductivity balance of original data.

Fig. S2 Time variations of SO$_2$, HNO$_3$, HCl, and NH$_3$ measured by four-stage filter pack and five-stage filter pack
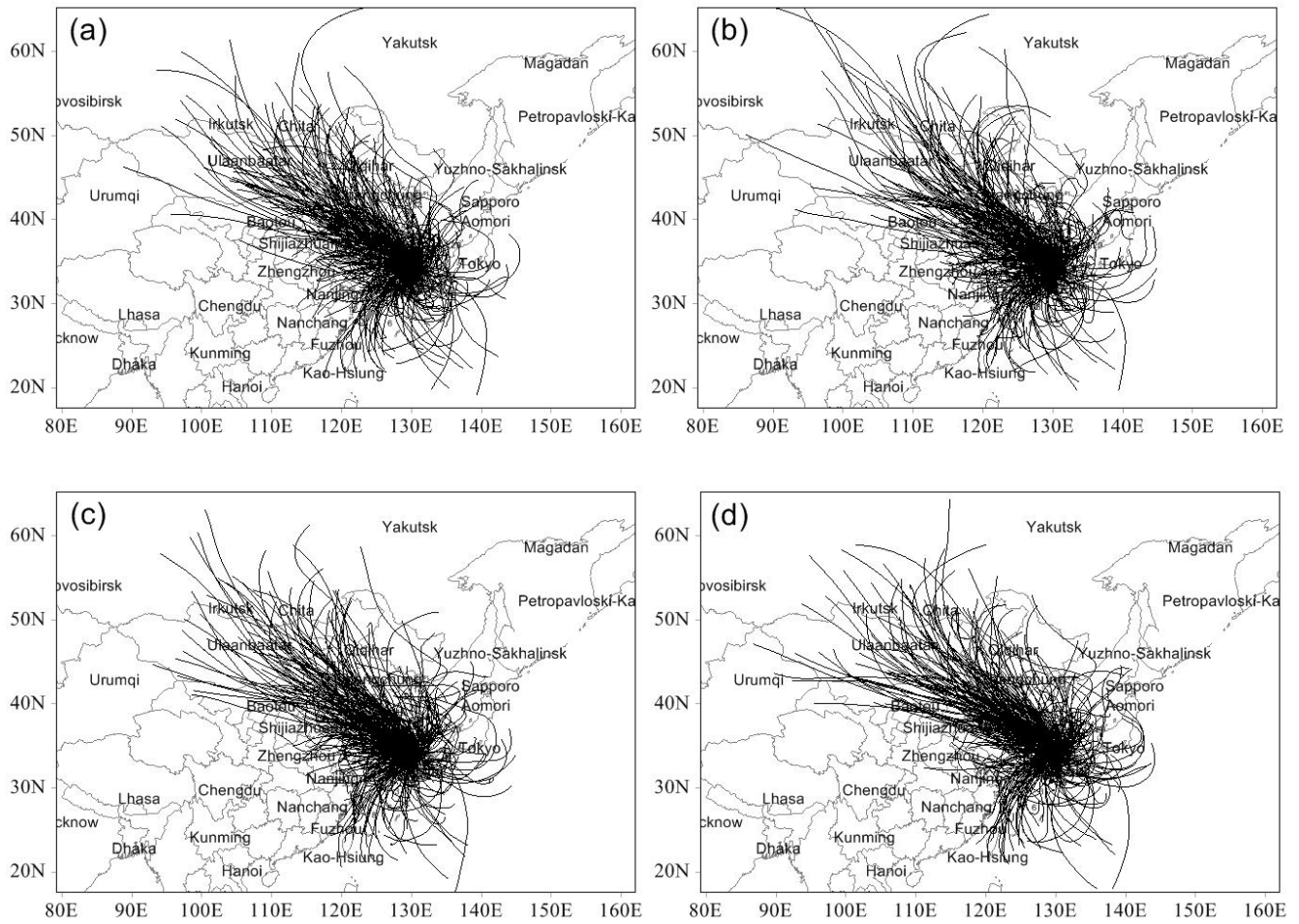
Fig. S3 The transport pathways of the daily air masses during the sampling period with the trajectory start hour of 03:00 (a),

09:00 (b), 15:00 (c), 21:00 (d), respectively (Note: Even each trajectory start hour was different, the transport pathways of

daily air masses were very similar, moreover, the sampling intermediate time in this study was 15:00 (UTC); hence, we

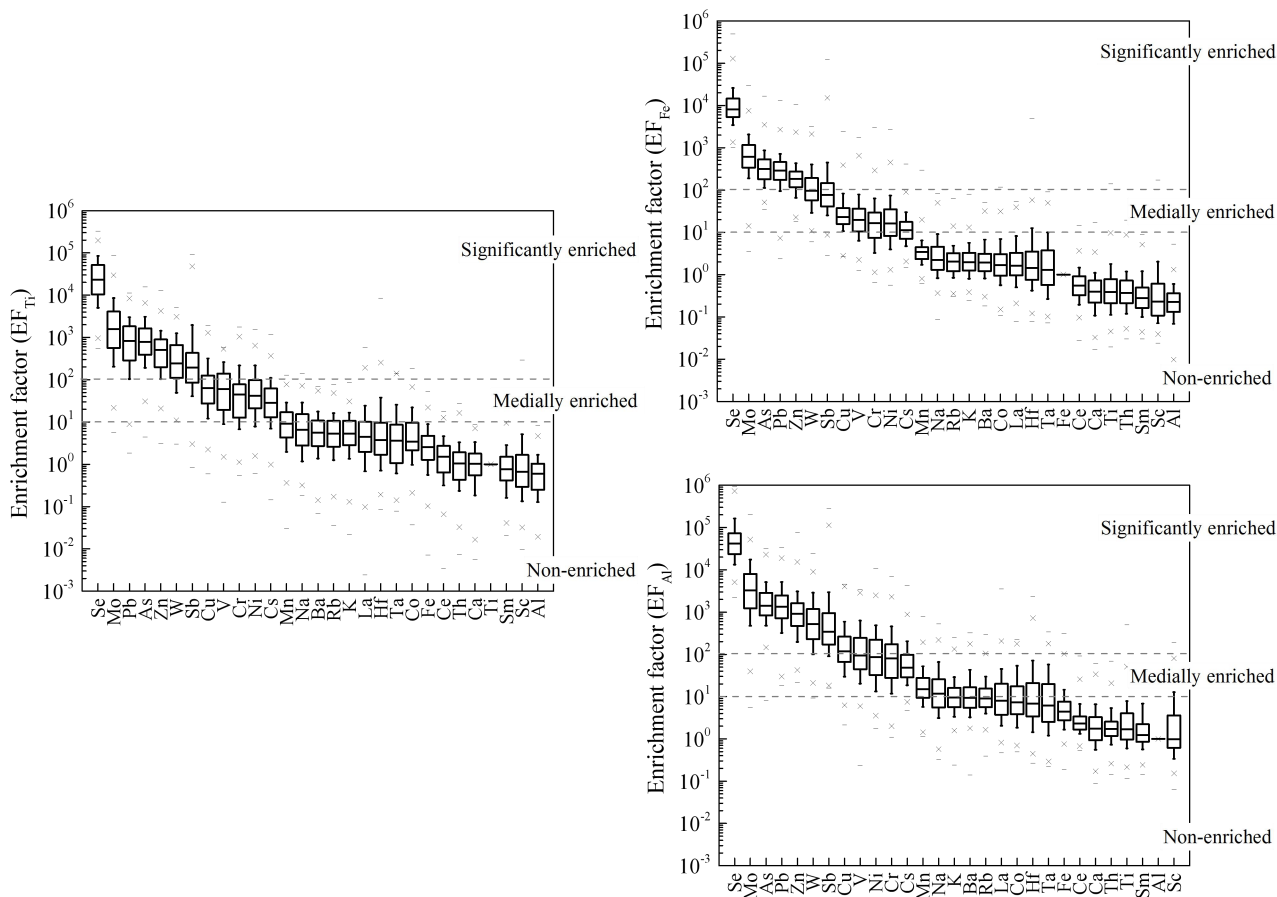finally choose this group of 365 trajectories.)

Fig. S4 The calculated enrichment factors of 29 heavy metals by choosing different reference metal (Ti, Fe, and Al).
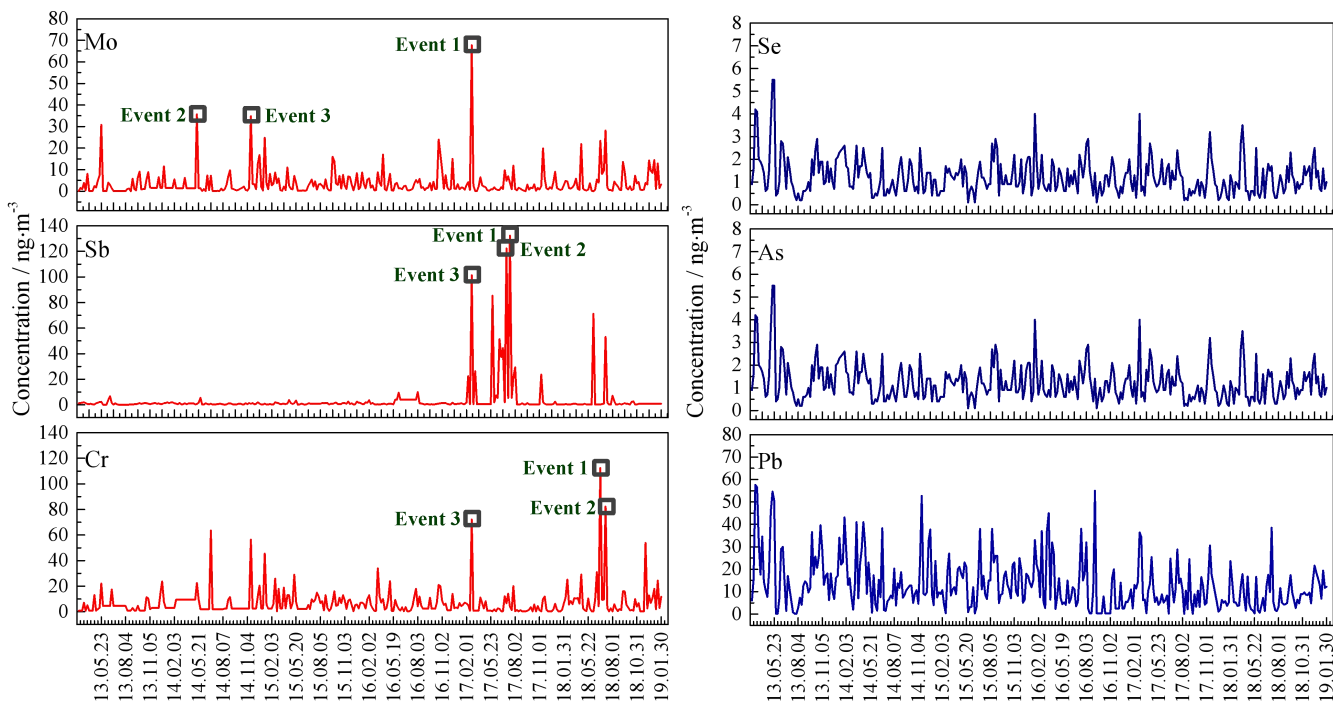

Fig. S5 Concentration variations of high risk metals during the whole sampling period and the extremely high

concentration (top three) events for Mo, Sb and Cr.

References

Behrooz, R.D., Kaskaoutis, D.G., Grivas, G., Mihalopoulos, N., 2021. Human health risk assessment for toxic elements in the extreme ambient dust conditions observed in Sistan, Iran. Chemosphere 262, 127835.

Fan, M.Y., Zhang, Y.L., Lin, Y.C., Cao, F., Sun, Y., Qiu, Y., Xing, G., Dao, X., Fu, P., 2021. Specific sources of health risks induced by metallic elements in $PM_{2.5}$ during the wintertime in Beijing, China. Atmospheric Environment 246, 118112.

Fang, B., Zeng, H., Zhang, L., Wang, H., Liu, J., Hao, K., Zheng, G., Wang, M., Wang, Q., Yang, W., 2021. Toxic metals in outdoor/indoor airborne $PM_{2.5}$ in port city of Northern, China: Characteristics, sources, and personal exposure risk assessment. Environmental Pollution 279, 116937.

Gao, P., Lei, T., Jia, L., Song, Y., Lin, N., Du, Y., Feng, Y., Zhang, Z., Cui, F., 2017. Exposure and health risk assessment of $PM_{2.5}$-bound trace metals during winter in university campus in Northeast China. Science of The Total Environment 576, 628-636.

Hu, X., Zhang, Y., Ding, Z., Wang, T., Lian, H., Sun, Y., Wu, J., 2012. Bioaccessibility and health risk of arsenic and heavy metals (Cd, Co, Cr, Cu, Ni, Pb, Zn and Mn) in TSP and $PM_{2.5}$ in Nanjing, China. Atmospheric Environment 57, 146-152.

Jiang, N., Yin, S., Guo, Y., Li, J., Kang, P., Zhang, R., Tang, X., 2018. Characteristics of mass concentration, chemical composition, source apportionment of $PM_{2.5}$ and PM_{10} and health risk assessment in the emerging megacity in China. Atmospheric Pollution Research 9, 309-321.

Li, F., Yan, J., Wei, Y., Zeng, J., Wang, X., Chen, X., Zhang, C., Li, W., Chen, M., Lü, G., 2021. $PM_{2.5}$-bound heavy metals from the major cities in China: Spatiotemporal distribution, fuzzy exposure assessment and health risk management. Journal of Cleaner Production 286, 124967.

Liu, K., Ren, J., 2019. Characteristics, sources and health risks of $PM_{2.5}$-bound potentially toxic elements in the northern rural China. Atmospheric Pollution Research 10, 1621-1626.

Wang, H., Qiao, B., Zhang, L., Yang, F., Jiang, X., 2018. Characteristics and sources of trace elements in $PM_{2.5}$ in two megacities in Sichuan Basin of southwest China. Environmental Pollution 242, 1577-1586.

Wang, S., Hu, G., Yu, R., Shen, H., Yan, Y., 2021. Bioaccessibility and source-specific health risk of heavy metals in $PM_{2.5}$ in a coastal city in China. Environmental Advances 4, 100047.

Wang, X., He, S., Chen, S., Zhang, Y., Wang, A., Luo, J., Ye, X., Mo, Z., Wu, L., Xu, P., Cai, G., Chen, Z., Lou, X., 2018. Spatiotemporal Characteristics and Health Risk Assessment of Heavy Metals in $PM_{2.5}$ in Zhejiang Province. International Journal of Environmental Research and Public Health 15, 583.

Xie, J., Jin, L., Cui, J., Luo, X., Li, J., Zhang, G., Li, X., 2020. Health risk-oriented source apportionment of $PM_{2.5}$-associated trace metals. Environmental Pollution 262, 114655.

Xie, J.J., Yuan, C.G., Xie, J., Niu, X.D., He, A.E., 2020. $PM_{2.5}$-bound potentially toxic elements (PTEs) fractions, bioavailability and health risks before and after coal limiting. Ecotoxicology and Environmental Safety 192, 110249.

Xie, J.J., Yuan, C.G., Xie, J., Shen, Y.W., He, K.Q., Zhang, K.G., 2019. Speciation and bioaccessibility of heavy metals in $PM_{2.5}$ in Baoding city, China. Environmental Pollution 252, 336-343.

Xu, J., Jia, C., Yu, H., Xu, H., Ji, D., Wang, C., Xiao, H., He, J., 2021. Characteristics, sources, and health risks of PM$_{2.5}$-bound trace elements in representative areas of Northern Zhejiang Province, China. Chemosphere 272, 129632.

Zhai, Y., Liu, X., Chen, H., Xu, B., Zhu, L., Li, C., Zeng, G., 2014. Source identification and potential ecological risk assessment of heavy metals in PM$_{2.5}$ from Changsha. Science of The Total Environment 493, 109-115.

Zhang, J., Zhou, X., Wang, Z., Yang, L., Wang, J., Wang, W., 2018. Trace elements in PM$_{2.5}$ in Shandong Province: Source identification and health risk assessment. Science of The Total Environment 621, 558-577.